UNIVERSITY OF THESSALY

DEPARTMENT OF CIVIL ENGINEERING

LABORATORY OF HYDROLOGY AND AQUATIC SYSTEMS ANALYSIS

UNIVERSITÉ JOSEPH FOURIER

OBSERVATOIRE DES SCIENCES DE L'UNIVERS DE GRENOBLE I (OSUG)

LABORATOIRE D' ETUDE DES TRANSFERTS EN HYDROLOGIE ET ENVIRONEMENT

COMMON GREEK-FRENCH MASTER PROGRAM

"MANAGEMENT OF HYDROMETEREOLOGICAL HAZARDS - HYDROHASARDS"

THE IMPACTS OF CLIMATE CHANGE ON DROUGHTS IN ACHELOOS RIVER BASIN

LYSITSA GEORGIA

MASTER THESIS

VOLOS 2012

TABLE OF CONTENTS

ACKNOWLEDMENTS

iii

ABSTRACT

Despite uncertainties on future climates, climate variation will influence the hydrology of a region through changes in the timing, amount of precipitation, temperature, evapotranspiration and soil moisture, which in turn will affect the drought characteristics in a region. This study is focused on the influence of various climate change scenarios on droughts events and their characteristics in the river basin of Acheloos, Greece. Acheloos River is the second longest river in Greece and first in water contribution. It contains various reservoirs and constitutes the main source of water, both for the flat and the semi mountainous regions of Western Greece. The outputs of the Canadian Centre for Climate Modeling Analysis Global Circulation Model CGCM3 were applied for three socio-economic scenarios, namely SRES B1, SRES A1B and SRES A2 for the assessment of climate change impact on droughts. A statistical downscaling method has been applied to estimate monthly precipitation and temperature time series for two future periods 2030-2050 and 2080-2100. The methodology is based on multiple regression of GCM predictant variables with observed areal precipitation and temperature and the application of a stochastic time series model for precipitation and temperature residuals simulation. The Standardized Precipitation Index (SPI) and the Standardized Precipitation Evapotranspiration Index (SPEI) computed at various timescales were used as indicators of meteorological droughts for present and future climate conditions. The analysis of the SPI and SPEI time series indicated an impact of climate change on the frequency of dry months and the allocation on various severity classes for the three SRES scenarios. SPEI indicated a larger increase in the frequency of dry months than SPI, due to the dependence of the index on the temperature. Comparison of the drought characteristics for the historical period (1980-2000) and the future periods indicated that the severity, maximum cumulative severity and maximum duration increased for the three under study scenarios for the period 2080-2100.

ΠΕΡΙΛΗΨΗ

Παρόλη την αβεβαιότητα στα μελλοντικά κλίματα, η κλιματική διακύμανση θα επηρεάσει την υδρολογία μιας περιοχής μέσω αλλαγών στην χρονική κατανομή και στη ποσότητα της βροχόπτωσης, στην θερμοκρασία, στην δυνητική εξατμισοδιαπνοή και στην εδαφική υγρασία, οι οποίες στη συνέχεια θα επηρεάσουν τα χαρακτηριστικά της ξηρασίας της υπό μελέτη περιοχής. Η επίδραση των διάφορων κλιματικών σεναρίων στα γεγονότα ξηρασίας και στα χαρακτηριστικά αυτών στην λεκάνη απορροής του Αχελώου ποταμού αποτελεί το πεδίο μελέτης της παρούσας εργασίας. Ο Αχελώος είναι ο δεύτερος σε μήκος ποταμός της Ελλάδας και ο πρώτος στην παροχή ύδατος. Περιέχει αρκετούς ταμιευτήρες και αποτελεί την κύρια πηγή νερού για τις πεδινές και ημιορεινές περιοχές της Δυτικής Ελλάδας. Από τα αρχεία του παγκόσμιου μοντέλου κυκλοφορίας CGCM3 του CCCMA (Canadian Centre for Climate Modeling Analysis) εξήχθησαν οι μεταβλητές για τα τρία κοινωνικό-οικονομικά SRES σενάρια, B1, A1B και B2 με σκοπό την εκτίμηση της επίδρασης της κλιματικής αλλαγής στη ξηρασία. Εφαρμόστηκε η μέθοδος του στατιστικού καταβιβασμού κλίμακας για να εκτιμηθούν οι μηνιαίες χρονοσειρές βροχόπτωσης και θερμοκρασίας για τις μελλοντικές χρονικές περιόδους 2030-2050 και 2080-2100. Η μεθοδολογία βασίζεται στη μέθοδο της πολλαπλής γραμμικής παλινδρόμησης των ανεξάρτητων μεταβλητών πρόγνωσης (predictands) που εξήχθησαν από το GCM και της παρατηρούμενης επιφανειακής βροχόπτωσης και θερμοκρασίας, καθώς επίσης και στην στοχαστική προσομοίωση των υπολοίπων βροχόπτωσης και θερμοκρασίας. Ο κανονικοποιημένος δείκτης βροχόπτωσης SPI (Standardized Precipitation Index) και ο κανονικοποιημένος δείκτης βροχόπτωσης εξατμισοδιαπνοής SPEI (Standardized Precipitation Evapotranspiration Index) υπολογίστηκαν για πολλαπλές χρονικές κλίμακες και χρησιμοποιήθηκαν σαν δείκτες για την εκτίμηση ξηρασίας για παρόντα και μελλοντικά κλίματα. Η ανάλυση των χρονοσειρών των δεικτών SPI και SPEI έδειξε μια επίδραση της κλιματικής αλλαγής στην συχνότητα των ξηρών μηνών και στην κατανομή τους στις διάφορες κατηγορίες δριμύτητας για τα τρία εξεταζόμενα σενάρια. Ο δείκτης SPEI έδειξε μεγαλύτερη αύξηση στην συχνότητα των ξηρών μηνών συγκριτικά με τον SPI, εξαιτίας της εξάρτησης του δείκτη από

την θερμοκρασία. Συγκρίνοντας τα χαρακτηριστικά των γεγονότων ξηρασίας της ιστορικής (1980-2000) και της μελλοντικής περιόδου (2080-2100), η δριμύτητα, η μέγιστη αθροιστική δριμύτητα και η μέγιστη διάρκεια των επεισοδίων ξηρασίας φάνηκε να αυξάνεται για τα τρία SRES σενάρια .

RÉSUMÉ

Malgré les incertitudes sur le climat futur, les variations climatiques influenceront l'hydrologie d'une région à travers des changements dans le temps de réaction, la quantité de précipitation, la température, l'évapotranspiration ou l'humidité des sols qui affecteront les caractéristiques de sécheresse d'une région. Cette étude se concentre sur divers scénarios de changement climatique d'évènements de sécheresse et leurs caractéristiques sur le bassin versant de Acheloos, Grèce. La rivière Acheloos est la deuxième plus grande rivière de Grèce et la première pour la contribution en eau. Elle possède plusieurs réservoirs et constitue la première ressource en eau des régions de plaines et de montagnes de la Grèce occidentale. Les sorties de modèle du Canadian Centre for Climate Modeling Analysis Global Circulation (CGCM3) ont été appliquées à trois scénarios socio-économiques respectivement nommés SRES B1, SRES A1B et SRES A2 pour la prévision de l'impact du changement climatique sur les sécheresses. Une méthode de descente d'échelle statistique a été appliquée pour estimer les précipitations mensuelles et les séries temporelles de température pour la période 2030-2050 et 2080-2100. La méthodologie est basée sur une régression multiple des variables prédictives des GCM avec les précipitations et températures régionales observées ainsi que sur l'application d'un modèle stochastique de série temporelle pour les résidus de précipitations et températures modélisées. L'Indice de Précipitation Standardisé (SPI) et l'Indice d'Evapotranspiration et de Précipitation Standardisés (SPEI) calculés à différentes échelles de temps ont été utilisés comme indicateurs des sécheresses météorologiques pour le climat présent et futur. L'analyse des séries temporelles de SPI et SPEI indique un impact du changement climatique sur la fréquence des mois secs ainsi que sur l'allocation de divers classes de sévérités pour les 3 scénarios SRES. Le SPEI prévois un plus grande augmentation de la fréquence des mois secs que le SPI due à sa dépendance à la température. La comparaison des caractéristiques de sécheresse de la période historique (1980-2000) avec les futures périodes, indique que la sévérité, la sévérité cumulative maximale et la durée maximale ont augmenté pour les 3 scénarios étudiés sur la période 2080-2100.

1. INTRODUCTION

1.1. Climate change

The diversity of climate change impacts is a major environmental problem facing the globe and a point of global concern of the scientists and decision makers since the observed changes of meteorological variables, mainly in precipitation and temperature, have shown that extreme events such as floods and droughts are already on rise. Global surface temperature has been increased significantly during the last century and will continue to rise unless greenhouse gas (GHG) emissions are drastically reduced (IPCC, 2001, 2007). According to Intergovernmental Panel on Climate Change report (IPCC, 2007) global GHG emissions due to human activities have grown since pre-industrial times, with an increase of 70% between 1970 and 2004.

In the 4th Assessment Reports of the IPCC (IPCC, 2007), a recent summary of observed changes in hydroclimatological variables is provided. Records of global surface temperature for 150 years (1850-2006) show that the eleven years from the period 1995–2006 rank among the twelve warmest years. Analysis of historical meteorological observations indicated that the 100-year linear trend (1906-2005) of 0.74 [0.56 to 0.92] °C is larger than the corresponding trend of 0.6 [0.4 to 0.8] °C (1901-2000) given in the Third Assessment Report (IPCC, 2001). However, the extend of climate change varies regionally, even locally due to interactions between atmospheric processes, oceans, land surfaces. Studies in the Mediterranean region have shown that temperature exhibits a positive trend in west Mediterranean and a negative trend in the east Mediterranean over the 20th century (National Observatory of Athens, 2001). A 5% decrease was observed in the precipitation over much of the land bordering the Mediterranean Sea, except for central North African coast (Tunisia and Libya). In the last decade a general drying is evident over most of southeastern Mediterranean and Greece. A precipitation decrease has been well documented in the central-west Mediterranean over the last 50 years (National Observatory of Athens, 2001; IPCC, 2007).

In 1990 and 1992 the IPCC developed long-term emissions scenarios, which widely used in the analysis of possible climate change, its impacts and option to mitigate climate change. Scenarios are alternative images of how the future might unfold and are an appropriate tool with which to analyze how driving forces may influence future emission outcomes and to assess the associated uncertainties. In 1996 a new set of scenarios, the SRES scenarios, were developed to update the IS92 series (IPCC, 2000). Four narrative storylines were developed to describe the relationships between emission driving forces and their evolution, each of which represents different demographic, social, economic, technological and environmental developments. For each storyline several different scenarios were developed using different modeling approaches. Six models were used and this resulted in 40 different scenarios. All scenarios based on the same storyline constitute a scenario family.

The A1 storyline and scenario family describes a future world of very rapid economic growth, low population growth, and the rapid introduction of new and more efficient technologies. Major underlying themes are convergence among regions, capacity building and increased cultural and social interactions, with a substantial reduction in regional differences in per capita income. It is divided into three groups that describe alternative directions of technological change in the energy system: fossil intensive (A1FI), non-fossil energy resources (A1T) and a balance across all sources (A1B).

The B1 scenario describes a convergent world, with the same population as A1, but more rapid changes in economic growth, emphasizing local solutions to economic structures toward a service and information economy and with reductions in material intensity, and the introduction of clean and resource-efficient technologies. The emphasis is on global solutions to economic, social, and environmental sustainability, including improved equity, but without additional climate initiatives.

B2 scenario describes a world in which the emphasis is on local solutions to economic, social, and environmental sustainability. It is a world with moderate population growth, intermediate levels of economic development, and less rapid

and more diverse technological change than in the B1 and A1 storylines. While the scenario is also oriented toward environmental protection and social equity, it focuses on local and regional levels.

A2 describes a very heterogeneous world. The underlying theme is self-reliance and preservation of local identities. Fertility patterns across regions converge very slowly, which results in high population growth. Economic development is primarily regionally oriented and per capita economic growth and technological change, are more fragmented and slower than in other storylines.

In order to capture the global climate system, General Circulation Models (GCMs) have been developed and used. GCMs are used to study the effects of the increasing concentration of carbon dioxide and the other greenhouse gases on the Earth's climate. These models link atmospheric processes with ocean and land surface processes and can be used to provide projections of the changes in temperature, precipitation and other climate variables in response to changes in greenhouse gas emissions. The two main types of General Circulation Models are Atmospheric (AGCM) and Ocean (OGCM) models. Separately they account for the changes within the atmosphere and the ocean respectively. An AGCM and an OGCM can be coupled together to form an atmosphere-ocean coupled general circulation model (AOGCM). With the addition of other components (such as a sea ice model or a land model), the AOGCM becomes the basis for a full climate model. Projections made by GCMs are reflections of the current state of knowledge of the processes in the climate system, but they still contain uncertainties. Unfortunately, GCMs are restricted in their usefulness for local impact studies due to their coarse spatial resolution in the order of hundreds of kilometers and they are unable to represent local sub-grid scale features and dynamics, such as local topographical features and convective cloud processes (Dibike and Coulibaly, 2006). However, in most climate change impact studies, such as hydrological impacts of climate change, sub-grid scale phenomenon is required to be simulated and therefore input data such as precipitation and temperature at sub-grid scales are required. Hence, it is necessary to convert the GCM outputs at the scale of the watershed for which the hydrological impact is going to be investigated. The methods used for converting the GCM outputs into

local meteorological variables that are required for reliable modeling of water resources systems are referred to as downscaling techniques (Wilby et al., 2002).

There are two main techniques of downscaling, the dynamical and statistical. Dynamical downscaling has the potential for capturing meso-scale nonlinear effects and providing coherent information among multiple climate variables. These models are formulated using physical principles and they can credibly reproduce a broad range of climates around the world, which increases confidence in their ability to downscale realistically future climates. The parameterization schemes that the dynamical models use to represent sub-grid scale processes in future climates that may be operating outside the range for which they were designed, as well as their computational cost are the main drawbacks of dynamical models. Statistical downscaling methods use cross-scale relationships that have been derived from observed data, and apply these to climate model data. These methods have the advantage of being computationally inexpensive, able to access finer scales than dynamical methods. Observational data at the desired scale for a long enough period are required in order to trained and validated. Unfortunately the statistical downscaling methods assume that the derived cross-scale relationships remain stable when the climate is perturbed. Other shortcomings of these techniques are that they cannot effectively accommodate regional feedbacks and, in some methods, can lack coherency among multiple climate variables.

There are applications related criteria in a particular context in order an appropriate downscaling method to be chosen (Mearns et al., 2004; Wilby et al., 2004). However, there are assumptions involved in both statistical and dynamical techniques which are difficult to verify a priori and contribute to the uncertainty of results (Giorgi et al., 2001). Many climate impact studies exist for developing and intercomparing statistical downscaling techniques (Wilby and Wigley, 1997; Xu 1999; Giorgi et al., 2001; Varis et al., 2004; Xu et al., 2005; Fowler et al., 2007).

i.   Projections of future changes in climate

According to IPCC, carbon dioxide concentrations, globally averaged surface temperature, and sea level are projected to increase under all IPCC emissions scenarios during the 21st century.

All SRES emissions scenarios result in an increase in the atmospheric concentration of CO_2. The projected concentrations of CO_2 -the primary anthropogenic greenhouse gas- for the six illustrative SRES scenarios, in the year 2100 range from 540 to 970 ppm, compared to about 280 ppm in the pre-industrial era and about 368 ppm in the year 2000. These projections include the land and ocean climate feedbacks.

The possibility of either increases or decreases in anthropogenic aerosols is included in the SRES scenarios, depending on the extent of fossil-fuel use and policies to abate polluting emissions. Sulfate aerosol concentrations are projected to fall below present levels by 2100 in all SRES scenarios. This would result in warming relative to present day. As a result of changes in climate, natural aerosols (e.g., sea salt, dust, and emissions leading to sulfate and carbon aerosols) are projected to increase.

An increase by 1.4 to 5.8°C of the globally averaged surface temperature is projected over the period 1990 to 2100. This is about two to ten times larger than the central value of observed warming over the 20th century. It is very likely that nearly all land areas will warm more rapidly than the global average, particularly those at northern high latitudes in winter. More hot days and heat waves and fewer cold and frost days are projected over nearly all land areas. Increases in mean temperature will lead to increases in hot weather and record hot weather, with fewer frost days and cold waves.

Furthermore, globally averaged annual precipitation is projected to increase during the 21st century as well as globally averaged water vapor and evaporation. At the regional scale, both increases and decreases in precipitation are projected, typically of 5 to 20%. It is likely that precipitation will increase

over high latitude regions in both summer and winter. Increases are also projected over northern mid-latitudes, tropical Africa and Antarctica in winter, and in southern and eastern Asia in summer. Australia, Central America, and southern Africa show consistent decreases in winter rainfall. Larger year-to-year variations in precipitation are very likely over most areas where an increase in mean precipitation is projected.

The amplitude, duration, location and frequency of extreme precipitation events will increase over many areas and the return period for extreme precipitation events are projected to decrease. This would lead to more frequent floods and landslides with attendant loss of life, health impacts (e.g., epidemics, infectious diseases and food poisoning), property damage, loss to infrastructure and settlements, soil erosion, pollution loads, insurance and agriculture losses, amongst others. A general drying of the mid-continental areas during summer is likely to lead to increases in summer droughts and could increase the risk of wild fires, due to a combination of increased temperature and potential evaporation that is not balanced by increases in precipitation.

Especially for Europe and the Mediterranean region, the models results showed an increase in the annual mean temperature more than the global mean. Northern Europe will face higher temperature in winter and Mediterranean area higher temperature in summer. The lowest winter temperatures will increase more than average winter temperature in northern Europe, and the highest summer temperatures are likely to increase more than average summer temperature in southern and central Europe.

An increase to the annual precipitation is projected in most of northern Europe as well as to extremes of daily precipitation. In most of the Mediterranean area the annual precipitation will decrease. The annual number of precipitation days is expected to decrease. In central Europe, precipitation is likely to increase in winter but decrease in summer. As a consequence the risk of summer drought will increase in both Mediterranean area and central Europe.

1.2. Drought

As it was mentioned before climate change is expected to primarily affect precipitation, temperature and potential evapotranspiration, and, thus, is likely to affect the occurrence and severity of meteorological droughts. Droughts are natural phenomena that affect nearly every region in the world and more people than any other natural disaster (Wilhite, 2000; Wilhite and Buchanan, 2005). It can be regarded as having been the most serious climatic risk in the 20th century (Obasi, 1994) with a devastating damage potential on agriculture, economy, environment and society. Drought has received special attention from researchers examining the Global Change hypothesis (Changnon et al., 2000).

Droughts generally originate from a deficiency of precipitation, soil moisture and water resources over an extended period of time, resulting in water shortage for sustaining and supplying the socio-economic activities of a region (Loukas and Vasiliades, 2004). Due to the multi-discipline character of this natural hazard, numerous definitions on the drought have been developed. A broad review of definitions for drought can be found on technical notes published by the Worldwide Meteorological Organization (WMO, 1967); other sources as Subrahmanyam (1967), Sandford (1979), Dracup, et al (1980), group the drought into three kinds: meteorological, hydrological and agricultural. The most well-known and widely used classification of droughts is the classification initially proposed by Dracup and his associates (Dracup et al., 1980) and integrated later by Wilhite and Glantz (1985), where four categories are identified. This drought classification system was adopted by the American Meteorological Society (2004). Based on the nature of the water deficit, four types of droughts are defined: a) the meteorological drought which is defined as a lack of precipitation over region for a period of time, b) the hydrological drought which is related to a period with deficiency in surface and subsurface water supplies of a given water resources management system, c) the agricultural drought, which, links impacts of meteorological drought to agricultural and usually refers to a period with declining soil moisture and consequent crop failure without any reference to surface water resources, d) the socio-economic drought which is associated to the failure of water resources

systems to meet the water demands and thus, associating droughts with supply of and demand for an economic good (water). The first three categories are referred as environmental droughts, and the socio-economic drought is considered as water resources systems drought (Wilhite, 2000). A similar classification is used by Tate and Gustard (2000) where droughts are classified into climatological, agrometeorological, river flow and groundwater droughts.

Droughts differ from one another in three essential characteristics; intensity, duration and spatial coverage (Wilhite, 2000). It is very difficult to objectively quantify their characteristics in terms of intensity, magnitude, duration and spatial extent due to the adversity of defining their onset, extend and end. However, it is necessary for the analysis of droughts to detect their features and to link the drought variability to climate (Piechota and Dracup, 1996). For this purpose, much effort has been devoted to developing techniques in order to analyze, monitor and evaluate the droughts. Among these, drought indices are the most widely used. Drought indices are employed to characterize droughts and its statistical properties. Several generations of researchers during the 20th century have proposed numerous of indices in the domains of meteorology, hydrology, agriculture research and application, remote sensing and water resources management. Many reviews such as Du Pisani et al. (1998); Heim (2000, 2002); Keyantash and Dracup (2002); Vogt and Somma (2000); Hayes et al.(2007); Niemeyer (2008) and the International Water Management Institute (IWMI, 2008) have been published giving a brief overview of existing drought indices. Many attempts have been made in the last decades in order to produce new drought indices and improve the existing ones (González and Valdés, 2004; Keyantash and Dracup, 2004; Wells et al., 2004; Tsakiris et al., 2007; Vicente-Serrano et al., 2010).

Along the various meteorological indices, the most commonly used are: 1) Discrete and cumulative precipitation anomalies, 2) the Z-score or Standardized Rainfall Anomalies (Jones and Hulme, 1996) , 3) Rainfall deciles (Gibbs and Maher, 1967), 4) the Palmer Drought Severity Index (PDSI) (Palmer, 1965), 5) the Bhalme – Mooley Drought Index (BMDI) (Bhalme and Mooley, 1980), 6) the Rainfall Anomaly Index (RAI) (van Rooy, 1965), and 7) the Standardized

Precipitation Index (SPI) (McKee et al., 1993). However, the Palmer Drought Severity Index (PDSI), based on a soil water balance equation, and the Standardized Precipitation Index (SPI), based on a precipitation probabilistic approach, were widely accepted and used in most studies related to drought analysis.

The Standardized Precipitation Index uses the precipitation as the only determinant. It is simpler than PDSI and it can be applied at any location. The SPI quantifies the precipitation deficit for multiple time scales and reflects the impact of drought on the availability of different types of water resources including soil moisture, ground water, snowpack, river discharges, and reservoir storages. For example, the moisture stored in the soil is highly affected by the short-term precipitation anomalies, whereas streamflow, groundwater and reservoir storage slowly respond to longer-term precipitation anomalies. Due to the normalized character, the SPI can represent wetter and drier climates in the same way.

Recently the Standardized Precipitation-Evapotranspiration Index (SPEI) was proposed by Vicente- Serrano et al. (2010) for identifying drought periods. It is based on precipitation and PET and combines the sensitivity of PDSI and to changes in evaporation demand (caused by temperature fluctuations and trends) with the simplicity of calculation and the multi-temporal nature of the SPI. According to recent studies (Vicente-Serrano et al., 2010; Potop, 2011) the role of temperature increase on drought conditions was not recognized using the precipitation-based SPI drought index, but was indentified for the drought in the decade of 2000 using the SPEI index.

Many studies in the international literature have tested the effectiveness of the drought indices in monitoring and analyzing the regional droughts. The Standardized Precipitation Index was used by Hayes and his associates (Hayes et al., 1999) in order to monitor the drought of 1996 in the southern and southwestern USA. They concluded that the SPI has the ability to detect the onset of the drought and monitor its progression and compared the results with the PDSI, where they found that the onset of the drought was detected at least one

month earlier using the SPI. Earlier, Guttman (1998) with a spectral analysis, compared historical time series of PDSI with time series of SPI and demonstrated the spatially invariance of the spectral characteristics of the SPI in contrast with those of the PDSI which are spatially variable. For this reason, he concluded that SPI is a better drought index for interregional comparison of drought events. In his study, Guttman (1998) also found that the 12-month SPI oscillations were found to be in phase with the oscillations of PDSI. Loukas et al. (2003) in an intercomparison of SPI, Zscore, RAI, the PDSI and the Palmer moisture anomaly index (Z-Index) (Palmer, 1965) at 28 meteorological stations in Greece found similar results. In that study, the oscillations of the SPI were found to be in phase with the oscillations of the Z-score and the RAI for the same time-scales and with the oscillations of the PDSI for time-scales larger than 6-months.

The SPI was used in recent regional drought analyses in the Mediterranean region using rain gauge data (Bordi et al., 2001; Lana et al., 2001), gridded rain gauge data (Lloyd-Hughes and Saunders, 2002; Tsakiris and Vangelis, 2004), and NCEP/NCAR reanalysis gridded precipitation data (Bordi and Sutera, 2001). The above studies indicate that the Mediterranean region have been afflicted by severe and more or less prolonged periods of drought in the last 50 years.

Furthermore, various studies (Vasiliades and Loukas, 2006, 2009; Vasiliades et al., 2011; Vicente-Serrano and Lopez-Moreno, 2005) examined the relationship between the timescales of the SPI and PDSI indices and the types of drought. Vicente- Serrano and Lopez-Moreno analyzed the usefulness of different SPI timescales to monitor droughts in river discharges and reservoir storages. They have shown that the response of the river discharges to higher timescales than 3-months is very low and the usefulness of higher timescales to monitor river flow droughts in the mountain hydrological system is very debatable. On the other hand, the timescales of SPI useful to analyze droughts in the reservoir storages are longer than for river discharges. Vasiliades and Loukas (2006) comparing SPI and the Palmer four indices showed that SPI is better related to hydrological drought. However, different timescales of SPI were best correlated to hydrological drought for the study watersheds depending on their area, geophysical, and hydroclimatic characteristics.

Although many studies have been performed for the effectiveness of the drought indices in monitoring and analyzing the droughts, few studies on climate change impacts on droughts have employed meteorological drought indices which require less input data when compared to weather, soil and land use as the tools for assessing drought responses (Kothavala, 1999; Blenkishop and Fowler, 2007; Mavromatis, 2007; Loukas et al., 2007, 2008; Vasiliades et al., 2009).

Vicente- Serrano et al.(2010), compared time series of three drought indices for a set of observatories with different climate characteristics located in different parts of the world. They used the SPI, the sc-PDSI and the proposed Standardized Precipitation Evapotranspiration Index (SPEI) and they concluded that under global warming conditions only the sc-PDSI and SPEI identified an increase in drought severity associated with higher water demand due to evapotranspiration. Comparing the two indices, the SPEI is crucial for drought analysis and monitoring due to its multi-scalar character.

11

2. METHODOLOGY

The aim of this study is to evaluate a statistical downscaling method for monthly precipitation and temperature and the subsequent estimation of climate change impacts on droughts. The downscaling method was developed using the outputs of the Canadian Centre for Climate Modeling Analysis General Circulation Model (CGCMa3) for the base historical period (1980–2000), and used to estimate monthly precipitation and temperature time series for two future periods (2030–2050 and 2080– 2100). The droughts have been assessed using the most commonly used drought index, the Standardized Precipitation Index (SPI) and the most recent drought index the Standardized Precipitation-Evapotranspiration Index (SPEI). Both the SPI and SPEI time series were estimated at multiple timescales for the historical base period 1980–2000 for observed and downscaled monthly precipitation and water balance respectively, as well as for the two future periods 2030-2050 and 2080-2100 for assessing drought severity classes, and used for evaluating future climate change impacts on droughts.

2.1. Climate downscaling

2.1.1. Global circulation Model

Global Circulation Models (GCMs) have been used to study the effects of the increasing concentration of carbon dioxide and the other greenhouse gases on the Earth's climate. These models link atmospheric processes with ocean and land surface processes and can be used to provide projections of the changes in temperature, precipitation and other climate variables in response to changes in greenhouse gas emissions. In this study the third generation of the Canadian Centre for Climate Modelling and Analysis (CCCma) Coupled Global Climate Model (CGCM3) and for three socio-economic development scenarios was used in order to assess the climate change impacts on monthly precipitation, temperature and evapotranspiration in Acheloos watershed. The third version of the Canadian Centre for Climate Modelling and Analysis (CCCma) CGCM3 makes use of the same ocean component as that used in the earlier, the Second Generation Coupled Global Climate Model (CGCM2), but it makes use of the

12

substantially updated atmospheric component the Third Generation Atmospheric General Circulation Model (AGCM3). CGCM3.1 was run at two different resolutions. The T47 version was used in this study. It has a surface grid whose spatial resolution is roughly 3.75 degrees lat/lon and 31 levels in the vertical. The ocean grid shares the same land mask as the atmosphere, but has four ocean grid cells underlying every atmospheric grid cell. The ocean resolution in this case is roughly 1.85 degrees, with 29 levels in the vertical. The development of CGCM3 was a team effort involving G. Flato, G. Boer, D.Y. Robitaille, W.G. Lee, W. Merryfield, and O. Saenko, along with many contributions from the AGCM development team.

CCCma performed experiments with CGCM3.1 for three scenarios, SRES A1B, SRES A2, and SRES B1, as well as for the so-called "Committed" scenario in which the greenhouse gas concentrations and aerosol loadings were held fixed at the year 2000 level.
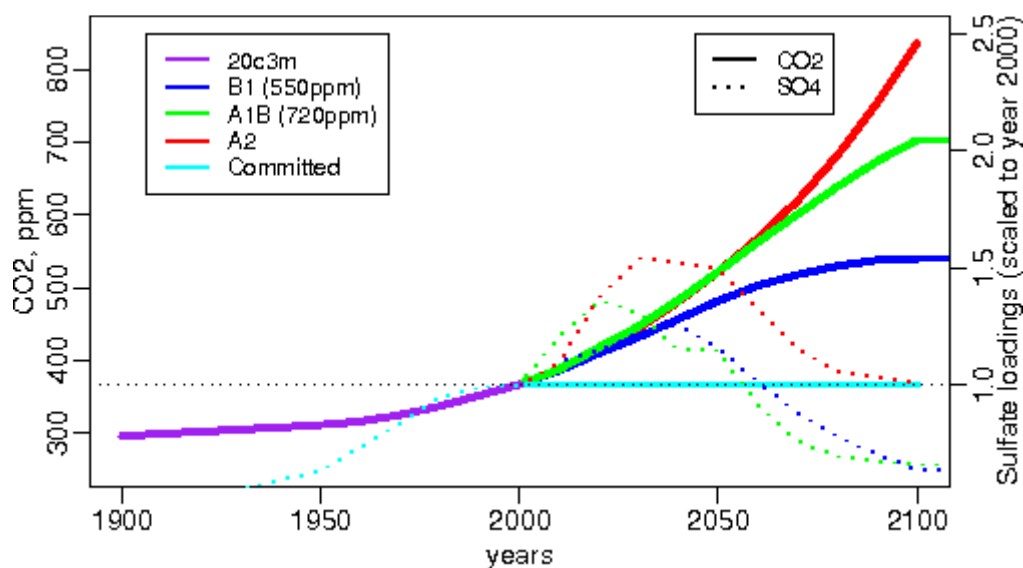
Figure 2.1. Time evolution of the CO_2 concentrations (solid line curves, the range is on the left hand y-axis) and globally averaged sulphate aerosol loadings scaled to year 2000 (dotted line curves, the range is on the right hand side y-axis) as prescribed in the IPCC 20-th century (20C3M, purple), SRES B1 (blue), SRES A1B (green) and SRES A2 (red) experiment.

The CGCM3.1 model output that used for the downscaling is:

- **20C3M:** The IPCC 20-th Century experiment with CGCM3.1/T47 for years 1850-2000.

13

–   **SRES A1B:** The IPCC SRES A1B 720 ppm stabilization experiment with CGCM3.1/T47 for years 2001-2100, initialized from the end of the 20C3M experiment.

–   **SRES B1:** The IPCC SRES B1 550 ppm stabilization experiment with CGCM3.1/T47 for years 2001-2100, initialized from the end of the 20C3M experiment.

–   **SRES A2:** The IPCC SRES A2 experiment with CGCM3.1/T47 for years 2001-2100, initialized from the end of the 20C3M experiment.

As already mentioned A1B scenario assumes a very rapid economic growth, global population that peaks in mid-century and declines thereafter, and rapid introduction of new and more efficient technologies. In this world developments of energy technologies are balanced across energy sources.

According to Intergovernmental Panel on Climate Change, SRES B2 scenario emphasizes the protection of the environment and social equity, but also relies on local solutions to economic, social, and environmental sustainability. It represents a low emission scenario.

The third scenario that used in the study is the SRES A2 scenario which describes a strong, but regionally oriented economic growth and fragmented technological change with an emphasis on human wealth and represents a high emissions scenario.

The differences between developed and developing countries according to these scenarios remain strong. Scenario runs were taken over two time periods: 2030–2050 and 2080–2100.

The commonly used approach in climate change studies is to combine the output of the GCMs with an impact model. This approach is quite realistic although there are inherent uncertainties about the details of regional climate changes. These uncertainties arise from a number of sources, such as uncertainties in GCM outputs, downscaling of GCM outputs and specification of the climate change scenarios. The limitation of the spatial resolution and the resolution of the output are the major shortcoming of the current generation of GCMs, since the

14

output of GCMs is given for a much larger scale than the scale of a watershed. Methods to overcome the spatial resolution limitation of the GCMs have been proposed in the literature. Interpolation techniques (McCabe and Wolock, 1999), statistical downscaling (Brandsma and Buishand, 1997; Wilby et al., 2002) and downscaling through coupling of GCM output and regional meteorological models (Giorgi et al., 2001) are methods that have been used to. Uncertainty increases within and between every link of the approach.

The uncertainty depends on four factors, on the quality of the GCM simulations, concerning the variables for downscaling and the uncertainty of the emission scenarios; the quality of the downscaled scenarios, due to inhomogeneities in observed data and drawbacks of the applied technique; the quality and the resolution of the impact models which are often strong simplification of reality; and finally on the errors of the input data due to instrumentation or sample data error (Vasiliades et al., 2009). Concerning the GCMs uncertainty, it can be assessed by using different GCMs or using Monte Carlo experiments with one GCM starting with different initial conditions. In order to assess the downscaling techniques uncertainty, different downscaling techniques can be used, otherwise by varying parameterizations of the downscaling models. Furthermore, uncertainties of impact models can be estimated by varying input parameters, taking into account, e.g. sampling errors. In this study, two types of uncertainty are addressed the downscaling technique and the impact model uncertainty.

2.1.2. Statistical downscaling

General Circulation Models (GCMs) have resolutions in the order of hundred kilometers while Regional Climate Models (RCMs) may be as tens of kilometers. However there is a mismatch between the grid resolution of the climate models and the resolution needed by impacts studies. Fine resolution climate change information can be obtained via downscaling.

Statistical downscaling is based on the view that the regional climate is conditioned by two factors the large scale climatic state and regional/local physiographic features as topography, land-sea distribution and land use (von Storch, 1995, 1999). Therefore, regional or local climate information is derived

by first determining a statistical model which relates large-scale climate variables (predictors) to regional variables (predictands). Local and regional climate characteristics are estimated by feeding this statistical model with the large-scale output of a GCM simulation. The advantages by using these techniques consist the inexpensive computational and thus can be applied to output from different GCM experiments, and the fact that they can be used to provide site-specific information, which can be critical for many climate change impact studies. The major drawback of statistical downscaling methods is that the basic assumption is not verifiable, i.e. that the statistical relationships developed for the present day also hold under the different forcing conditions of possible future climates- a limitation that also applies to the physical parameterizations of dynamical models (Wilby et al., 2004).

<u>Methods of statistical downscaling</u>

Statistical downscaling involves developing quantitative relationships between large-scale atmospheric variables (predictors) and local surface variables (predictands) (Varis et al., 2004; Xu et al., 2005; Fowler et al., 2007). The main statistical downscaling techniques are weather classification schemes, regression models and weather generators (Wilby et al., 2004; Giorgi et al., 2001)

- The **weather classification** methods group days into a finite number of discrete weather types or states according to their synoptic similarity.
- **Regression models** are a conceptually simple means of representing linear or nonlinear relationships between predictands and the large scale atmospheric forcing. Commonly applied methods include multiple regression (Murphy, 1999), canonical correlation analysis (CCA) (von Storch et al., 1993) and artificial neural networks which are akin to nonlinear regression (Wilby and Wigley, 1997; Crane and Hewitson, 1998).
- **Weather generators (WGs)** are models that replicate the statistical attributes of a local climate variable such as the mean and variance, but not observed sequences of events (Wilks and Wilby, 1999). These models are based on representations of precipitation occurrence via Markov

processes for wet-/ dry-day or spell transitions (**Table** Σφάλμα! Δεν υπάρχει κείμενο καθορισμένου στυλ στο έγγραφο.**.1**).

It is important to be aware of several assumptions when downscaling climate model output for current and projected climates (Hewitson and Crane, 1996; Giorgi et al., 2001)

1. Predictors relevant to the local predictand should be adequately reproduced by the host climate model at the spatial scales used to condition the downscaled responses.
2. The relationship between the predictors and predictand remain valid for periods outside the fitting period (time invariance).
3. The predictor set sufficiently incorporates the future climate change signal.
4. The predictors used for determining future local climate should not lie outside the range of the climatology used to calibrate the statistical downscaling model.

Table 2.1. A summary of the strengths and weaknesses of the main statistical downscaling methods (Wilby et al., 2004).

Method	Strengths	Weaknesses
Weather typing (e.g. analogue method, hybrid approaches, fuzzy classification, self organizing maps, Monte Carlo methods).	• Yields physically interpretable linkages to surface climate • Versatile (e.g., can be applied to surface climate, air quality, flooding, erosion, etc.) • Compositing for analysis of extreme events	• Requires additional task of weather classification • Circulation-based schemes can be insensitive to future climate forcing • May not capture intra-type variations in surface climate
Weather generators (e.g. Markov chains, stochastic models, spell length methods, storm arrival times, mixture modelling).	• Production of large ensembles for uncertainty analysis or long simulations for extremes • Spatial interpolation of model parameters using landscape • Can generate sub-daily information	• Arbitrary adjustment of parameters for future climate • Unanticipated effects to secondary variables of changing precipitation parameters
Regression methods (e.g. linear regression, neural networks, canonical correlation analysis, kriging).	• Relatively straightforward to apply • Employs full range of available predictor variables • 'Off-the-shelf' solutions and software available	• Poor representation of observed variance • May assume linearity and/or normality of data • Poor representation of extreme events

Statistical downscaling is the process of building an empirical model:

$$y = F(x) \tag{2.1}$$

17

for a small-scale feature y, not adequately described in GCMs, and large-scale features x, well resolved. As predictands, y has been used as weather variables, such as monthly temperatures and monthly precipitation amounts. The predictor x has often been chosen as characteristics of the weather circulation. If the function F is linear, Eq. (2.1) becomes

$$F(x) = \alpha x + \varepsilon \qquad (2.2)$$

with ε drawn from a normal distribution with zero mean and standard deviation σ and 0<α<1. The variations in ε are assumed to be independent from x. In this setting, the randomness in y stems from the randomness in ε. Hence, Eq. (2.1) must be understood as a stochastic equation (Von Storch, 1999).

In this study, the GCM grid point outputs were downscaled using multiple regression equations between GCM predictor output variables and areal monthly precipitation and temperature. Stepwise screening of gridpoint data was found to be the best statistical model among canonical correlation analysis, singular value decomposition, and multiple regression models on principal components (PCs) of predictor fields for downscaling daily temperature in Europe (Huth, 1999).

The predictors used in such analyses should be: a) well simulated by the GCM, b) strongly correlated with the predictand variable (precipitation and temperature), and c) available. Using these criteria, 46 predictor grid variables were used (Table 2.2). The output data from 20CM3 experiment of the CGCM3.1/T47 model for the period 1850-2000 were used.

The first step of the downscaling is the correlation analysis between the 46 independent predictors and the dependent local variables (precipitation, temperature). The predictors that will be chosen should be uncorrelated with each other and explain the more of the variance of the predicted variable. For this purpose a procedure based on forward selection stepwise regression technique and included testing with various linear and non-linear regression models was employed. All of these models rely on homogeneous long timeseries of the target parameter on the local scale and one or several atmospheric predictors on the large-scale. A major limitation is the assumption that the

relationships obtained under present conditions will also hold true under a changing climate.

The forward stepwise regression starts by choosing the independent variable which explains most of the variation in the dependent variable. Then a second variable is chosen which explains most of the residual variation and the regression coefficients are recalculated. Variables that do not significantly add to the success of the model are excluded. This procedure continues until no variables significantly explain residual variation.

The above method, which was applied in order to predict monthly precipitation for the period 1980-2000, has unveiled that the most significant predictors the precipitation are the Toa outgoing longwave flux (Rlut, w/m^2) and the Surface downward eastward stress (Tauu, Pa). Dummy variables (a set of twelve categorical variables assigned to the 12 months of the year) are used to account for the effect of the "month" on precipitation and the areal precipitation was transformed using natural logarithms (ln) to enhance the model's accuracy. The coefficient of determination R^2 was used as goodness of fit measure for the regression models (Table 2.3). The best regression downscaling model containing monthly dummy variables is expressed as:

$$P_{MLR} = \alpha_1 b_1 + \alpha_2 b_2 + \alpha_3 b_3 + _{...} a_{12} b_{12} + a_{13}(Rlut) + a_{14}(Tauu) + c \qquad (2.3)$$

where P_{MLR} is the logarithmically transformed monthly precipitation, $b_1, b_2, b_3, . . . , b_{12}$ are the monthly weighing dummy variables, $\alpha_1, \alpha_2, \alpha_3, ... , a_{12}$ are regression coefficients, and c is the regression constant. Dummy variables, $b_1 - b_{12}$, are assigned binary values, 0 or 1, depending on the month in which precipitation is referred. For example, if month is October, then, b_1, takes the value of 1 and all the other dummy variables, $b_2 - b_{12}$, take the value of 0. Similarly, if month is November, then, b_1 takes the value of 0, b_2 takes the value of 1 and all the other dummy variables, $b_3 - b_{12}$, take the value of 0 and so on. However, the monthly downscaled precipitation (P_{MLR}) values will always have smaller variance than the local values (i.e. areal observed precipitation) (Von Storch, 1999). It is obvious from Figure 2.1 that the model simulates quite well the average observed areal precipitation but not with the highest accuracy.

Table 2.2. Predictor variables for statistical downscaling of precipitation and temperature.

A/A	Variable	Measurement unit	Initials
1	Air pressure at sea level	Pa	Psl
2	Precipitation flux	kg/m²s	Pr
3	Near-surface daily-mean air temperature	K	Tas
4	Moisture content of soil layer	kg/m²s	Mrsos
5	Soil moisture content	kg/m²s	Mrso
6	Surface downward eastward stress	Pa	Tauu
7	Surface downward northward stress	Pa	Tauv
8	Surface snow thickness	m	Snd
9	Surface upward latent heat flux	w/m²	Hfls
10	Surface upward sensible heat flux	w/m²	Hfss
11	Surface downwelling longwave flux in air	w/m²	Rlds
12	Surface upwelling longwave flux in air	w/m²	Rlus
13	Surface downwelling shortwave flux in air	w/m²	Rsds
14	Surface upwelling shortwave flux in air	w/m²	Rsus
15	Surface temperature	K	Ts
16	Surface air pressure	Pa	Ps
17	Snowfall flux	kg/m²s	Prsn
18	Convective precipitation flux	kg/m²s	Prc
19	Atmosphere water vapor content	kg/m²	Prw
20	Soil frozen water content	kg/m²	Mrfso
21	Surface runoff flux	kg/m²s	Mrros
22	Runoff flux	kg/m²s	Mrro
23	Surface snow amount where land	kg/m²s	Snw
24	Surface snow area fraction where land	(%)	Snc
25	Surface snow melt flux where land	kg/m²s	Snm
26	Near-surface eastward wind	m/s	Uas
27	Near-surface northward wind	m/s	Vas
28	Toa incoming shortwave flux	w/m²	Rsdt
29	Toa outgoing shortwave flux	w/m²	Rsut
30	Toa outgoing longwave flux	w/m²	Rlut
31	Net downward radiative flux at top of atmosphere	w/m²	Rtmt
32	Surface downwelling shortwave flux in assuming clear sky	w/m²	Rsdscs
33	Surface upwelling shortwave flux in assuming clear sky	w/m²	Rsuscs
34	Surface downwelling longwave flux in assuming clear sky	w/m²	Rldscs
35	Toa outgoing longwave flux assuming clear sky	w/m²	Rlutcs
36	Toa outgoing shortwave flux assuming clear sky	w/m²	Rsutcs
37	Atmosphere cloud condensed water content	kg/m²	Cllwvi
38	Atmosphere cloud ice content	kg/m²	clivi
39	Sea ice thickness	m	Sit
40	Sea ice outward velocity	m/s	Usi
41	Sea ice northward velocity	m/s	Vsi
42	Air temperature (10m-1000m)	K	Ta
43	Eastward wind (10m-1000m)	m/s	Ua
44	Northward wind (10m-1000m)	m/s	Va
45	Lagrangian tendency of air pressure (10m-1000m)	Pa/s	Wap
46	Geopotential height (10m-1000m)	m	Zq

Table 2.3. Modification of coefficient of determination of the under study regression downscaling models for predicting precipitation

Watershed	R^2	R^2 with Dummies
Acheloos	0.4492	0.5496
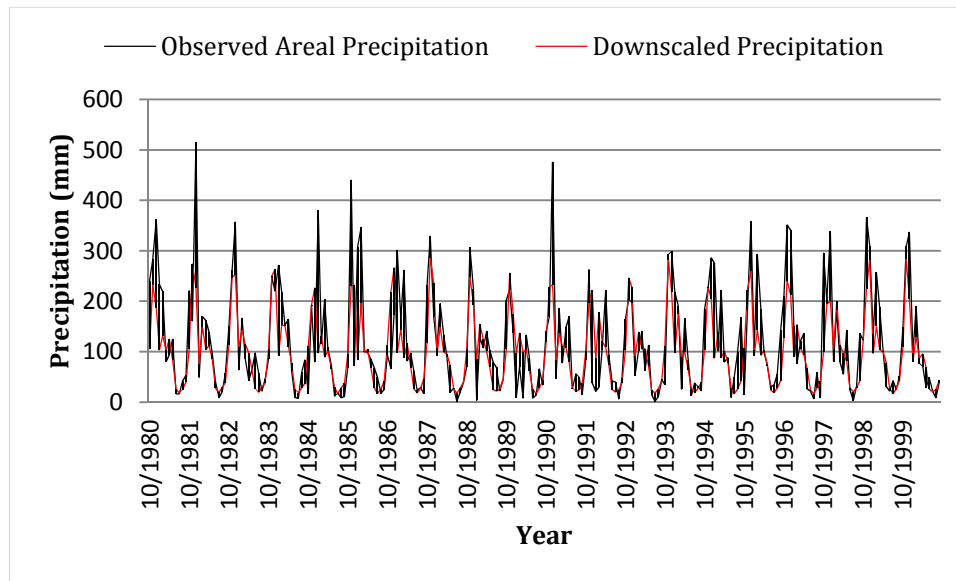
Figure 2.2. Comparison of observed average monthly areal precipitation and average monthly downscaled precipitation in Acheloos watershed.

The same method was used in order to estimate monthly temperature of the Acheloos watershed for the same 20-years period (1980-2000). The regression analysis for the temperature is less complicated than the precipitation one, since extreme events emerge rarely comparing to extreme events of precipitation and with minimum standard deviation.

Forward stepwise regression was applied in monthly temperature and the predictors that explained the most variation of the observed temperature were the Surface Downwelling shortwave flux in air (Rsds, w/m^{2}) and the Geopotential height at 50hPa (Zg_50, m). Dummy variables were used to account for the effect of the "month" on temperature as in the case of precipitation. The regression downscaling model containing monthly dummy variables is expressed as:

$$T_{MLR} = \alpha_1 b_1 + \alpha_2 b_2 + \alpha_3 b_3 + \ldots a_{12} b_{12} + a_{13}(Rsds) + a_{14}(Zg\_50) + c \qquad (2.4)$$

where T_{MLR} is the monthly temperature, $b_1, b_2, b_3, \ldots, b_{12}$ are the monthly weighing dummy variables, $\alpha_1, \alpha_2, \alpha_3, \ldots, a_{12}$ are regression coefficients, and c is the regression constant.

Table 2.4 indicates the modification of the coefficient of determination of the downscaled models with and without the dummy variables. Furthermore, Figure

21

2.2 shows that the model that was used simulates the average monthly temperate very well. However, the extreme values of the observed temperature are not simulated adequately.

Table 2.4. Modification of coefficient of determination of the under study regression downscaling models for predicting temperature.

Watershed	R^2	R^2 with Dummies
Acheloos	0.9413	0.9644
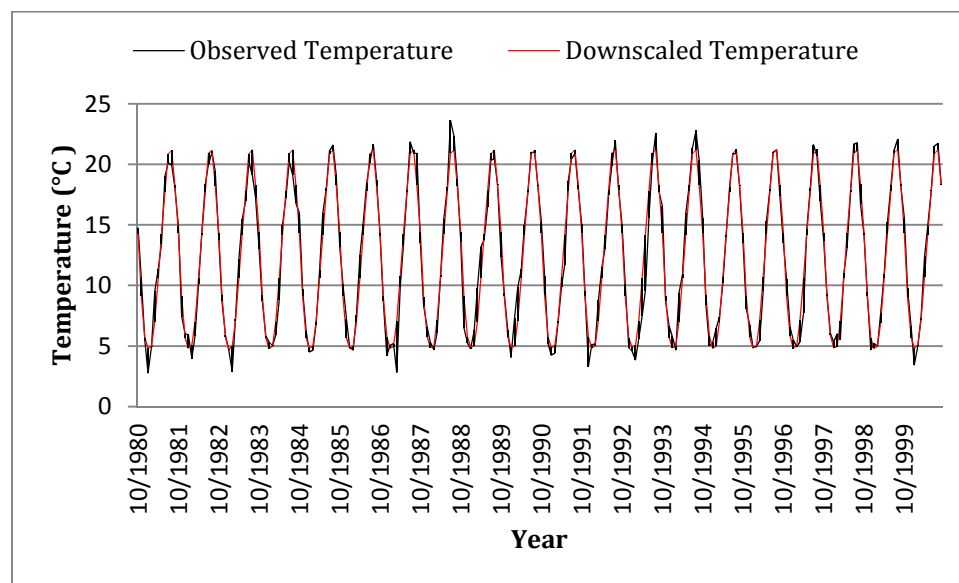
Figure 2.3. Comparison of observed average monthly temperature and average monthly downscaled temperature in Acheloos watershed.

In many climate impact studies the variance of the downscaled time series should be the same with the variance of the observed values. To meet this requirement various methods have been proposed such as variance inflation (Karl et al., 1990; Huth, 1999), expanded downscaling (Burger, 1996), and randomization (Dehn and Buma, 1999). In this study, to preserve the variability of the observed series, the estimated precipitation, as well as temperature, was combined with the residual values of the regression. These can be viewed as a noise component, statistically independent of the large-scale climate. In the formula:

$$P = P_{MLR} + P_{residual} \qquad (2.5)$$

22

with P is the observed monthly precipitation, P_{MLR} is monthly precipitation explained by multiple linear regression and $P_{residual}$ is the residuals of MLR. If this operation is carried out on the estimated series of the regression fitting period (October 1980–September 2000), the result is the observed series Concerning the temperature the following equation was used:

$$T = T_{MLR} + T_{residual} \qquad (2.6)$$

where T is the observed monthly temperature, T_{MLR} the monthly temperature explained by the multiple linear regression and $T_{residual}$ the residuals of the MLR.

For the climate scenarios, P_{MLR} is obtained by downscaling the GCM outputs while $P_{residual}$ remains unchanged. In this way, the problem of limited correlation between predictor and predictand variables may be tackled. However, in order to estimate the uncertainty of the downscaling method stochastic time series modelling was applied for the treatment of the residuals.

2.1.3. Stochastic simulation of the residuals of the downscaled precipitation and temperature

Stochastic models are used for generating long synthetic time series of climate data which are random numbers and are modified to preserve the statistical properties (in terms of mean, variance, skew, long-term persistency, etc.) of the observed series which they are based. Each stochastic replicate (sequence) is different and has different characteristics compared to the historical data, but the average of each characteristic from all stochastic replicates is the same as the historical data (Box et al., 2008). Stochastic climate data can be used as inputs to complex hydrological and ecological models for the quantification of uncertainty in environmental systems as a result of climatic variability (Salas, 1993).

Using historical climate data as inputs into hydrological models provides results that are based on only one realization of the past climate. However, using stochastic climate data provide alternative realizations that are equally likely to occur. Stochastic climate data are traditionally used in storage yield analysis to estimate reservoir size for a given demand and reliability, or to estimate system reliability (number and levels of water restrictions) for a given storage size and demand characteristics.

In the past, data generation models assumed that there was no variation in the model parameters between years and only the seasonal or monthly variations within a year were taken into account. However, there is a growing awareness of long term persistence in the climatic data in the form of wet and dry years or ENSO cycles, so the parameters of the models should be varied in some way to model the wet and dry spells. There has been very little research on this aspect (Srikanthan and McMahon, 2001).

The generation of rainfall and other climate data needs a range of models depending on the time and spatial scales involved. Cox and Isham (1994) presented three broad types of rainfall models, namely, empirical statistical models, models of dynamic meteorology and intermediate stochastic models, a classification based on the amount of physical realism incorporated into the model structure.

In empirical statistical models, empirical stochastic models are fitted to the data available. The models for the generation of annual, monthly and daily rainfall and climate data are of this type. In the models of dynamic meteorology, large systems of simultaneous nonlinear partial differential equations representing, fairly realistically, the physical processes involved, are solved numerically. These are generally used for weather forecasting rather than for data generation. In intermediate stochastic models, few parameters are used to represent the rainfall process, the parameters being intended to relate to underlying physical phenomena such as rain cells, rain bands and cell clusters. These types of models are used for the analysis of data collected at short time intervals such as hourly. The model used in this study is of the first type, namely, empirical statistical models and was applied in order to simulate and generate synthetic monthly time series of precipitation and temperature residuals, resulted from statistical downscaling for the Acheloos watershed for the base period (1980-2000). A special characteristic that must be preserved in stochastic modeling of climate data is the cross-correlation between variables. Hence, for the assessment of the uncertainty of the residuals time series, the potential evapotranspiration, which was calculated with the Thornthwaite method, was also added as input in the model for the stochastic simulation of the current climate.

24

i.   Generation of annual climate data

The generation of climate data is based on the following three methodologies:

- AR(1) Model without parameter uncertainty. Srikanthan and McMahon (1985) recommended a first order Markov model incorporating the Wilson-Hilferty transformation to generate annual rainfall data. This model degenerates into a white noise model when the coefficient of skewness and the lag one auto-correlation coefficient are close to zero.

- AR(1) Model with parameter uncertainty. It is based on the previous methodology but it uses the Box-Cox transformation.

- Hidden State Markov (HSM) model. Thyer and Kuczera (2000) developed a Hidden State Markov (HSM) model with Bayesian inference to generate annual rainfall data. The model assumes that the climate is composed of two states, either a dry state (low rainfall year) or a wet state (high rainfall year). Each state has separate Normal annual rainfall distributions. The transition from one state to the other is governed by the transition probabilities. If the transition probabilities to other states are sufficiently low then the climate may persist in one state for a number of years. This provides an explicit mechanism for the HSM model to simulate the influence of a quasi-periodic phenomenon such as El Nino.

In the current study the AR(1) model without parameter uncertainty was applied for the generation of annual climate data. In a previous study, the method applied in meteorological stations in Thessaly and indicated that it is a reliable method for generation of stochastic annual precipitation and temperature data for Mediterranean and continental climate. Moreover, this method is satisfactory for the simulation of wet and dry years and the preservation of the long term persistence (Vasiliades, 2010).

The AR(1) Model is a first order autoregressive model and it is used to generate annual climate data. The AR(1) model simulates the annual precipitation or temperature which depends only on the previous time step and a random Gaussian component is added. The annual residuals of rainfall and temperature data have small variance, meaning that the variables simulate the normal

distribution. Hence, a first order autoregressive [AR(1)] or a random model is adequate for most cases. The AR(1) model is of the form:

$$X_t = r_1(X_{t-1}) + (1 - r_1^2) - \eta_t \qquad (2.7)$$

where X_t are the standardised rainfall residuals in time step t, η_t normally distributed random component with zero mean and unit variance and r is lag one autocorrelation coefficient.

The residuals of annual precipitation is obtained from

$$x_t = \overline{X} + sX_t \qquad (2.8)$$

where x_t the rainfall residuals at time t, $\overline{X}$ the mean annual rainfall residuals and s the standard deviation of the annual rainfall residuals. If the annual data are skewed, the skewness in the data can be modelled through the Wilson-Hilferty transformation:

$$\varepsilon_t = \frac{2}{g_\varepsilon}\left[\left(1 + \frac{g_\varepsilon \eta_t}{6} - \frac{g_\varepsilon^2}{36}\right)^3 - 1\right] \qquad (2.9)$$

where g_ε is the skewness of ε_t which is related to the skewness of annual data through:

$$g_e = \frac{(1 - r^3)}{(1 - r^2)^{3/2}} g \qquad (2.10)$$

Because the variability (Cv), skewness (Cs), and lag one autocorrelation (r_1) of annual climate data are low (Cv < 0.5, Cs <1 and r_1 < 0.5) a first order autoregressive model with Wilson-Hilferty transformation (Wilson and Hilferty, 1931) is adequate for the generation of annual climate data. Since the climate data are cross correlated a first order autoregressive multivariate model needs to be used to generate annual climate data to preserve the cross and autocorrelations.

A multivariate model to generate annual climate data is of the form:

26

$$X_t = AX_{t-1} + B\varepsilon_t \tag{2.11}$$

X_t is a (3x1) matrix of standardized climate data for year t, A and B (3x3) coefficient matrices to preserve the correlations, and ε_t random component with zero mean and unit variance. The matrices A and B are determined from the following (Matalas, 1967).

$$A = M_1 M_0^{-1} \tag{2.12}$$

$$BB^T = M_0 - M_1 M_0^{-1} M_1^T \tag{2.13}$$

where M_0 and M_1 are the lag zero and lag one cross correlation matrices respectively. The elements of M_0 and M_1 corresponding to variables i and j are given by:

$$m_0^{ij} = \frac{1}{n}\sum_{t=1}^{n} X_i X_j \tag{2.14}$$

$$m_1^{ij} = \frac{1}{n-1}\sum_{t=1}^{n-1} X_i X_{j-1} \tag{2.15}$$

The matrix A can be obtained from Equation 2.12. The matrix BB^T is symmetric and should be positive semi-definite for solving for B. The matrix B can be obtained by the Cholesky decomposition where the matrix B is assumed to be lower triangular. The elements b_{ij} of B are obtained from the recursive relationships:

$$b_{ij} = 0, \qquad\qquad j > i \tag{2.16}$$

$$b_{11} = \sqrt{c_{11}} \tag{2.17}$$

where c_{ij} is the element of matrix $B = BB^T$. The remaining elements in the first column of B are given by:

$$b_{1j} = c_{1j}/b_{11} \tag{2.18}$$

For $j > 1$, the jth diagonal element is obtained from

27

$$b_{jj} = c_{jj} - \sum_{k=1}^{j-1} b_{jk}^2 \,, \qquad j = 2, 3 \qquad\qquad (2.19)$$

The solution is complete when $j = 3$. Otherwise, the other elements of column j of B are computed from:

$$b_{jj} = \frac{c_{jj} - \sum_{k=1}^{j-1} b_{ik} b_{jk}}{b_{jj}} \, j = 2 \qquad\qquad (2.20)$$

Once matrices A and B are determined, standardized normally distributed values are generated using Equation 2.11. The skewness is then input to the generated values by the Wilson-Hilferty transformation, rescaled by the standard deviation and the mean added to obtain the generated annual climate data. In order to evaluate generated annual climate data the following parameters were estimated from 100 replicates each of length equal to the historical record (20 years): Mean ($\bar{x}$), standard deviation (s), coefficient of skewness (g), lag one autocorrelation coefficient (r_1), maximum, minimum, and cross correlation between the climate variables. One hundred replicates, each of length equal to the length of historical data were generated. The above parameters were estimated from each replicate and from these values the 0, 25, 50, 75, 100 percentile values and the mean were calculated.

ii. Generation of monthly climate data

Monthly rainfall and temperature data are used in the simulation of water resources systems, and in the estimation of water yield from large catchments. In order to assess the system response to climatic variability, long replicates of stochastically generated monthly data are used. However the monthly rainfall data are not suitable for most regions, where there is large number of months of no rainfall. In earlier studies (Srikanthan and McMahon, 1985; Hipel and McLeod, 1994) recommended the method of fragments to disaggregate the annual rainfall data generated by a first order autoregressive model. The main drawbacks of this approach are the inability to preserve the monthly correlation between the first month of a year and the last month of the previous year and the occurrence of similar patterns from a short length of historic data (Salas, 1993). Maheepala

and Perera (1996) proposed a modification to the selection of fragments that preserves the year-end monthly correlation to improve on the first drawback and Porter and Pink (1991) used synthetic fragments from a Thomas-Fiering monthly model to overcome the second drawback. For sites with considerable number of zero rainfall months, there will be problems with the application of the Thomas-Fiering monthly model to generate the synthetic fragments. Moreover the extended model developed by Mejia and Rousselle (1976) can be used to disaggregate the generated annual rainfalls to monthly rainfalls. Here again, the condensed form of the model developed by Lane (1979) can be used at the expense of not preserving some of the cross correlations.

In the current study the Modified method of synthetic fragments proposed by Maheepala and Perera (1996) was applied for generate synthetic monthly climate data. The method applied in meteorological stations in Thessaly and indicated that is a reliable method for the generation of stochastic monthly precipitation and temperature data for Mediterranean and continental climate (Vasiliades, 2010).

The annual climate data were generated by a first order autoregressive multivariate model (AR(1)) and the monthly climate data by the modified method of fragments. The observed monthly climate data are standardized year by year so that the sum of the monthly climate data in any year equals to unity. This is carried out by dividing the monthly climate data in a year by the corresponding annual climate data. In the case of temperature, the mean annual temperature was first multiplied by 12. By doing so, from a record of n years, one will have n sets of fragments of monthly climate data. The generated annual climate data are disaggregated by selecting a fragment whose annual climate data are closer to the generated annual climate data by using the following indices

$$\alpha_i = \sum_{j=1}^{3} \left(\frac{x_k^j - x_i^j}{s_x^j} \right)^2 \tag{2.21}$$

29

$$\beta_i = \sum_{j=1}^{3} \left(\frac{y_{k-1}^j - y_{i-1}^j}{s_y^j} \right)^2 \tag{2.22}$$

where x_k^j is generated annual climate data for variable j and year k, x_i^j the observed annual climate data for variable j and year i, s_x^j standard deviation of the observed annual climate data for variable j, y_{k-1}^j the disaggregated monthly climate data for variable j for the last month of year k-1, y_{i-1}^j the disaggregated monthly climate data for variable j for the last month of year i-1 and s_y^j the standard deviation of the observed monthly climate data for variable j for the last month of the year.

A set of fragments are selected for which the sum ($\alpha_i + \beta_i$) is minimum and multiplying the generated annual climate data by each set of the 12 fragments to give generated monthly climate data.

For the evaluation of the generated monthly climate data, apart from the annual parameters, monthly parameters were also estimated such as the mean, standard deviation, coefficient of skewness, correlation coefficient between successive months, maximum, minimum and cross correlation between the monthly climate variables.

Finally the downscaled time series of precipitation and temperature were added to the stochastic replicates of the rainfall and temperature residuals so as to reproduce 100 synthetic time series of the historical precipitation and temperature. The previous statistical monthly and annual parameters were calculated for each of the 100 synthetic time series of precipitation and temperature and from these values the 0, 25, 50, 75, 100 percentile values and the mean were calculated. Synthetic time series were reproduced as well as for the potential evapotranspiration, which were calculated from the synthetic time series of temperature with the method of Thornthwaite.

Concerning the future period, the developed MLR equation (Eq.2.3 and Eq.2.4) were used to downscale monthly GCM precipitation and temperature time series P_{MLR} and T_{MLR} for the future periods 2030–2050, and 2080-2100, and then the

precipitation residuals ($P_{residual}$) as well as the temperature residuals ($T_{residual}$) were added to P_{MLR} using Eq. (2.5) and T_{MLR} using Eq. (2.6) respectively, assuming that the precipitation and temperature residual time series in the future have the same statistical characteristics of the historical period. Essentially, the precipitation and temperature residual time series for the future periods were the time series generated by Eq. (2.11) for the historical base period.

2.2. Drought Indices

Many indices have been used for the identification of more than one type of drought (Tate and Gustard, 2000; Keyantash and Dracup, 2002) and their categorization may not be appropriate, although it is widely used (Wilhite and Glantz, 1985; AMS, 2004). In this study two drought indices were used in order to identify the impacts of climate change on droughts. The first is the Standardized Precipitation Index proposed by McKee and his associates (1993) and the second is the Standardized Precipitation-Evapotranspiration Index recently proposed by Vicente-Serrano et al. (2010). Both indices were calculated for multiple time scales for the historical period as well as for the future periods of 2030-2050 and 2080-2100. The justification for using two different drought indices is the fact that the SPI only accounts for precipitation effects, whereas the SPEI accounts for inputs (precipitation) and outputs (evapotranspiration) to the system. Precipitation is the main variable explaining the frequency, duration and severity of droughts (Chang and Cleopa, 1991; Heim, 2002). However, recent studies have shown that the effect of temperature (or evapotranspiration) is significant (Hu and Willson, 2000), particularly under global warming scenarios (Dubrovsky et al., 2008). Abramopoulos et al. (1988) showed that evaporation and transpiration can consume up to 80% of rainfall, and found that the efficiency of drying due to temperature anomalies is as high as that due to rainfall shortage. Moreover, Syed et al. (2008) showed that precipitation dominates terrestrial water storage variation in the tropics, but evapotranspiration explains the variability at middle latitudes. In addition,

studies have shown that anomalous high temperatures related to warming processes have in recent years exacerbated the impact of climatic droughts on water resources (Nicholls, 2004; Cai and Cowan, 2008).

2.2.1. Standardized Precipitation Index

The Standardized Precipitation Index (SPI) has been developed by McKee and his associates (1993) and used to define and monitor droughts. Among others, the US Colorado Climate Center, the US Western Regional Climate Center, and the US National Drought Mitigation Center use the SPI to monitor drought in the United States. SPI can be calculated for multiple time-scales. This is very important because the timescale over which precipitation deficits accumulate functionally separates different types of drought (McKee et al., 1995) and, therefore, allows to quantify the natural lags between precipitation and other water usable sources such as river discharge, soil moisture and reservoir storage. Recent studies have used SPI as indicator of hydrological and water resources variables, like soil moisture, surface runoff and reservoir storage (Loukas and Vasiliades, 2005; Vicente-Serrano and Lopez- Moreno, 2005).

The SPI is calculated by adjusting the precipitation series to a given probability distribution. Initially, the Gamma distribution was used to calculate the SPI (McKee et al., 1993). Computation of the SPI involves fitting a Gamma probability density function to a given frequency distribution of precipitation totals for a station, area or a watershed. The alpha and beta parameters of the Gamma probability density function are estimated for each station, for each timescale of interest (1, 3, 6, 9, 12 months, etc.), and for each month of the year. The Gamma distribution is defined by its probability density function:

$$g(x) = \frac{1}{\beta^{\alpha}\Gamma(\alpha)} x^{\alpha-1} e^{-x/\beta} \text{ for } x>0 \tag{2.23}$$

where $\alpha, \beta >0$ are the shape and scale parameters respectively, $x >0$ is the precipitation amount and $\Gamma(\alpha)$ is the gamma function. The unbiased Probability Weighted Moments are used to estimate α and β.

The Gamma distribution is not defined for x=0 and a precipitation distribution may contain zeros. In this study a "naïve" method has been applied. According to this method the null precipitation is substituted with a small amount of precipitation, for example 0.1 mm. This substitution does not affect the distribution of precipitation and circumvent the problem. The error introduced by this method depends on the number of months with null precipitation and it is usually evident for the 1-month precipitation.

The estimated parameters are then used to find the cumulative probability, *H(x)*, of an observed precipitation event for the given month and timescale for the station in question. The cumulative probability, *H(x)*, is then transformed to the standard normal random variable z with mean equal to zero and variance of one, which is the value of the SPI. Once standardized the strength of the anomaly is classified as set out in Table 2.5. This table also contains the corresponding probabilities of occurrence of each severity arising naturally from the Normal probability density function. Thus, at a given location for an individual month, moderate dry periods (SPI ≤ -1) have an occurrence probability of 15.9%, whereas extreme dry periods (SPI ≤ -2) have an event probability of 2.3%. Extreme values in the SPI will, by definition, occur with the same frequency at all locations. Negative SPI values indicate droughts and positive SPI values denote wet weather conditions (Table 2.5).

Table 2.5 . Drought classification by SPI values and corresponding event probabilities.

SPI value	Category	Probability (%)
2.00 or more	Extremely wet	2.3
1.50 to 1.99	Severely wet	4.4
1.00 to 1.49	Moderately wet	9.2
-0.99 to 0.99	Near normal	68.2
-1.49 to -1.00	Moderately dry	9.2
-1.99 to -1.50	Severely dry	4.4
-2 or less	Extremely dry	2.3

In this study the observed and areal averaged monthly precipitation were used for the estimation of the monthly SPI for the watershed of Acheloos for 1-, 3-, 6-, 9-, 12-, 24- month time scales for the historical period (1980-2000). Thereafter, the downscaled time series for the two future periods of 2030-2050 and 2080-2100 were used in order to calculate the future climate time series of SPI for the same time scales and compared to the respective historical SPI time series. The parameters of the gamma distribution, α and β, are assumed unchanged in the future. Hence, their respective values for the historical period have been used. Several studies that assessing climate change impacts on drought indices have adopted the same technique (Loukas et al., 2007; Dubrovsky et al., 2008; Loukas et al., 2008; Vasiliades et al., 2009).

The SPI time series were analyzed in order to identify the frequency of each category of droughts events (moderate, severe and extreme) in the historical and future periods, for all time scales. The percentile values 0, 25, 50, 75, 100 and the mean of the 100 SPI time series for all time scales and for all periods were calculated. Using the threshold level method, the average deficit, maximum severity and maximum duration were identified.

2.2.2. Standardized Precipitation-Evapotranspiration Index

Recently Vicente-Serrano et al. (2010) proposed a new multi-scalar drought index. The Standardized Precipitation Evapotranspiration Index (SPEI). It is based on precipitation and temperature data, and has the advantage of combining a multi-scalar character with the capacity to include the effects of temperature variability on drought assessment. The calculation procedure of SPEI is based on this of the original SPI. The SPI is calculated using monthly (or weekly) precipitation as the input data. The SPEI uses the monthly (or weekly) difference between precipitation and Potential Evapotranspiration (PET). This represents a simple climatic water balance (Thornthwaite, 1948) which is calculated at different time scales to obtain the SPEI. The first step, calculation of the PET, is difficult because of the involvement of numerous parameters including surface temperature, air humidity, soil incoming radiation, water vapor pressure and ground-atmosphere latent and sensible heat fluxes (Allen et al.,

1998). Different methods have been proposed to indirectly estimate the PET from meteorological parameters measured at weather stations. According to data availability, such methods include physically based methods (e.g. the Penman‑Monteith method; PM) and models based on empirical relationships, where PET is calculated with fewer data requirements. Although some methods in general provide better results than others for PET quantification (Droogers and Allen, 2002), the purpose of including PET in the drought index calculation is to obtain a relative temporal estimation, and therefore the method used to calculate the PET is not critical. Mavromatis (2007) recently showed that the use of simple or complex methods to calculate the PET provide similar results when a drought index such as the PDSI is calculated. Therefore, the simplest approach to calculate PET (Thornthwaite, 1948) was followed, which has the advantage of only requiring data on monthly mean temperature. With a value of PET, the difference between the precipitation (P) and PET for the month i is calculated according to:

$$D_i = P_i - PET_i \tag{2.24}$$

which provides a simple measure of the water surplus or deficit for the analyzed month. The calculated D_i values are aggregated at different time scales, following the same procedure as that for the SPI:

$$D_n^k = \sum_{i=0}^{k-1} P_{n-i} - PET_{n-i} \tag{2.25}$$

Where k (months) is the timescale of the aggregation and n is the calculation month. In quantifying the SPEI, a three parameter distribution is needed to used, since in two parameter distributions the variable x (precipitation) has a lower boundary of zero ($0 > x < \infty$), whereas in three parameter distributions x can take values in the range ($\gamma > x < \infty$, where γ is the parameter of origin of the distribution), consequently, x can have negative values, which are common in D series. To model D_i values at different time scales the probability density function of a three parameter Log-logistic distribution are used:

$$f(x) = \frac{\beta}{\alpha} \left(\frac{x-\gamma}{\alpha}\right)^{\beta-1} \left(1 + \left(\frac{x-\gamma}{\alpha}\right)^{\beta}\right)^{-2} \tag{2.26}$$

where α, β and γ are scale, shape and origin parameters, respectively, for D values in the range ($\gamma > D < \infty$). Parameters of the Log-logistic distribution can be obtained following different procedures. Among them, the unbiased Probability

35

Weighted Moments can be used and therefore the parameters of the Pearson III distribution can be obtained following Singh et al. (1993):

$$\beta = \frac{2w_1 - w_0}{6w_1 - w_0 - 6w_2} \tag{2.27}$$

$$\alpha = \frac{(w_0 - 2w_1)\beta}{\Gamma(1 + 1/\beta)\Gamma(1 - 1/\beta)} \tag{2.28}$$

$$\gamma = w_0 - \alpha\Gamma(1 + 1/\beta)\Gamma(1 - 1/\beta) \tag{2.29}$$

where $\Gamma(\beta)$ is the gamma function of β. The Probability Weighted Moments of order *s* are calculated as:

$$w_s = \frac{1}{N}\sum_{i=1}^{N}(1 - F_i)^s D_i \tag{2.30}$$

where D_i is the time series of precipitation and F_i is a frequency estimator calculated following the approach of Hosking (1990):

$$F_i = \frac{i - 0.35}{N} \tag{2.31}$$

where *i* is the range of observations arranged in increasing order, and *N* is the number of data points.

The Log-logistic distribution adopted for standardizing the *D* series for all time scales is given by:

$$F(x) = \left[1 + \left(\frac{\alpha}{x - \gamma}\right)^\beta\right]^{-1} \tag{2.32}$$

F(x) value is then transformed to a normal variable by means of the following approximation (Abramowitz and Stegun, 1965):

$$SPEI = W - \frac{C_0 + C_1 W + C_2 W^2}{1 + d_1 + d_2 W^2 + d_3 W^3} \tag{2.33}$$

where $C_0, C_1, C_2, d_1, d_2, d_3$ are similar constants as for SPI and W is probability-weighted moments:

$$W = \sqrt{-2\ln(P)} \qquad \text{for } P \leq 0.5 \tag{2.34}$$

where *P* is the probability of exceeding a determined *D* value, P =1-F(x). If P > 0.5, *P* is replaced by *1−P* and the sign of the resultant SPEI is reversed. The

36

constants are: C_0, = 2.515517, C_1, = 0.802853, C_2, = 0.010328, d_1, = 1.432788, d_2, = 0.189269, d_3 = 0.001308. The average value of SPEI is 0, and the standard deviation is 1. The SPEI is a standardized variable, and it can therefore be compared with other SPEI values over time and space. An SPEI of 0 indicates a value corresponding to 50% of the cumulative probability of D, according to a Log-logistic distribution.

The SPEI time series, as the SPI series, were calculated for the observed and stochastic time series for the historical period for multiple time scales (1-, 3-, 6-, 9-, 12-, 24- month). Furthermore SPEI time series were calculated for the future periods of 2030-2050 and 2080-2100 for the same time scales. The parameters of the log-logistic distribution are assumed unchanged in the future, as was applied for the estimation of the future time series of SPI. For the estimation of the SPEI the time series of PET, which were calculated with the method of Thornthwaite from the observed and synthetic time series of temperature, were used for the historical and future period.

The SPEI time series were investigated firstly, in order to identify the frequency of each category of droughts events (moderate, severe and extreme) in the historical and future periods, for all time scales. The percentile values 0, 25, 50, 75, 100 and the mean of the 100 SPEI time series for all time scales and for all periods were calculated. Furthermore the average deficit, maximum severity and maximum duration were identified using the threshold level method.

2.2.3. The threshold level method

The most frequently applied quantitative definition of a drought is based on defining a threshold, Q_0, below which the river flow is considered as a drought (also referred to as a low flow spell in the literature). There are two main methods to select and characterize deficits, namely the threshold level method and the sequent peak algorithm. The threshold level method was initially named method of crossing theory (Tallaksen, 2000). It is also referred to as run sum analysis because it generally study runs below or above a given threshold. The method is relevant for storage/yield analysis and is associated with hydrological design and operation of reservoir storage systems. Important areas of

application are hydropower and water management, water supply systems and irrigation schemes.

The threshold level Q_0 is also referred to as the truncation level and is used to define whether the flow in a river is in deficit. The deficit starts when the flow goes below the threshold and ends as soon as the flow returns above the threshold. Thus, the beginning and the end of a deficit can be defined. In addition the following deficit characteristics can be defined:

– The duration, which is the period of time where the flow is below the threshold level and is also referred to as drought duration, low-flow spell or run length (d_i);

– The volume or cumulative severity, which is also referred to as drought volume or run sum (v_i);

– The intensity, which is also referred to as deficit or drought severity/ magnitude, (m_i) is the ratio between deficit volume and deficit duration;

– The minimum value of each deficit event (Q_{min});

– The end of occurrence, for example, the starting date, the mean of the onset and termination, or the date of minimum value.
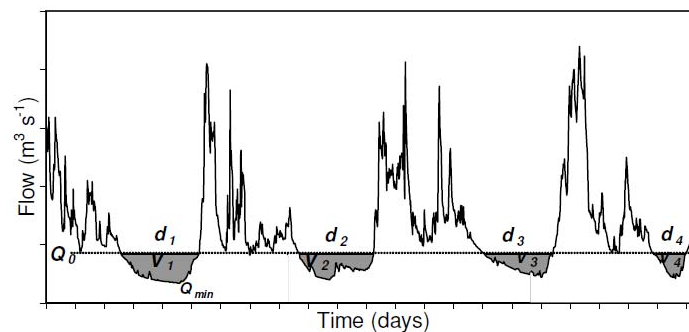
Figure 2.4. Definition of low flow and drought characteristics (modified from Tallaksen, 2000).

Based on the time series of the deficit characteristics, it is possible to determine indices, such as the average deficit duration or average deficit volume. The threshold might be chosen in a number of ways and the choice is amongst other a function of the type of water deficit to be studied (Dracup et al., 1980). The choice is influenced by the purpose and region of the study and the data availability.

In Acheloos watershed the method of threshold was applied in order to identify the average deficit, maximum severity and maximum duration for the observed time series of SPI and SPEI as well as for each replicate that were produced from the synthetic time series of precipitation and water balance, for 6-, 12- and 24-month time scale for the base period (1980-2000). Moreover, the above characteristics were identified for the future period of 2080-2100 for the two scenarios of B1 and A2 for the same time scales. The threshold level was chosen to have the value of -1, since SPI and SPEI values bellow -1 (Table 2.5) identify drought event.

3. STUDY AREA

3.1. Description

The study area is focusing on Acheloos watershed in western Greece (fig.3.1), near Ionian coastal zone and west of Pindos Mountain. Acheloos River is the second longest river in Greece, with total length of 220 km, and first in water contribution. It constitutes the main source of water both for the flat and the semi mountainous regions of Aitoloakarnania. The river basin is about 2986 km² and extends from 21.08°E, 38.29°N to 21.92°E, 39.73°N. The maximum altitude of the area is 2420 m.

Acheloos springs from Lakmos Mountain in the central Pindos Range. The river initially flows in the western part of prefecture of Trikala, then flows southward at the boundaries of prefectures of Trikala and Arta, and then at the boundaries of Karditsa and Arta. It continues through the limits of prefectures of Evritania and Aitoloakarnania. In this part Acheloos is linked with the rivers Agrafiotis, Tavropos and Trikeriotis and continues its southward flow. In the area of Agrinio it turns westward towards the Aitoliki basin. Then flows again southward, it is enriched with surplus water from the lakes Lysimachia and Trixonida and finally goes westward in the area of Neochori and flows into Ionian Sea shaping an extensive deltaic field. In its wider basin of flow, four natural lakes exist (Trichonida, Lisimachia Amvrakia, Ozeros), and four dams and reservoirs (Kremaston, Kastrakiou, Stratos I & Stratos II) have been constructed and several hydroelectric power stations of Greek Power Authority (Public Enterprise of Electricity) have been constructed.

The drainage basin of Acheloos may be divided into three individual sub basins: a) the upper part, which is defined by the administrative boundaries of Trilofo community, b) the middle part, which is delimited in the south by Stratos village and includes Tavropos, Kremasta, Kastraki and Stratos reservoirs, and c) the lower part, which includes the Trichonida, Lisimahia, Amvrakia and Ozeros natural lakes, the alluvial plain and the Mesologi, Etoliko and Klisova lagoons (Liakouris, 1971).
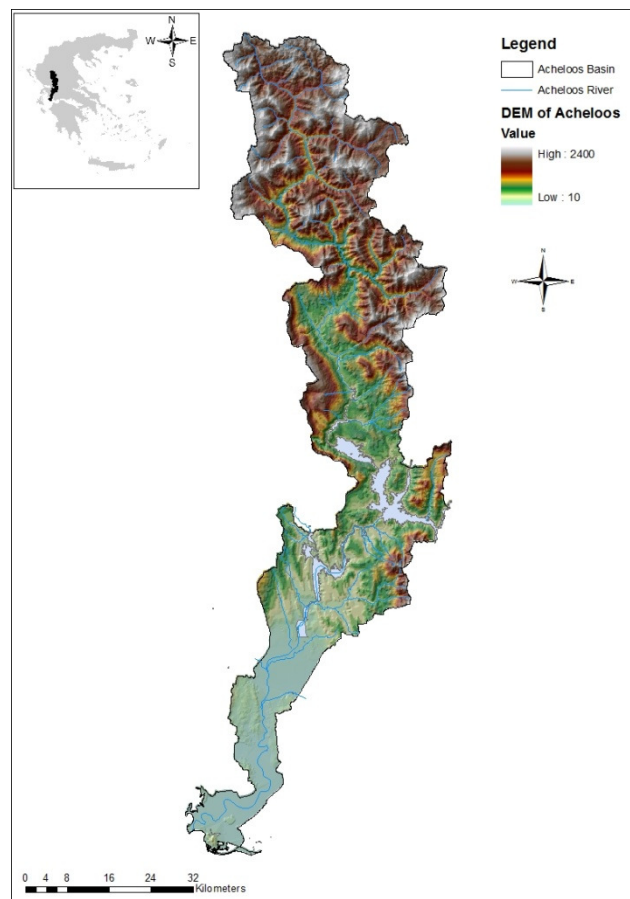
Figure 3.1. Digital elevation model of Acheloos watershed.

The climate in the Acheloos basin belongs to the mild Mediterranean type and tends to Continental type in north and north-eastern regions (Liakouris, 1971). In particular, the warmer month of the year is July (average temperature: 27,40°C), while the coolest is January (average temperature: 8,30°C). The annual height of rain is approximately 1.100-1.200mm.

3.2. Database

Monthly data of precipitation were available from precipitation stations for the period 1980-2000 for the Acheloos watershed. Rain gauges generally measure rainfall at individual points. However, many hydrological applications require the average depth of rainfall occurring over an area which can then be compared directly with runoff from that area. Hence, average areal rainfall is required. The areal precipitation has been estimated using the methods of Thiessen polygon and the precipitation gradient method. Similarly, for the estimation of the temperature of the Acheloos watershed, the temperature gradient was used,

41

using monthly data from the available meteorological stations for the base period.

i. Estimation of areal precipitation

The widely-used method of Thiessen method was proposed by A.M. Thiessen in 1911. The Thiessen polygon method accounts for the variability in spatial distribution of gauges and the consequent variable area which each gauge represents. The areas representing each gauge are defined by drawing lines between adjacent stations on a map. The perpendicular bisectors of these lines form a pattern of polygons (the Thiessen polygons) with one station in each polygon. Stations outside the basin boundary should be included in the analysis as they may have polygons which extend into the basin area. The area of a polygon for an individual station as a proportion of the total basin area represents the Thiessen weight for that station. Areal rainfall is thus estimated by first multiplying individual station totals by their Thiessen weights and then summing the weighted totals as follows:

$$Po = \sum \frac{(Ai \times Pi)}{A} = \sum \left(\frac{Ai \times Pi}{A} \right) \tag{3.1}$$

where A_i is the area of Thiessen polygon for station i, A the total area under consideration, P_i is the monthly precipitation for station i and P_0 the areal precipitation. In order to estimate the areal precipitation with this method, precipitation data from 51 raingages were used (Fig.3.2). Stations outside the watershed included in the analysis since they affected the basin area.

This method is not ideal for mountainous areas where orographic effects are significant or where rain gauges are predominantly located at lower elevations of the basin. Therefore the precipitation gradient method was used. The method is based on the assumption that rainfall increases as the elevation increases. It uses a linear relationship between elevation and precipitation and since a satisfactory correlation exists, it can be used in order to estimate rainfall at any elevation.

The first step was to find the linear relationship between the elevation of each station and the mean annual precipitation of each station. The coefficient of determination was not satisfied using the data from the stations that used for the

42

Thiessen method. Hence, 23 precipitation stations were included in the linear relationship (Fig. 3.3).
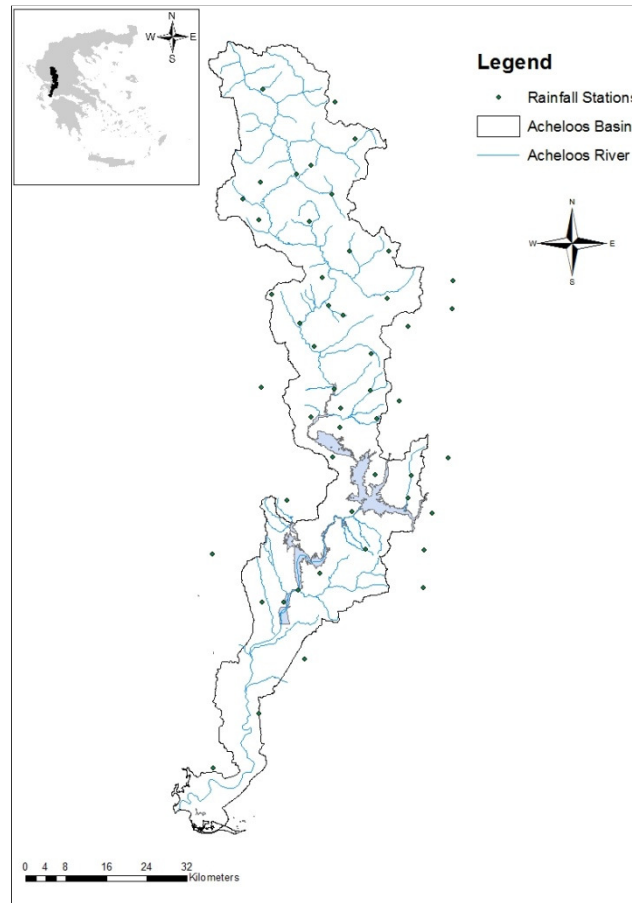
Figure 3.2. Location of the precipitation stations used in this study.

Thereafter, the mean annual precipitation of the watershed was estimated by the following equation:

$$P_k = P_{T(k)} - \frac{(Z_T - Z)b}{100} \tag{3.2}$$

where P_k is the mean annual areal precipitation of the watershed, $P_{T(k)}$ is the mean annual precipitation estimated with the Thiessen method, Z_T is the weighted mean elevation of the watershed estimated by Thiessen, Z is the elevation of the watershed estimated with the method of gradients and b is the slope of the linear relationship. The mean monthly precipitation is estimated by:

$$P_i^k = \frac{P_k P_{T(i)}^k}{P_{T(k)}} \tag{3.3}$$

where P_i^k is the monthly precipitation at the i month and k year, P_k is the mean annual areal precipitation of the watershed, $P_{T(i)}^k$ is the monthly precipitation at

43

the i month and k year estimated with the Thiessen method and , $P_{T(k)}$ is the mean annual precipitation estimated with the Thiessen method.

With the above method the mean monthly areal precipitation of the Acheloos watershed was estimated (Fig. 3.4).
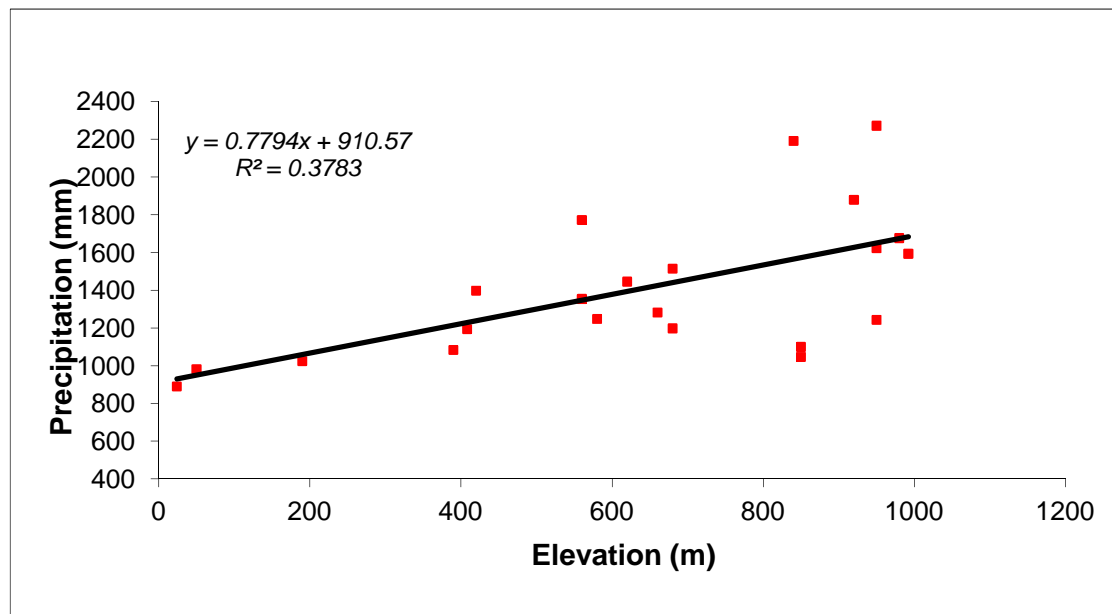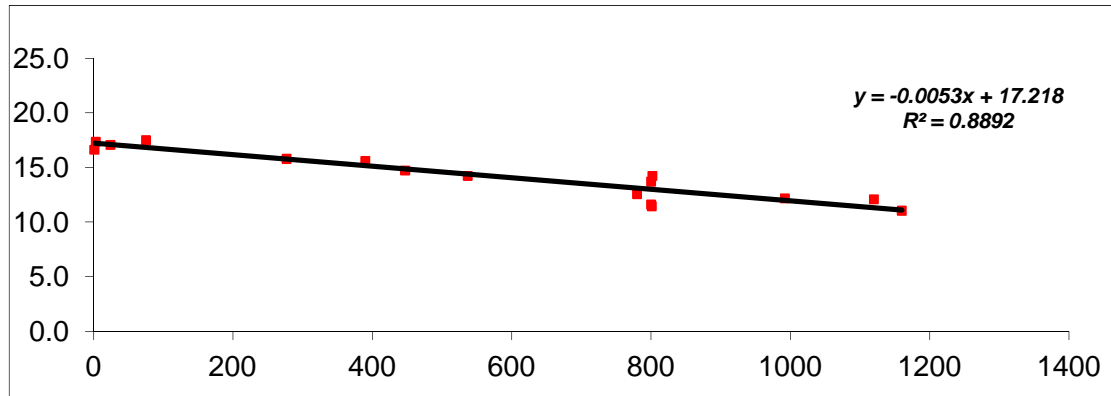

Figure 3.3. Precipitation gradient of Acheloos watershed.
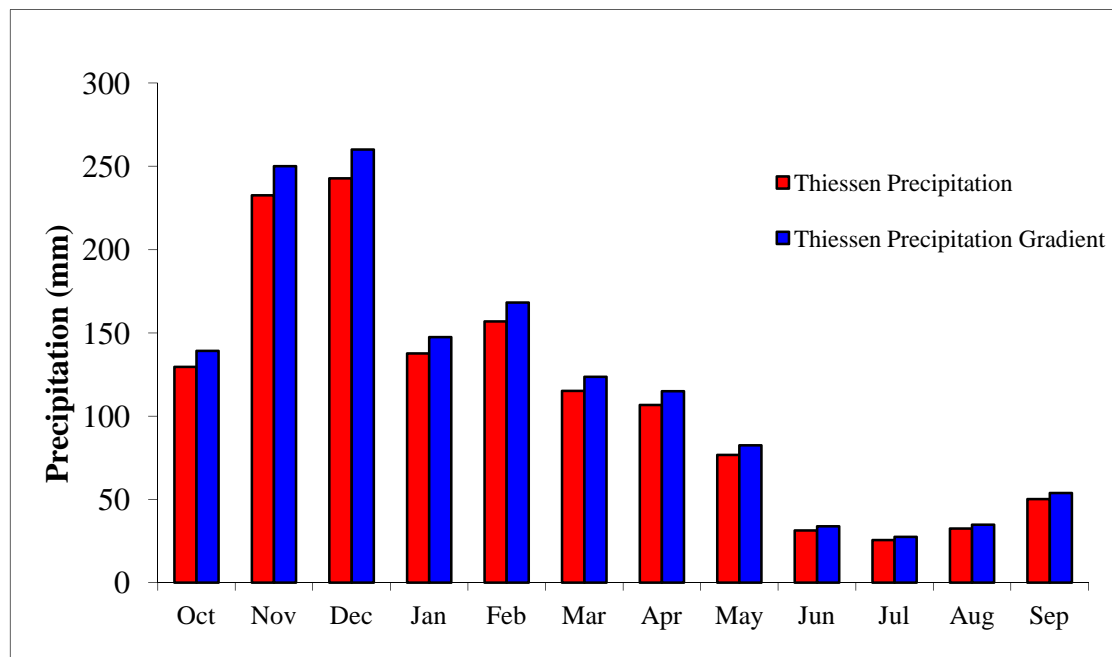
Figure 3.4. Monthly areal precipitation estimated with the method of Thiessen and the precipitation gradient method for the base period (1980-2000).

44

ii. Estimation of areal temperature

The temperature gradient method used for estimation of the areal temperature. According to this method the temperature decreases as the elevation increases per 100m. In order to estimate the mean annual and monthly temperature, the linear relationship between the elevation of each station and the mean annual temperature of each station should be found (fig.3.5).

$$y = -0.0053x + 17.218$$
$$R^2 = 0.8892$$

Figure 3.5. Precipitation gradient of Acheloos watershed.

The mean annual and monthly temperature according to the temperature gradient method is estimated using temperature data from a base station. Therefore, the temperature can be defined as:

$$T_k = T_{T(k)} - \frac{(Z_b - Z)b}{100} \tag{3.4}$$

$$T_i^{\ k} = \frac{T_k T_{T(i)}^{\ k}}{T_{T(k)}} \tag{3.5}$$

where $T_{T(k)}$ is the mean annual temperature at the base station at year k, T_k the mean annual temperature of the watershed at year k, $T_i^{\ k}$ the mean monthly temperature of the watershed at month i and year k, $T_{T(i)}^{\ k}$ the mean monthly temperature of the base station at month i and year k, b is the slope of the linear regression, Z_b is the elevation of the base station and Z is the elevation of the watershed. Figure 3.6 indicates the areal temperature estimated with the temperature gradient method as well as the temperature of the base station.
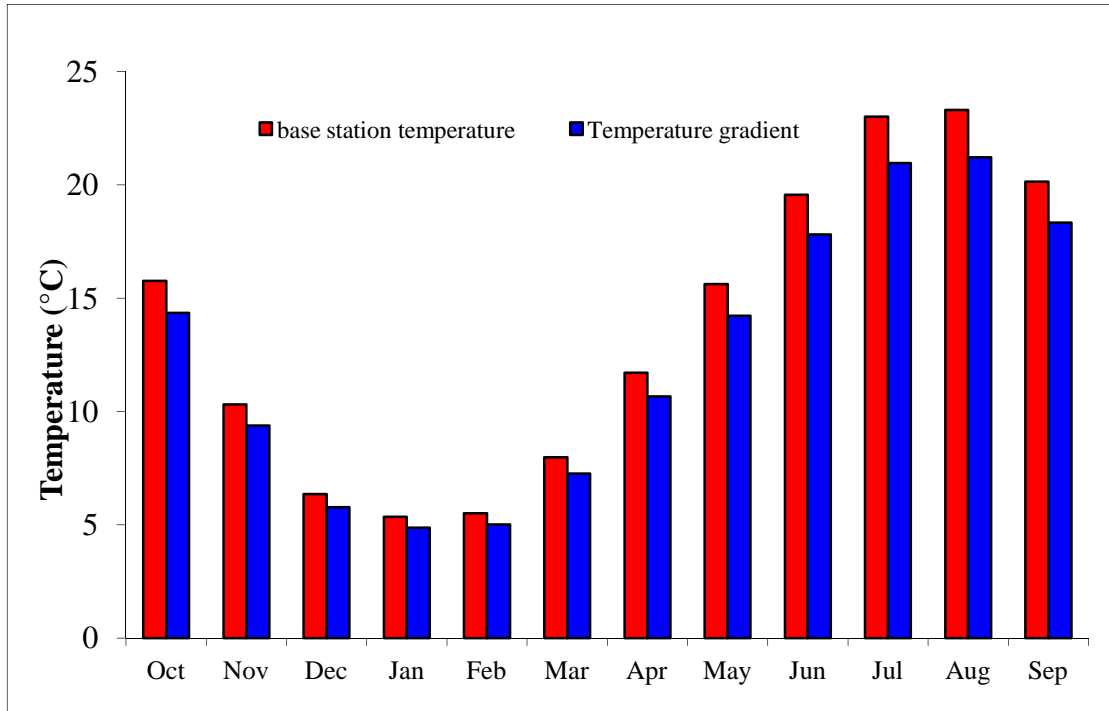
Figure 3.6. Monthly areal temperature of the base station and the Acheloos watershed estimated with the temperature gradient method for the base period (1980-2000).

iii.   Estimation of Potential Evapotranspiration.

Different methods have been proposed to estimate the PET from meteorological parameters. Thornthwaite (1948) proposed a simple approach to calculate PET using only monthly mean temperature. Following this method monthly PET (mm) is obtained by:

$$PET = 16 L_d \left(\frac{10 T_a}{I}\right)^a \tag{3.6}$$

where *T* is the monthly mean temperature in °C; *I* is a heat index, which is calculated as the sum of 12 monthly index values *i*, the latter being derived from mean monthly temperature using the formula:

$$i = \left(\frac{T}{5}\right)^{1.514} \tag{3.7}$$

a is a coefficient depending on *I*: $a = 6.75E^{-7}I^3 - 7.71E^{-5}I^2 + 1.79E^{-2}I + 0.492$ and L_d is a correction coefficient computed as a function of the latitude and month.

46

Therefore using the monthly temperature estimated with the temperature gradient method, monthly PET was calculated for the Acheloos watershed where it is obvious from figures 3.6 and 3.7 the relationship between them.
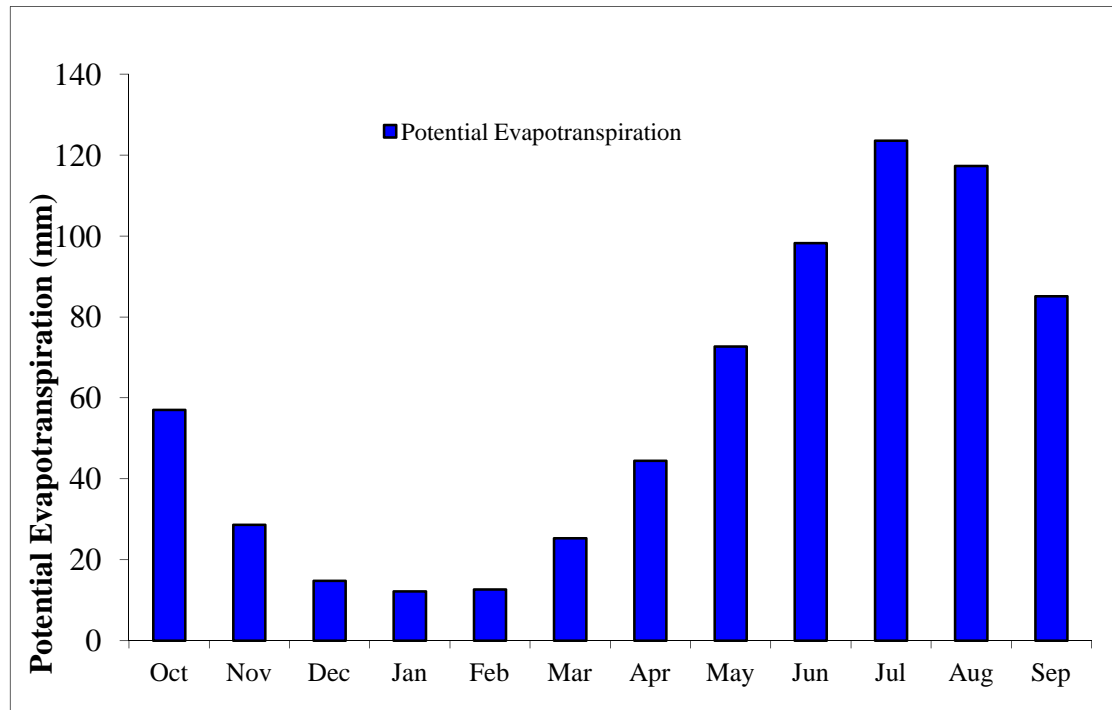
Figure 3.7. Monthly Potential Evapotranspiration in Acheloos watershed estimated with the method of Thornthwaite for the base period (1980-2000).

4. APPLICATION-RESULTS

The methods described in Chapter 2 were used firstly for the statistical downscaling of the monthly areal precipitation and temperature using information from the third generation Canadian Centre for Climate Modeling and Analysis GCM (CGCMa3) in Acheloos watershed. The statistical downscaling was developed for the historical period 1980-2000. Secondly, areal precipitation and temperature was estimated using the outputs from CGCMa3 for two future periods (2030-2050 and 2080-2100) and for three socio-economic scenarios (B1, A1B, A2). Moreover, the observed and the stochastically generated time series of areal precipitation and temperature, as well as potential evapotranspiration which was calculated from the temperature time series were used to estimate SPI and SPEI time series for the base period in order to identify drought events and their characteristics. The SPI and SPEI time series were calculated for various timescales. Finally future SPI and SPEI time series were calculated and the effect of climate change on droughts was assessed from the changes in the number of negative monthly SPI and SPEI values by severity classes.

4.1. Climate Downscaling

Statistical downscaling targeted in generating monthly time series of precipitation and temperature for evaluating climate change impacts on meteorological droughts. A combination of multiple linear regression and stochastic modeling of the residuals derived from MLR was used for the downscaling method of the parameters. The analysis results of the MLR has shown that the correlation coefficient, r, between the logarithmically transformed estimated downscaled monthly areal precipitation and the logarithmically transformed observed monthly basin-wide precipitation was equal to 0.74 for the base period, 1980-2000. Similar the correlation coefficient r between the estimated downscaled monthly temperature and the observed monthly temperature of the watershed was 0.98. The developed relationships has been found to be statistically significant at $\alpha=5\%$ significance level using the t-test.
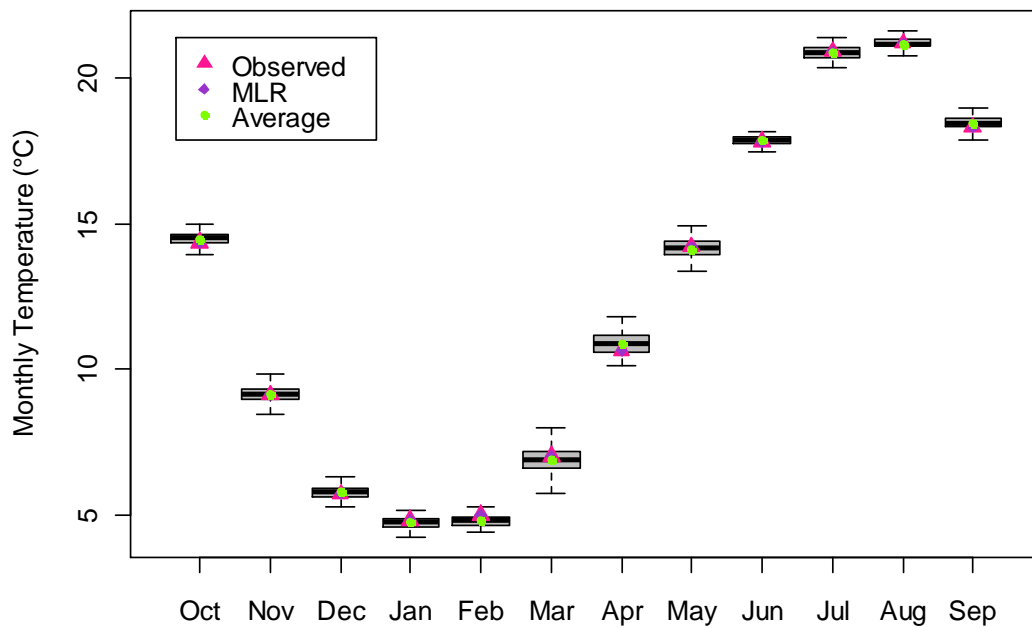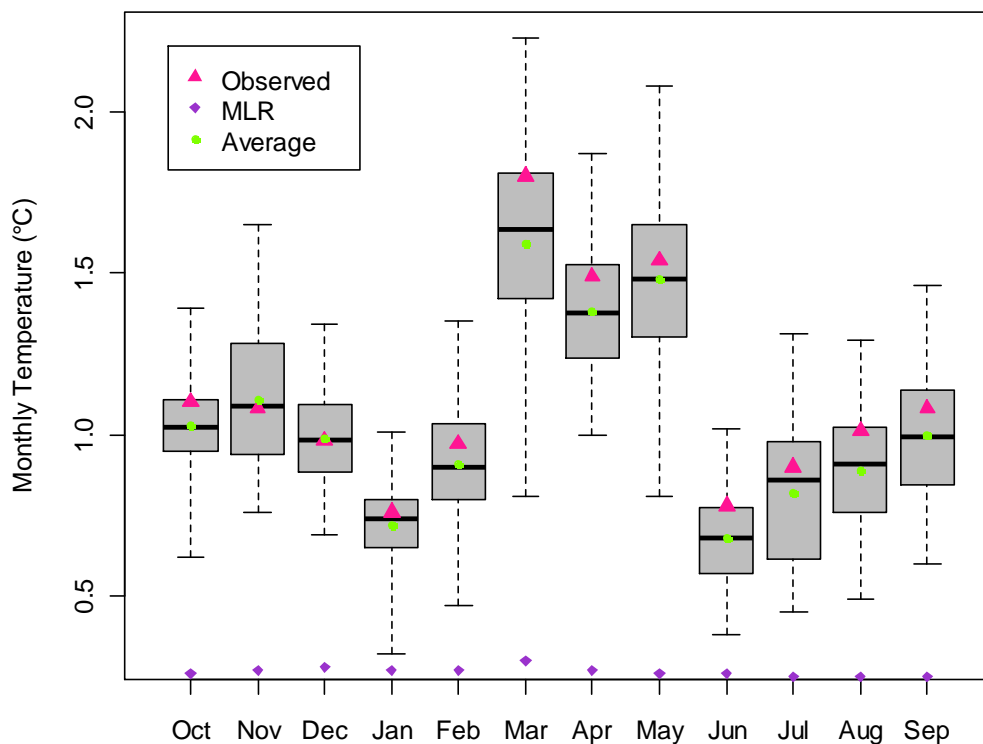
a)
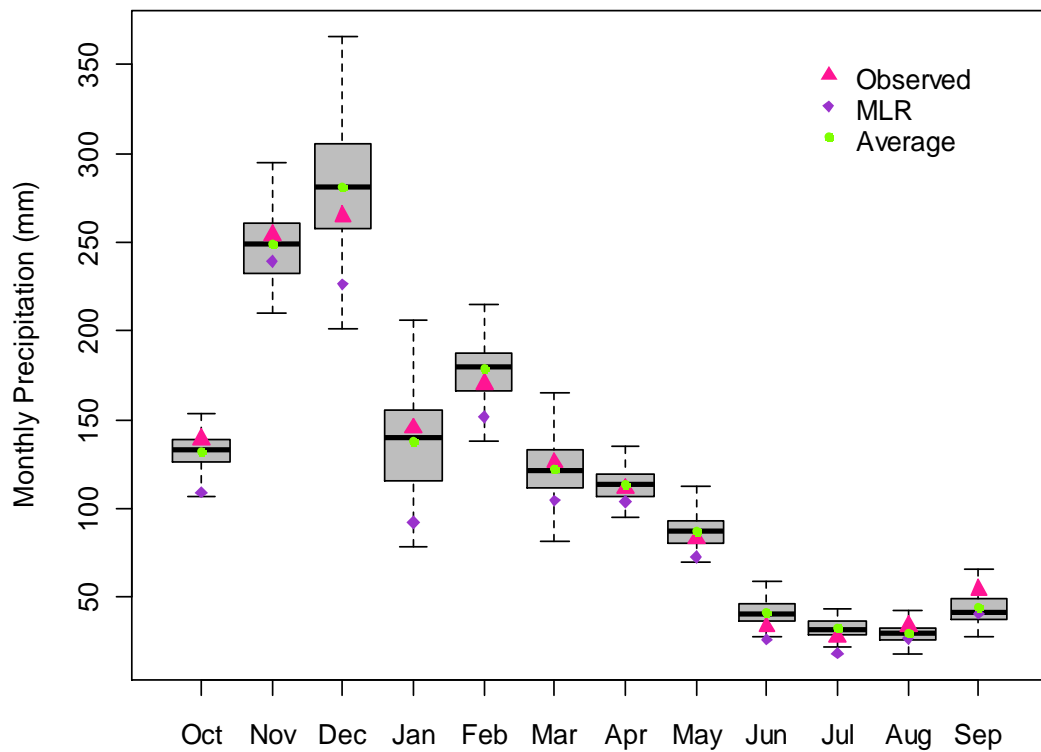
b)
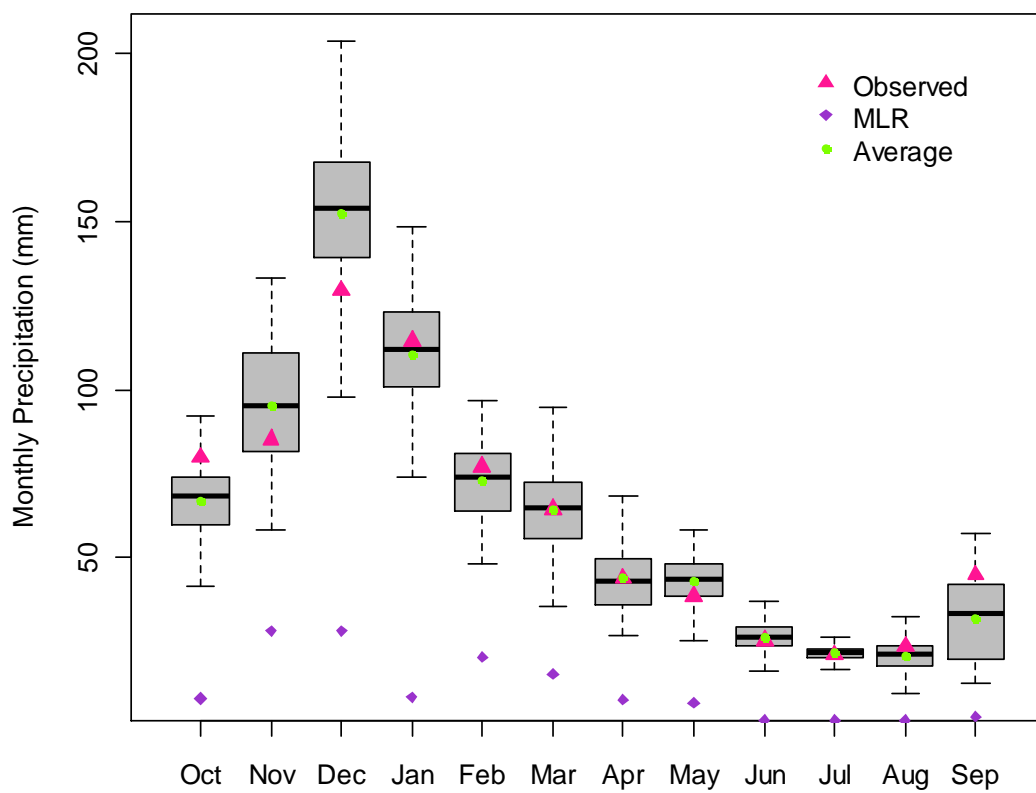
Figure 4.1. Statistical properties of the statistical downscaling procedure for the historical period 1980-2000 for a) average monthly precipitation and b) standard deviation.

49

a)

b)

Figure 4.2. Statistical properties of the statistical downscaling procedure for the historical period 1980-2000 for a) average monthly temperature and b)standard deviation of monthly temperature.

The regression model simulated quite well the mean monthly precipitation (Fig. 4.1) and temperature (Fig.4.2) for the historical period 1980-2000 but not the variance of the observed precipitation and temperature.

50

For the treatment of the residuals, stochastic time series theory was applied to preserve the variance of observed monthly precipitation. A first order autoregressive model (AR(1)) was applied and used to generate annual climate data. Moreover the modified method of fragments applied in order to disaggregate the annual data to monthly climate data. For the evaluation of the generated annual and monthly precipitation and temperature, annual and monthly parameters were estimated such as mean, standard deviation, coefficient of skewness, correlation coefficient between successive months, maximum, minimum and cross correlation between the monthly climate variables (precipitation-temperature, temperature-PET and precipitation-PET) for each of the 100 synthetic time series. From these values the 0, 25, 50, 75, 100 percentile values and the mean were calculated. Figures 4.1 and 4.2 show the statistical properties (average and standard deviation) of the monthly generated time series for the historical period. The Box-Whisker plots refer to stochastic simulations results, whereas MLR are the results obtained from the multiple linear regression. Furthermore, the average of the 100 replicates is added in the plot. The figures show that the method is able to reproduce the statistical properties of observed monthly precipitation and temperature time series for the period 1980-2000. Similar results are obtained from the other monthly parameters (coefficient of skewness, correlation coefficient between successive months, maximum, minimum and cross correlation between the monthly climate variables).

Table 4.1. Statistical properties of the statistical downscaling procedure for the historical period 1980-2000 for annual precipitation.

	Observed	MLR Downscaled	Stochastically Downscaled					
			Average	Min	25%	50%	75%	Max
Average	1442.70	1212.03	1453.74	1302.30	1413.14	1461.97	1492.54	1567.61
SD	233.84	46.04	216.97	143.70	189.46	213.89	239.12	333.39
Skewness	-0.57	0.09	-0.05	-1.60	-0.33	-0.04	0.29	1.27
Minimum	988.37	1126.36	1050.36	749.09	972.04	1048.11	1123.69	1304.46
Maximum	1787.40	1309.34	1855.49	1591.84	1777.30	1831.77	1931.21	2222.74
Acf_1	0.15	-0.19	0.09	-0.47	-0.02	0.10	0.22	0.54
Correl_rain-temp	0.02	-0.24	0.02	-0.60	-0.13	0.04	0.15	0.55

Table 4.2. Statistical properties of the statistical downscaling procedure for the historical period 1980-2000 for annual temperature.

Annual	Observed	MLR Downscaled	Stochastically Downscaled					
			Average	Min	25%	50%	75%	Max
Average	12.43	12.43	12.44	12.21	12.38	12.44	12.50	12.64
SD	0.46	0.01	0.44	0.26	0.39	0.44	0.50	0.64
Skewness	-0.04	-0.17	0.00	-1.29	-0.30	-0.04	0.33	1.21
Minimum	11.41	12.40	11.61	10.63	11.45	11.65	11.78	12.15
Maximum	13.45	12.45	13.26	12.95	13.12	13.23	13.38	13.82
Acf_1	-0.24	0.44	-0.26	-0.66	-0.40	-0.27	-0.13	0.12
Correl_rain-temp	0.02	-0.24	0.02	-0.60	-0.13	0.04	0.15	0.55

Furthermore, Tables 4.1 and 4.2 indicate that the statistical downscaling is able to reproduce the annual statistical characteristic of the annual observed time series of precipitation and temperature. The observed value is close to the median for most of the parameters and within the inter-quartiles range. Hence the generated data can be considered similar to the statistical characteristics of the historical data.

4.2. Drought Indices – Present Climate

SPI and SPEI time series were calculated from the observed and generated monthly time series at multiple time-scales (1-, 3-, 6-, 9-, 12- and 24-months). For the SPI time series the monthly precipitation time series were used, whereas for the estimation of SPEI the monthly water balance (Precipitation-PET) time series were used. The parameters of the gamma and log-logistic distributions were estimated based on the 100 generated time series of the historical period.

The results will be presented for SPI and SPEI timescales of -6, 12-, 24-months since there are representative of hydrological and water resources drought (Loukas and Vasiliades, 2005).
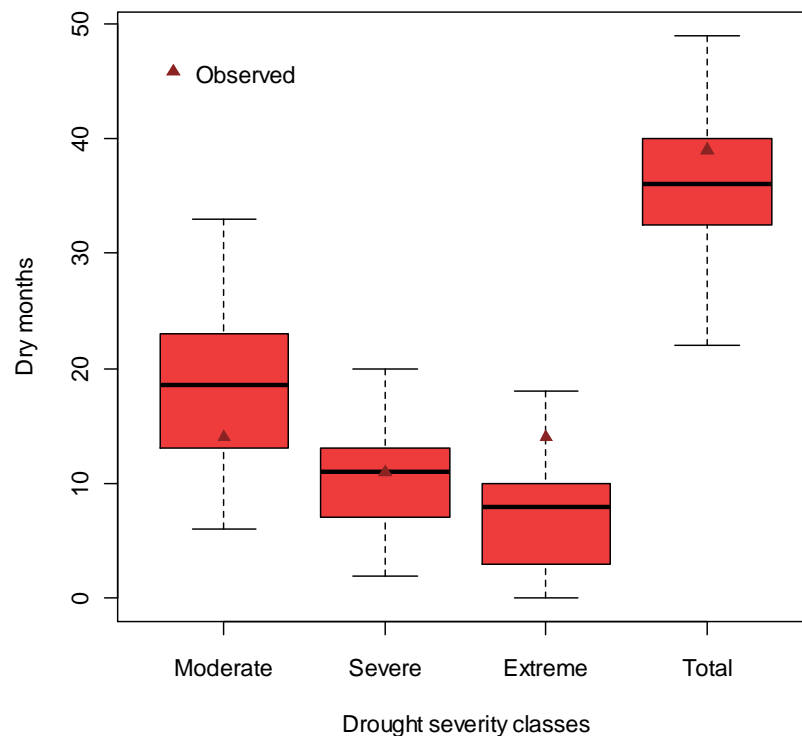
4.2.1. SPI

Firstly the temporal variation of observed and generated SPI time series was investigated, by comparing the number of months for which the SPI values for all

timescales indicated moderate drought (−1.50<SPI<−1.00), severe drought (−2.00<SPI<−1.50), and extreme drought (SPI<−2.00).

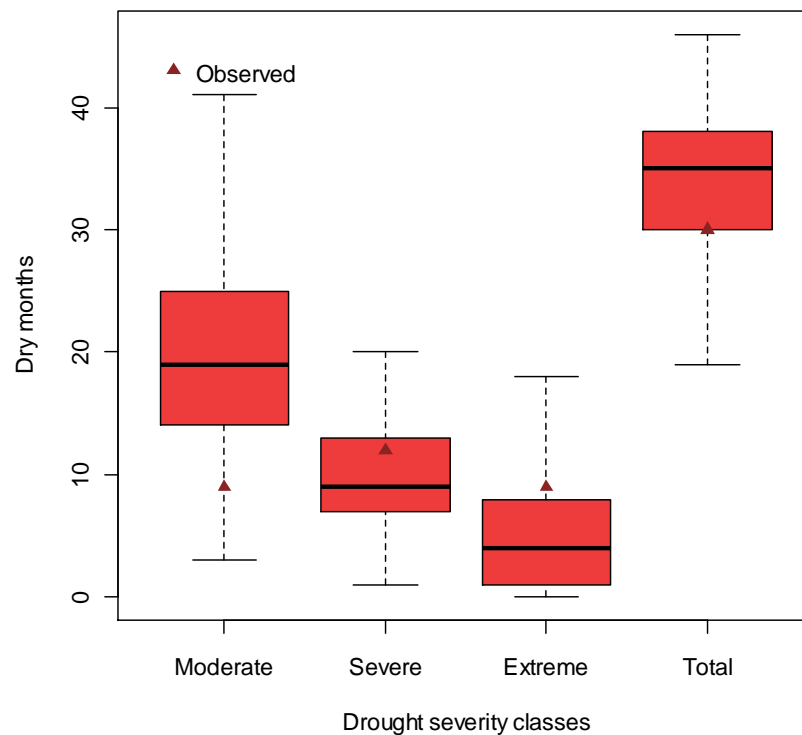a)
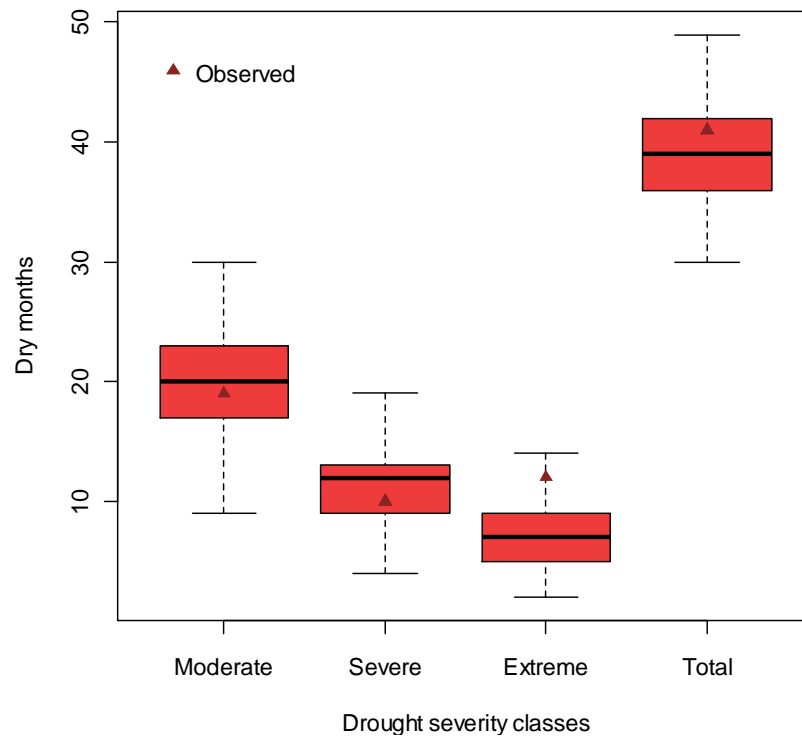
b)

c)

Figure 4.3. Total number of dry months (SPI≤-1) for various drought severity classes at a) 6-, b) 12- and c) 24-months timescale for 1980-2000.

Figure 4.3 indicate that Acheloos watershed experienced moderate, severe and extreme droughts for the base period (1980-2000). The statistical downscaling method is capable to simulate drought patterns, since the generated time series produce similar number of total dry months with the observed time series. However, the allocation of the dry months in the respective drought classes is quite different. The downscaling method simulates satisfactorily the moderate and severe droughts at all timescales, except moderate droughts at 24-months timescale, but produces smaller number of dry months for extreme drought. However, the observed drought pattern is in the range of the stochastic simulation.

Furthermore, from the analysis of drought events, indicated that about 17.45% of the time Acheloos watershed experienced drought for the historical period for SPI 6-month. Stochastic simulation results for the same timescale show that the watershed experienced droughts, on average, for 16.60 % of time with a range of 12.77% to 20.85%. Similar results are observed and for the other timescales. On the other hand, for 24-month timescale, stochastic simulation results show a

54

small increase in the drought time in the order of 16.06% with a range from 8.76% to 24.42%, whereas the observed is 13.9%. However, the difference in the time percentage of dry months is always within the range of the stochastic simulation results.

Using the threshold level method the average severity, average maximum cumulative severity and average maximum duration of the 100 generated SPI timeseries were identified at 6-, 12- and 24-months timescale. The threshold level was chosen to have the value of -1, since SPI values bellow -1 (Table 2.5) identify drought event. Table 4.3 shows the results of the method that was applied to the observed time series of SPI and the generated SPI time series. The statistical downscaling results show a decrease in the severity for all timescales that was applied. Moreover, maximum cumulative severity is underestimated for 6- and 12-months timescale. For 24-months timescale the simulated maximum cumulative severity is almost similar with the observed value. Finally, the observed maximum duration for the 6-month timescale is simulated well, whereas for the other timescales the stochastic method overestimates it. However the observed values are within the inter-quartiles range of the statistical downscaled values.

Table 4.3. Average deficit characteristics of the generated 6-, 12-, 24-months SPI timeseries for period 1980-2000.

|	Observed	Statistically Downscaled					
Timescale 6-months		**Average**	**Min**	**25%**	**50%**	**75%**	**Max**
Severity	0.69	0.60	0.32	0.53	0.59	0.66	0.93
Maximum cumulative severity	8.30	7.56	3.03	5.64	7.12	8.89	14.85
Maximum duration	8	8	4	6	7	9	14
Timescale 12-months							
Severity	0.70	0.62	0.29	0.46	0.59	0.75	1.37
Maximum cumulative severity	14	12.51	2.14	7.93	11.79	16.27	28.09
Maximum duration	11	14	5	11	13	15	36
Timescale 24-months							
Severity	0.74	0.54	0.15	0.38	0.51	0.64	1.37
Maximum cumulative severity	12.37	12.99	0.52	7.75	11.11	17.42	38.30
Maximum duration	13	18	2	13	18	23	35

4.2.2. SPEI

Drought events were also examined using the SPEI drought index. The number of months for which the SPEI values for all timescales indicated moderate drought (−1.50<SPI<−1.00), severe drought (−2.00<SPI<−1.50), and extreme drought (SPI<−2.00) was identified.

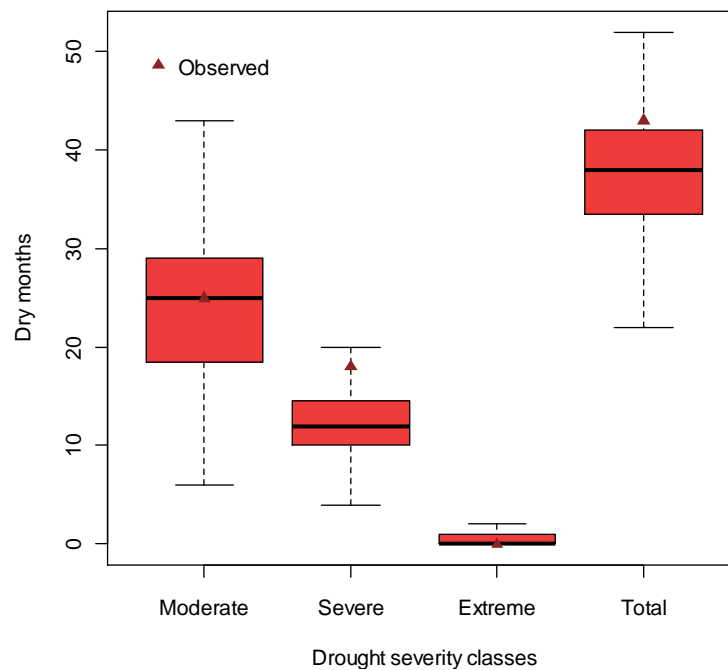a)
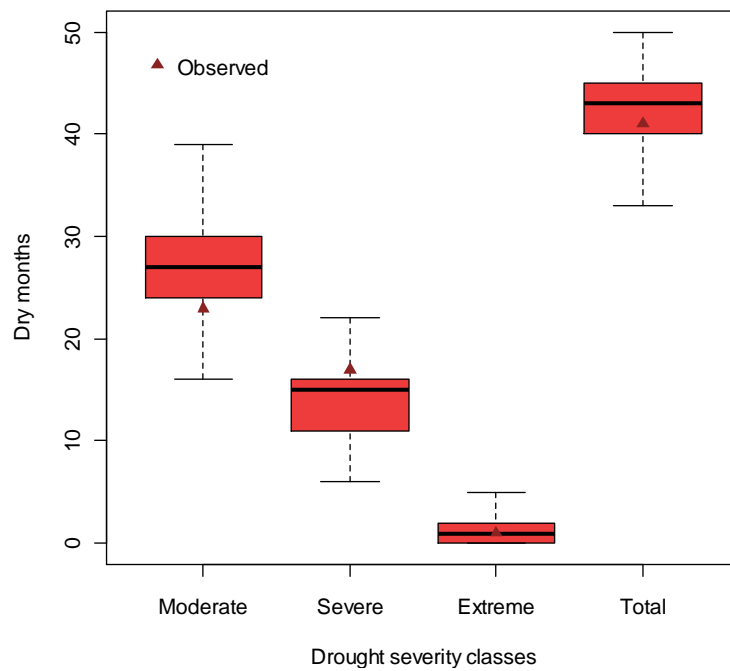
b)
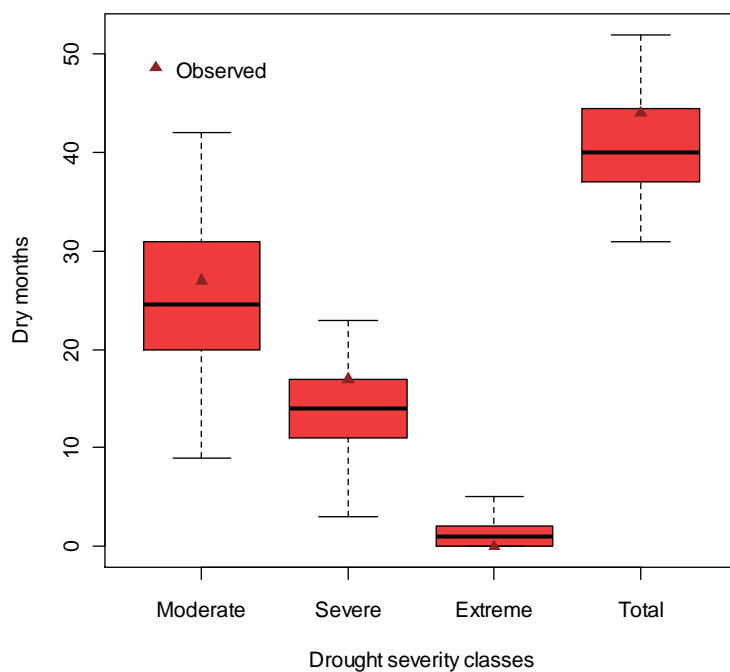
c)

Figure 4.4. Total number of dry months (SPEI≤-1) for various drought severity classes at a) 6-, b) 12- and c) 24-months timescale for 1980-2000.

Drought patterns are simulated quite well by the statistical downscaling method. The generated time series produce similar number of total dry months with the observed time series for all timescales, except the 24-months timescale where the observed dry months are 43 and the average total months that produced from the generated time series are 38 with a range from 22 to 52. The extreme drought events for all timescales are near 0 both for observed and generated time series. The number of moderate drought events simulated satisfactorily at almost all timescales. The statistical downscaling underestimates the severe drought events at all timescales. However, the observed drought pattern is in the range of the stochastic simulation.

Acheloos watershed experienced drought for the historical period for SPEI 6-months about 17.45% of the time. Stochastic simulation results for the same timescale showed that the watershed experienced droughts, on average, for 18.11% of time with a range of 13.19% to 21.28%. Similar results are observed and for the other timescales. For 12- and 24-month timescale, the stochastic simulation results showed 17.79% and 17.49% in the drought time with a range from 10.04% to 22.71% and from 10.14% to 23.96% respectively, whereas the observed is 19.21% for 12-months and 19.82% for 24-months timescale.

57

Table 4.4. Average deficit characteristics of the generated 6-, 12-, 24-months SPEI timeseries for period 1980-2000.

	Observed	Statistical Downscaling					
Timescale 6-months	**Average**	**Min**	**25%**	**50%**	**75%**	**Max**	
Severity	0.45	0.42	0.33	0.39	0.42	0.44	0.55
Maximum cumulative severity	5.27	4.85	2.72	4.12	4.84	5.47	8.88
Maximum duration	8	8	5	7	8	8	13
Timescale 12-months							
Severity	0.43	0.43	0.29	0.39	0.43	0.47	0.77
Maximum cumulative severity	7.36	8.86	3.61	6.60	8.42	10.63	18.31
Maximum duration	14	14	7	12	13	16	35
Timescale 24-months							
Severity	0.38	0.43	0.24	0.37	0.41	0.49	0.73
Maximum cumulative severity	7.21	10.31	3.49	7.31	10.56	13.17	20.30
Maximum duration	15	18	10	14	18	23	33

The threshold level method indicated that although the observed values are within the inter-quartiles range of the statistical downscaled values, there is an overestimation for the maximum cumulative severity and maximum duration at 24-months timescale compared with the observed values in the order of 43.04% and 22.27% respectively. Moreover, the method showed an increase in the average severity that produced from the generated series in the order of 15.13% at 24-months timescale.

4.3. Future Climate

The statistical downscaling method was used in order to generate future time series of precipitation and temperature. Firstly the multiple linear regression model was used to estimate the areal precipitation and temperature from the outputs of the CGCMa3 for three socio-economic scenarios. The downscaling was applied for two future periods 2030-2050 and 2080-2100. Thereafter the residuals of temperature and precipitation time series that were produced from the AR(1) model for the historical period, added to the downscaled time series,

assuming that the time series of the residuals remain unchanged in the future. Finally time series of PET were produced with the method of Thornthwaite for the three socio-economic scenarios and the two future periods.

Tables 4.3 and 4.4 show the statistical properties of the annual precipitation and temperature of the Acheloos river basin for all the socio-economic scenarios, for historical and future periods (2030-2050 and 2080-2100). The mean annual precipitation of the watershed is 1461.97 mm ranges from 1302.3mm to 1567.61mm, whereas the mean annual temperature is 12.44^{o}C with a range from 12.21^{o}C to 12.64^{o}C. For 2030-2050 the SRES B1 scenario projection indicates a slight increase in mean annual precipitation of 0.56% as well as in mean annual temperature of 0.61%. According to SRES A1B scenario, it is possible a slight decrease in precipitation of 0.02% and a slight increase in temperature of 0.79%. The third SRES scenario (A2) indicates a decrease in annual precipitation of 1.52% at 1439.70mm and a simultaneous increase in temperature of 0.82% at 12.54^{o}C. The standard deviation of precipitation is projected to decrease in the order of 0.77%, 1.08% and 0.49% for the B1, A1B and A2 scenarios respectively. The standard deviation of temperature remains unchanged for the three scenarios.

For the long-term period of 2080-2100 greater changes in precipitation and temperature are projected. For the more conservative SRES B1 scenario the precipitation and temperature increases in the order of 0.16% and 1.02% respectively. The SRES A1B scenario shows a decrease in precipitation in the order of 1.79% and an increase in the temperature in the order of 1.6%. Finally the SRES A2 scenario indicates slighter decrease in the precipitation at 1.52% and an increase in the temperature in the order of 2.17%. The changes in the values of standard deviation of precipitation and temperature are slighter for the three scenarios for the period 2080-2100.

The larger reduction for average annual precipitation was observed for the period 2080–2100 as expected. The average annual precipitation ranges from -1.52% to 0.56% for period 2030–2050 and from -1.79 to 0.16% for period 2080–2100 for the three scenarios. The average monthly precipitation is projected to

59

increase for most months of the two periods for the B1 SRES scenario. However, the other two scenarios showed a decrease of the average monthly precipitation in most months for both two periods (fig. 4.5 and 4.6).

Similar with precipitation the larger change in the average annual temperature was observed for the long-term period (2080-2100). The average annual temperature ranges from 0.61% to 0.81% for period 2030-2050 and from 1.02% to 2.17% for period 2080-2100. Figures 4.7 and 4.8 show the monthly average temperature of the watershed for the two future periods. There is a slight increase on temperature in all months.
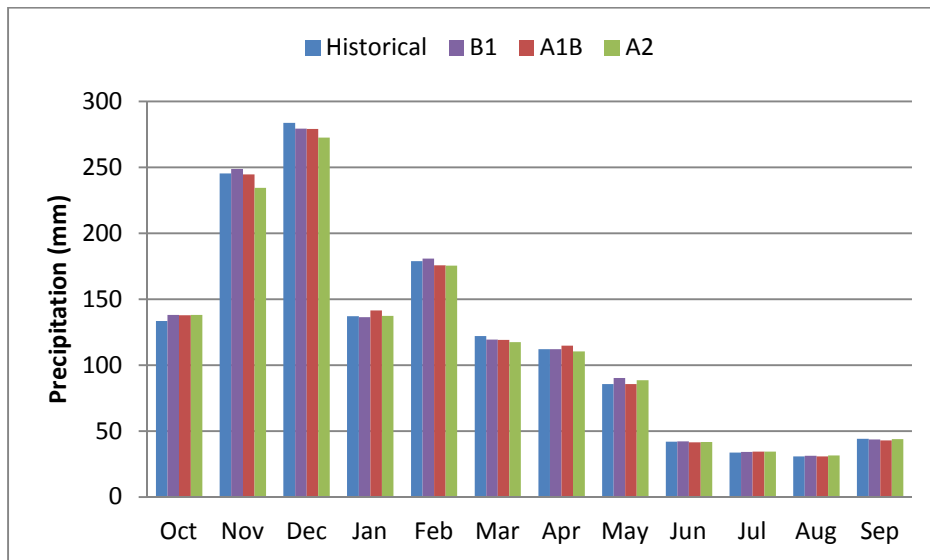
Figure 4.5. Monthly average precipitation for period 2030-2050.
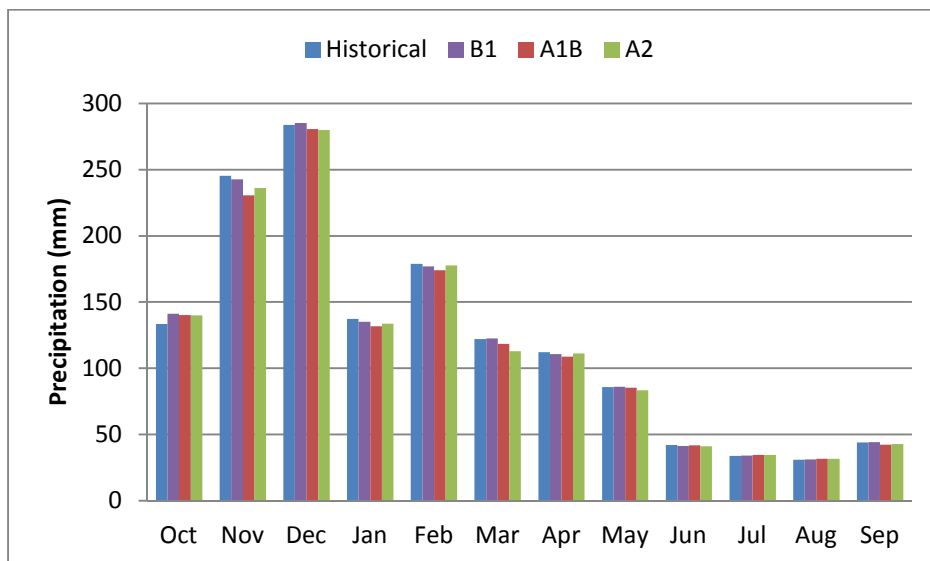
Figure 4.6. Monthly average precipitation for period 2080-2100.

60

Table 4.3. Statistical properties of annual precipitation of Acheloos watershed.

	Historical Period 1980-2000			Future Period 2030-2050			Future Period 2080-2100		
	Median	Maximum	Minimum	Median	Maximum	Minimum	Median	Maximum	Minimum
Average Annual Precipitation (mm)	1461.97	1567.61	1302.30						
SRES B1				1470.17	1575.37	1308.83	1464.27	1569.55	1304.04
SRES A1B				1461.71	1567.11	1303.35	1434.00	1539.48	1274.35
SRES A2				1439.75	1545.08	1281.09	1437.84	1543.74	1276.86
Standard deviation (mm)	213.89	333.39	143.70						
SRES B1				211.58	328.06	153.20	217.91	335.95	150.82
SRES A1B				212.84	314.93	154.42	214.16	350.93	142.11
SRES A2				212.24	333.73	144.60	213.17	322.79	141.81
Maximum (mm)	1831.77	2222.74	1591.84						
SRES B1				1859.56	2249.66	1629.15	1855.55	2215.33	1637.62
SRES A1B				1837.10	2214.93	1652.14	1819.00	2180.97	1587.06
SRES A2				1806.73	2170.20	1607.41	1818.06	2158.70	1825.46
Minimum (mm)	1048.11	1304.46	749.09						
SRES B1				1067.23	1294.81	739.86	1070.73	1315.92	707.65
SRES A1B				1053.08	1294.72	738.87	1017.30	1266.32	705.97
SRES A2				1043.04	1281.58	689.15	1031.63	1287.34	780.94

Table 4.4. Statistical properties of annual temperature of Acheloos watershed.

|	Historical Period 1980-2000			Future Period 2030-2050			Future Period 2080-2100		
	Median	Maximum	Minimum	Median	Maximum	Minimum	Median	Maximum	Minimum
Average Annual Temperature (oC)	12.44	12.64	12.21						
SRES B1				12.51	12.71	12.28	12.56	12.76	12.33
SRES A1B				12.53	12.73	12.31	12.64	12.84	12.41
SRES A2				12.54	12.74	12.31	12.71	12.91	12.48
Standard deviation (oC)	0.44	0.64	0.26						
SRES B1				0.44	0.64	0.26	0.44	0.63	0.26
SRES A1B				0.44	0.64	0.26	0.44	0.63	0.26
SRES A2				0.44	0.64	0.26	0.44	0.63	0.26
Maximum (oC)	13.23	13.82	12.95						
SRES B1				13.31	13.89	13.01	13.36	13.96	13.07
SRES A1B				13.33	13.92	13.06	13.44	14.02	13.16
SRES A2				13.34	13.93	13.04	13.50	14.07	13.22
Minimum (oC)	11.65	12.15	10.63						
SRES B1				11.72	12.22	10.68	11.79	12.26	10.74
SRES A1B				11.74	12.24	10.75	11.85	12.34	10.84
SRES A2				11.75	12.25	10.72	11.90	12.42	10.93

61
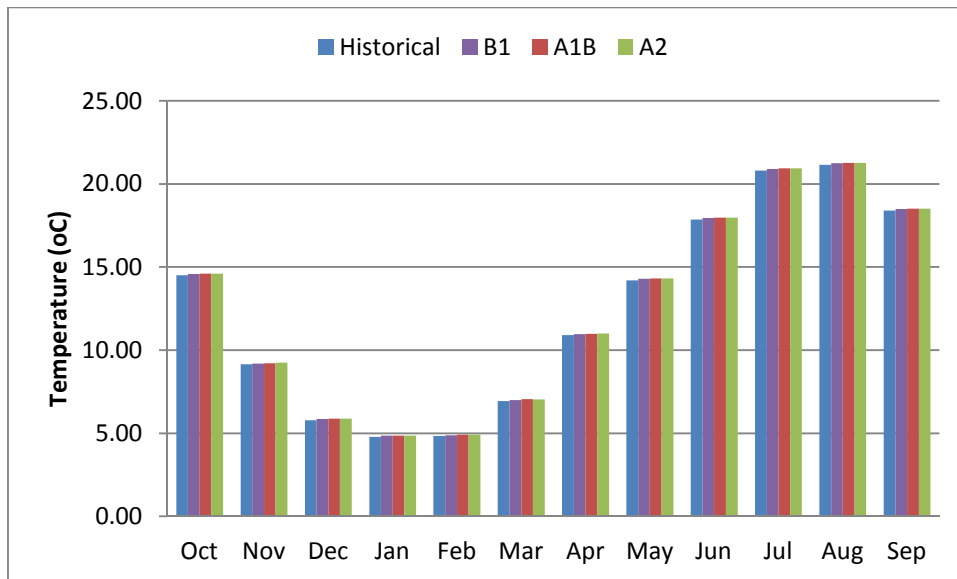
Figure 4.7. Monthly average temperature for period 2030-2050.
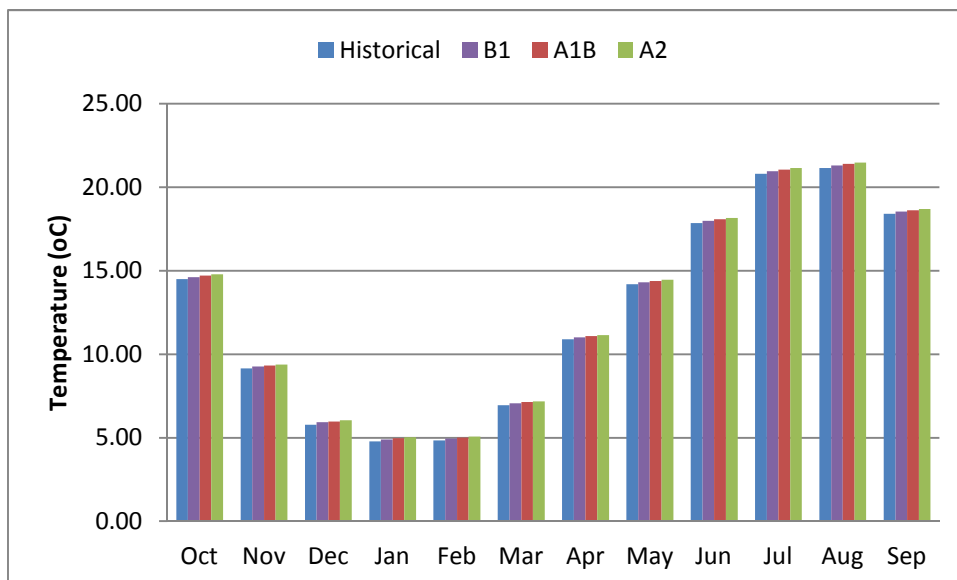

Figure 4.8. Monthly average temperature for period 2080-2100.

4.3.1. SPI

A. *Future Period 2030-2050*

The 100 future generated monthly precipitation time series for the three socio-economic scenarios and the two future periods were used for the estimation of SPI time series at multiple timescales (1-, 3-, 6-, 9-, 12-, 24- months). The parameters of the gamma distribution were assumed unchanged in the future and their respective values for the historical period have been used.

62
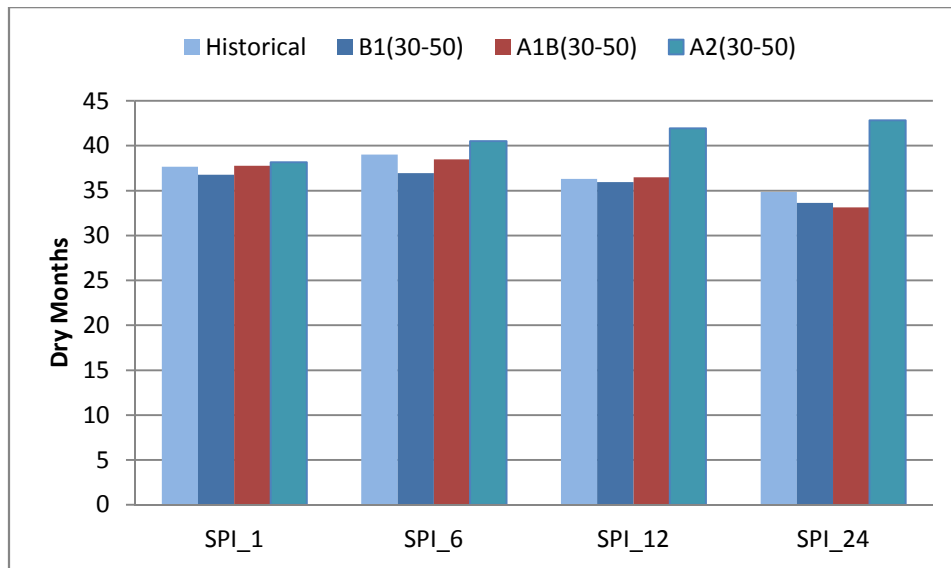
Figure 4.9. Total average dry months for SPI at multiple timescales for 2030-2050.

Figure 4.9 indicates that the total number of dry months (SPI<-1) will be increased for the A2 scenarios for period 2030-2050 at all time scales. For the B1 SRES scenario there is a decrease due to the slight increase of the annual precipitation for the same future period at all timescales. This is also obvious from the box-plots of 6-, and 24-months timescale for the three scenarios (fig.4.10 and 4.11). B1 scenario is more conservative that the others. For the downscaled time series of B1 scenario there is an average decrease of 5% and 3% that ranges from -31% to 20% and from -77% to 66% at 6- and 24-months respectively. A1B SRES scenario indicate an average decrease of 1% and 5% that ranges from -28% to 31% and from -54% to 52% at 6- and 24-months timescale. For 12-months timescale the average dry months simulated to be equal to the average dry months of the historical period with a range of -34% and 51%. Finally the number of negative values of the generated SPI time series of the A2 scenario will be increased at all timescales. The most increase will be at 24-months timescale by 23% with a range from -25% to 89%. At 6- and 12-months timescale the increase is lower at 4% and 15% that ranges from -28% to 28% and -20% to 51% respectively.

Figure 4.11 shows the number of dry months for the three socio-economic scenarios in period 2030-2050 at 12-months timescale, categorized with the severity of classes. According to this analysis, the total moderate dry months were increased for all scenarios. Similar patterns are observed in the other time scales. A2 scenario shows an average increase for the moderate dry months in the order of 9% with a range

from -68% to 99%, whereas B1 and A1B show an average increase of 2% and 5% with ranges from -73% to 132% and from -62% to 126% respectively at 12-months timescale. The extreme dry months were decreased at 6-, 12- and 24- months for the two scenarios, B1 and A1B, as well as a slight decrease in severe dry months were observed for period 2030-2050. However, A2 scenarios show an increase both in extreme and severe dry months with the highest increase at 24-months timescale in the order of 52% and 41% respectively.
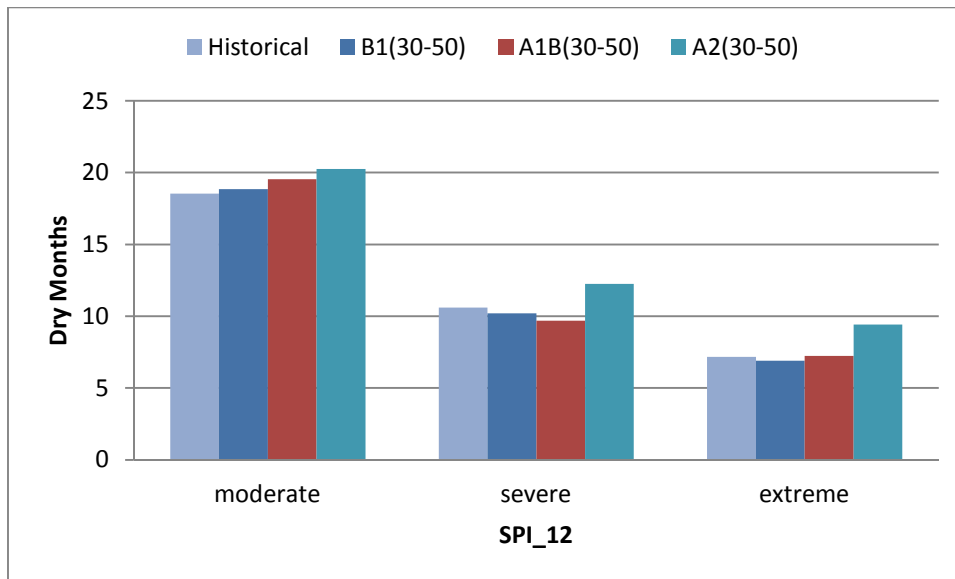
a)
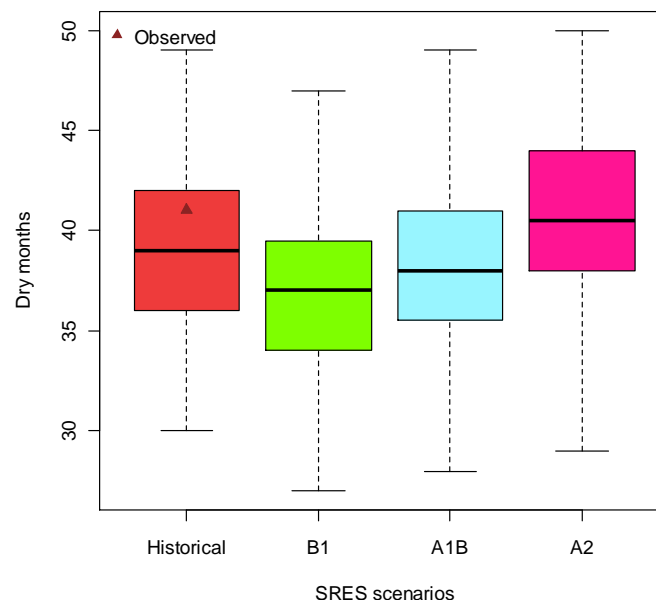
b)
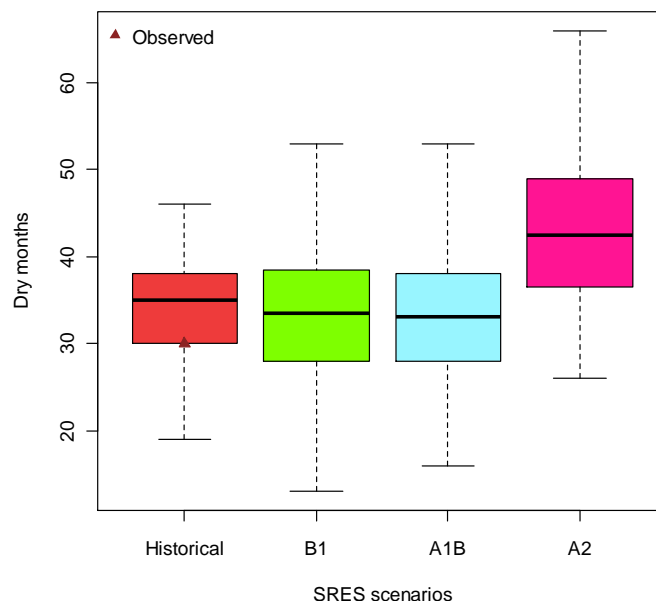
Figure 4.10. Total dry months for SPI for the three SRES scenarios at a)6- and b)24-months timescale for 2030-2050.

Figure 4.11. Total numbers of dry months (SPI≤-1) for various drought severity classes at 12-month timescale SPI for the three SRES scenarios and for period 2030-2050.

B. *Future Period 2080-2100*

Estimation of SPI time series for 2080-2100 for the three scenarios indicated an increase in the total dry months at almost all timescales (fig.4.12). For SPI at 6-months timescale an average increase of 12% and 8% was observed for A1B and A2 SRES scenario respectively.
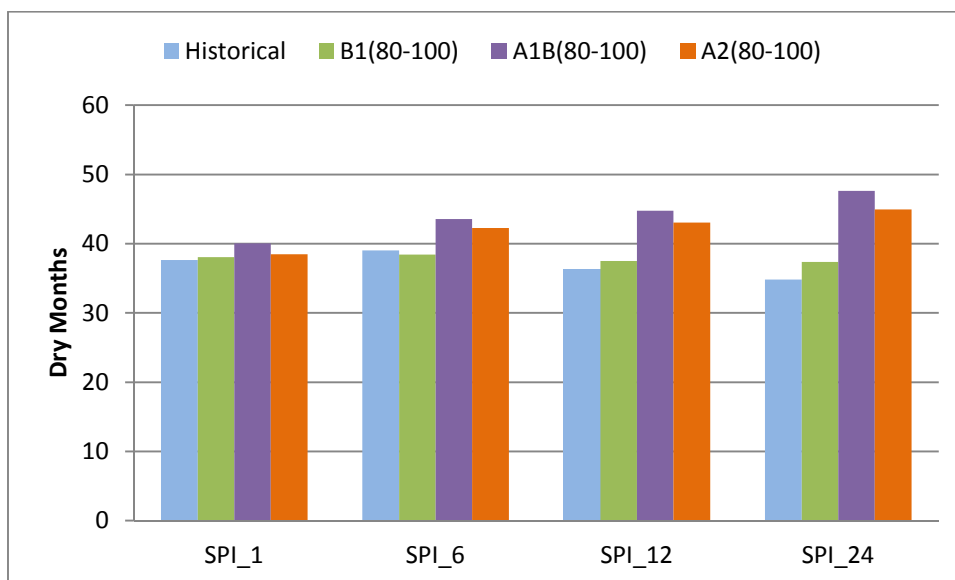

Figure 4.12. Total average dry months for SPI at multiple timescales for 2080-2100.

The median values of the generated SPI time series at 6-months timescale showed a decrease in the order of 3% with a range from 33% to 23% for the B1 scenario whereas at larger timescales a slight increase was indicated. For this period A1B seems more severe than the other two scenarios. As the timescale increases, an

65

increase in the average number of dry months is observed. Hence, at 12-months timescale the average increase for A1B scenario is 23% and ranges between -26% and 62% whereas at 24-months the increase is in the order of 37% with a range from -25% to 104%. Moreover, for the A2 SRES scenario the average increase in total dry months is 19% and 29% at 12- and 24-months timescale respectively (fig.4.13). SPI estimation is based on precipitation. Hence, there is an increase in the values of SPI for A1B and A2 scenario, since the downscaled procedure showed a slight decrease in the precipitation pattern for these scenarios. The annual precipitation for A1B scenario was projected with the highest decrease compared with the other two scenarios and this result is obvious in the estimation of SPI series for this period.
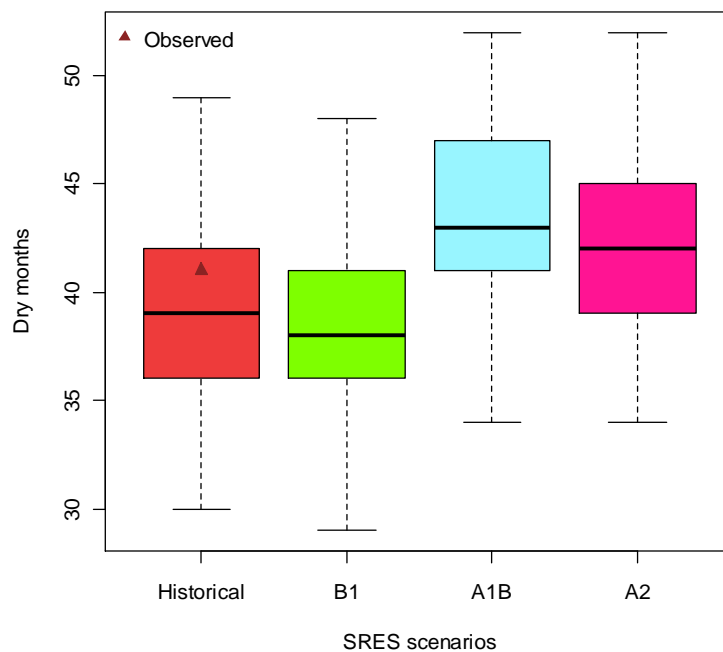
a)

b)
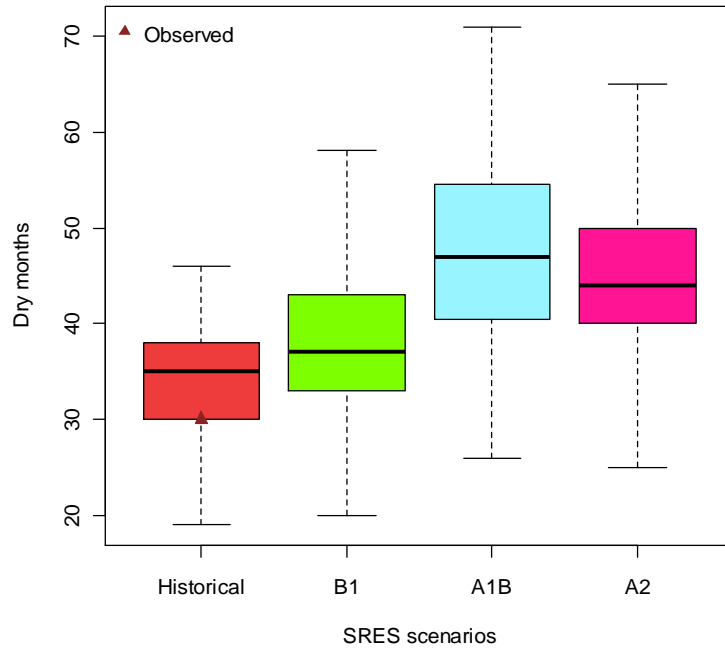
Figure 4.13. Total dry months for SPI for the three SRES scenarios at a)6- and b)24-months timescale for 2080-2100.

Figure 4.14. Total numbers of dry months (SPI≤-1) for various drought severity classes at 12-months timescale for the three SRES scenarios and for period 2080-2100.

Similar with the future period of 2030-2050, an increase in moderate dry months was indicated at all timescales and for all SRES scenarios (Fig. 4.14). Extreme dry months were increased at large timescales (12- and 24-months) for the three scenarios, where for B1 scenario the average increase is 6% and 11%, for A1B is 45% and 83% and finally for the A2 is 37% and 58% at 12- and 24-months timescale respectively. Moreover, severe dry months were increased compared with the historical period for

67

the two most severe scenarios A1B and A2 at all timescale. For B1 scenario a slight decrease was estimated at all timescales, except 24-months timescale where an increase of 15% is observed. Similar with the other drought severity classes, A1B scenario indicates larger number of severe dry months at all timescales than the other scenarios. The largest increase is at 24-months timescale where 52% is the average increase in severe dry months.

The results of the threshold level method are indicated in Table 4.5. The average severity for the three socio-economic scenarios was increased at all timescales by 3.35% for the B1 scenario, 9.40% for A1B and 8.56% for A2 scenario at 6-months timescale. For the three SRES scenarios the lower increase is observed at 12-months timescale and the largest at 24-months. A1B scenario is the most severe scenario for period 2080-2100 as the frequency analysis of dry months also showed. The statistics of the other deficit characteristics showed an increase at all timescales and for all scenarios, except the average maximum duration at 12-months timescale and for A1B and B1 scenario. Generally, there is an increase in most statistical characteristics of the average deficit characteristics of the generated SPI timeseries compared with the historical and as the timescale increases the difference between the historical and future statistical characteristics is rising.

Table 4.5. Average deficit characteristics of the generated 6-, 12-, 24-months SPI timeseries for period 2080-2100.
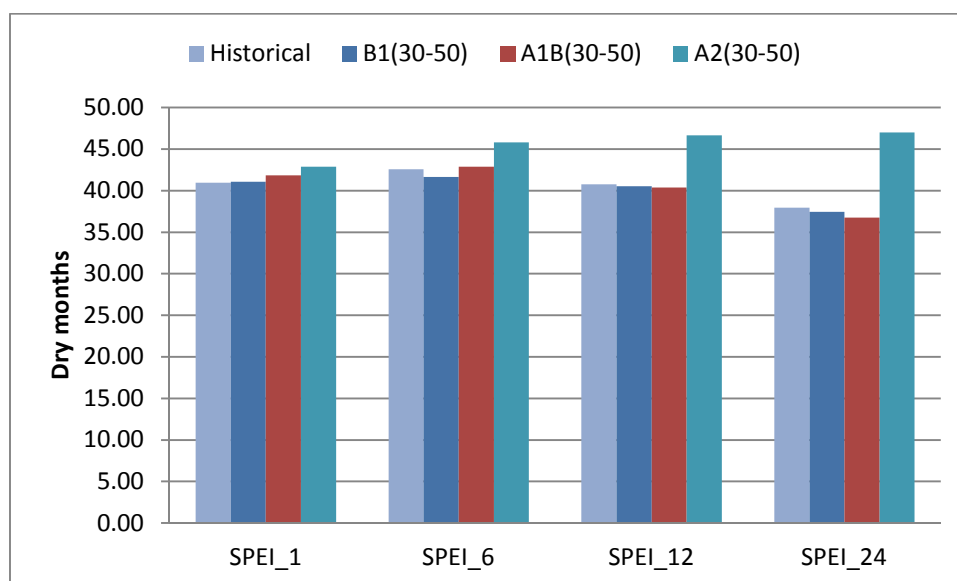
	Timescale 6-months				Timescale 12-months				Timescale 24-months			
	Average	Min	Median	Max	Average	Min	Median	Max	Average	Min	Median	Max
Severity												
Historical	0.60	0.32	0.59	0.93	0.62	0.29	0.59	1.37	0.54	0.15	0.51	1.37
B1	0.63	0.37	0.62	0.97	0.63	0.27	0.58	1.41	0.56	0.20	0.50	1.45
A1B	0.66	0.37	0.66	1.02	0.68	0.33	0.67	1.20	0.64	0.31	0.58	1.38
A2	0.66	0.43	0.65	0.99	0.67	0.36	0.64	1.30	0.60	0.14	0.57	1.26
Maximum cumulative severity												
Historical	7.56	3.03	7.12	14.85	12.51	2.14	11.79	28.09	12.99	0.52	11.11	38.30
B1	8.06	3.00	7.56	19.31	12.99	1.30	12.44	30.11	14.10	1.73	12.41	37.82
A1B	9.12	3.85	8.81	17.98	13.39	3.01	12.09	36.68	18.86	4.04	16.60	51.25
A2	8.95	3.63	8.19	21.44	15.02	4.19	13.94	33.02	17.32	0.57	15.28	49.10
Maximum duration												
Historical	8	4	7	14	14	5	13	36	18	2	18	35
B1	8	5	7	18	14	3	12	26	19	7	17	37
A1B	8	5	8	16	13	6	12	31	22	8	22	62
A2	8	5	8	17	15	7	13	28	21	5	22	62

68

4.3.2. SPEI

A. *Future Period 2030-2050*

The 100 future generated monthly time series of precipitation and evapotranspiration, which was calculated with the method of Thornwaite and is based on temperature, for the three socio-economic scenarios and the two future periods were used in order to estimate SPEI time series at multiple timescales (1-, 3-, 6-, 9-, 12-, 24- months). The parameters of the log-logistic distribution were assumed unchanged in the future. Hence, their respective values for the historical period have been used.

The analysis of the monthly SPEI time series for the period 2030-2050 showed that the total dry months (SPEI≤-1) will be increased for A2 SRES scenarios at all timescales (fig.4.12). For the B1 scenario there is a slight decrease at most timescales, whereas for A1B a slight decrease is observed at 12- and 24-months timescale. The largest average increase compared to the historical is observed for SPEI 24-months in the order of 24% and a range from -24% to 79%. At the same timescale the decrease in the SPEI time series is from -71% to 61% with a median decrease of -1% for the B1 scenario. For the A1B scenario the median decrease is -3% that ranges between -53% and 48% (fig.4.13).


Figure 4.12. Total average dry months for SPEI at multiple timescales for 2030-2050.

A2 seems more severe than the others for period 2030-2050 at all timescales. SPEI estimation is based on precipitation and temperature. Hence, there is an increase in the values of SPEI for A2 scenario, since the downscaled procedure showed a slight decrease in the precipitation pattern for this scenario and an increase in the temperature that probably affected the PET.

An increase in extreme dry months indicated from figure 4.14 for the three scenarios. Similar patterns are observed for all time scales. A2 has larger average increase in extreme dry months which is 157% with range from -100% to 1072%, while 68% and 76% is for B1 and A1B scenarios at 12-months timescale. Severe and moderate dry months for 12- and 24-months timescale were decreased for both B1 and A1B scenarios. Moderate dry months were increased by 6% and 8% for SPEI 12- and 24-months timeseries for A2. For the same timescales and the same scenario severe dry months were increased by 16% and 42% with ranges from -93% to 118% and from -76% to 169% respectively.
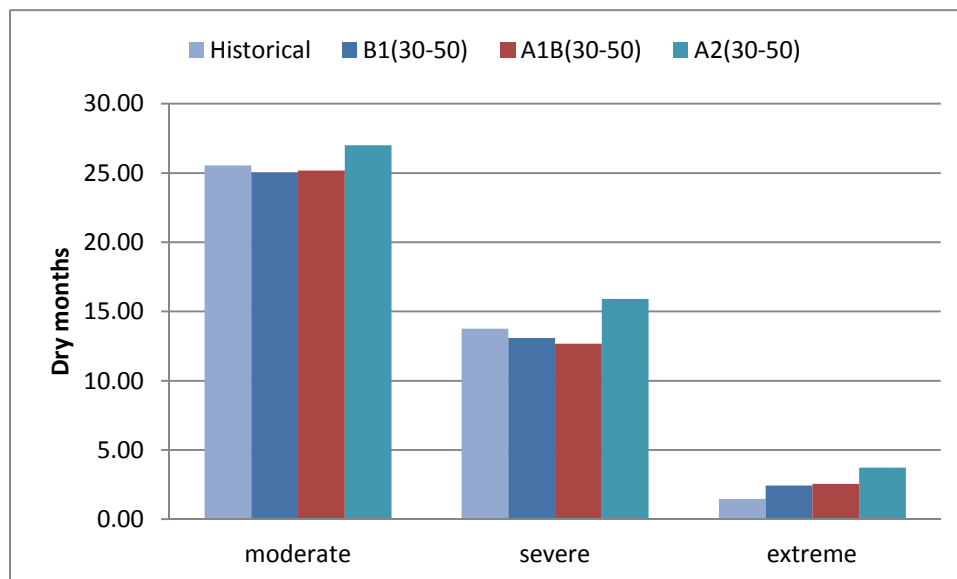
a)
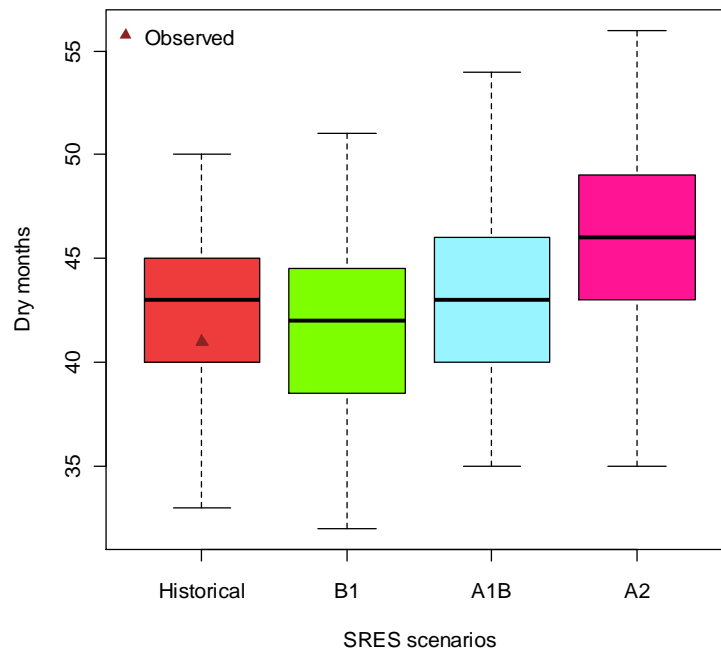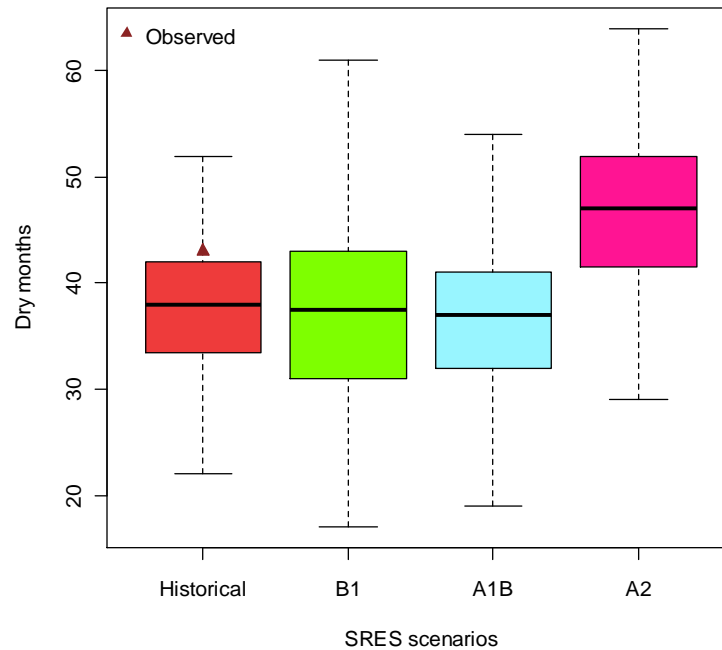
70

b)

Figure 4.13. Total dry months for SPEI for the three SRES scenarios at a)6- and b)24-months timescale for 2030-2050.
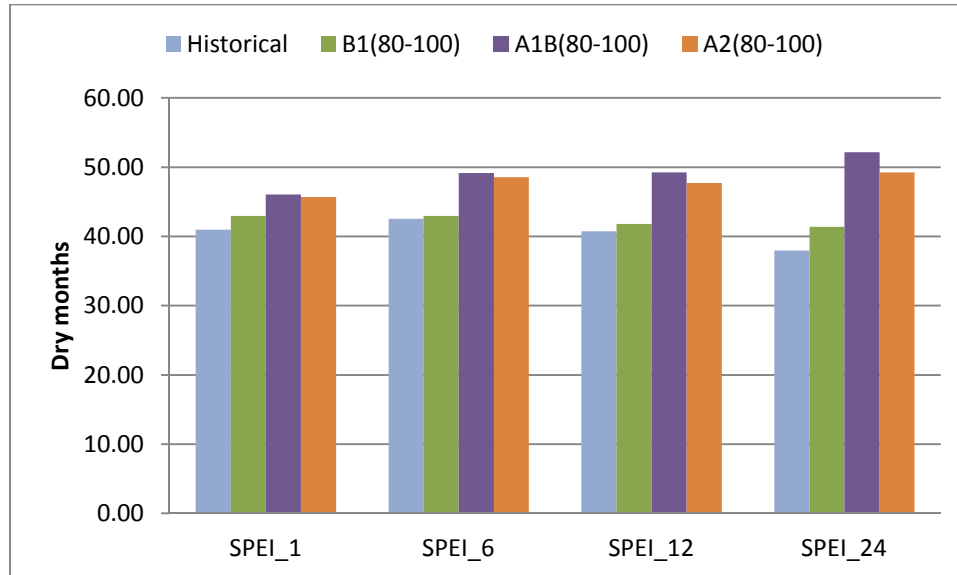

Figure 4.14. Total numbers of dry months (SPEI≤-1) for various drought severity classes at 12-months timescale for the three SRES scenarios and for period 2030-2050.

B. Future Period 2080-2100

For the future period 2080-2100 the SPEI time series indicated an increase in total dry months compared to the historical dry months at all timescales. Similar with SPI timeseries for the same period, A1B is the most severe scenario and B1 the most conservative (fig.415) for this period. According to figure 4.16, SPEI time series indicate larger increase at 24-months timescale compared to the historical than at
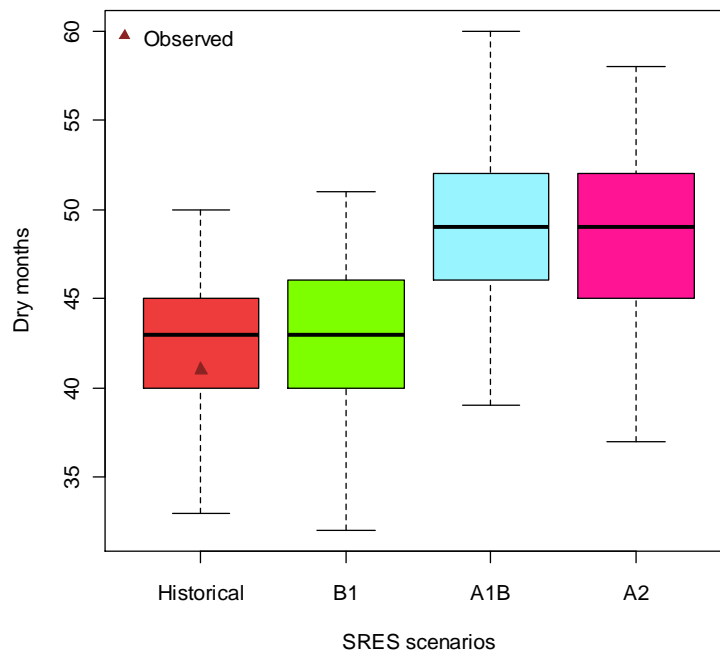
71

smaller timescales for all scenarios. An average increase of 3%, 21% and 17% was observed from the 100 time series of SPEI for B1, A1B and A2 respectively at 12-months timescale. At 24-months the average increase for B1 is 9%, for A1B 37% and 30% for A2 SRES scenario.
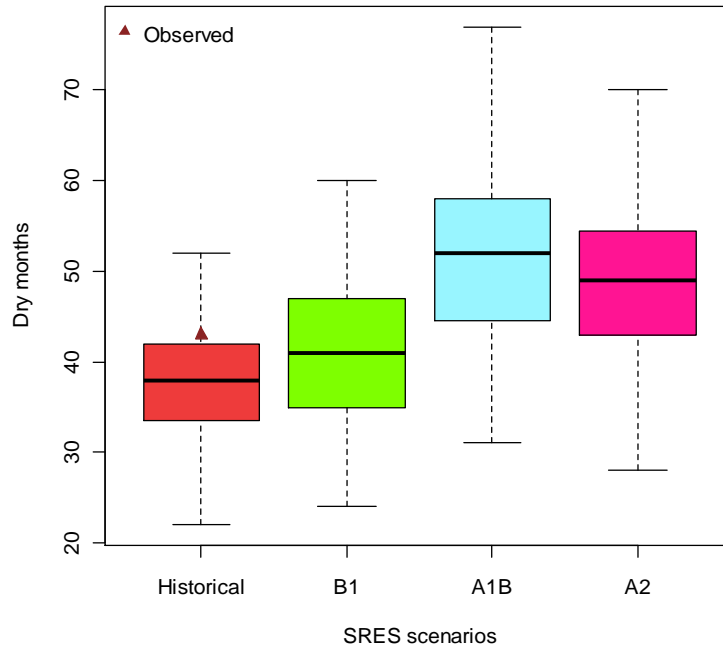

Figure 4.15. Total average dry months for SPEI at multiple timescales for 2080-2100.

a)

b)

Figure 4.16. Total dry months for SPEI for the three SRES scenarios at a) 6- and b)24-months timescale for 2080-2100.
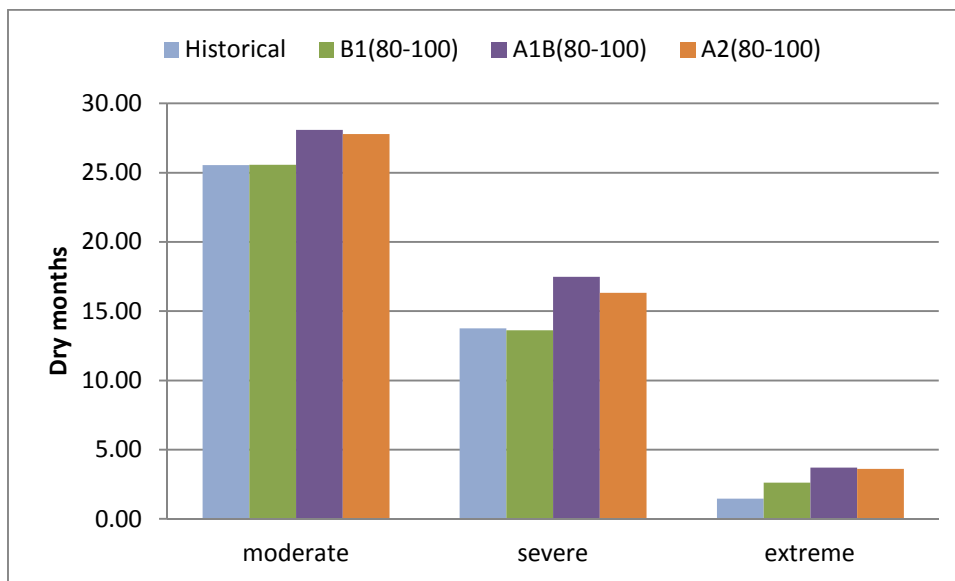
Figure 4.17. Total numbers of dry months (SPEI≤-1) for various drought severity classes at 12-months timescale for the three SRES scenarios and for period 2080-2100.

For all scenarios moderate, severe and extreme dry months at almost all timescales have increased whereas severe dry months for SPEI 12-months and moderate dry months for SPEI 6-months have been decreased for the B1 scenarios. At large timescales (12- and 24-months) extreme dry months have been increased and indicated that B1 scenario has the smallest and A1B the largest increase. The increase of extreme dry months for SPEI 12- and 24-months timeseries is 80% (range from -

73

100% to 590%) and 49% (range from -100% to 885%) for B1 scenario. However, for the other two scenarios the increase of extreme dry months is rising at larger timescales. For A1B SRES scenario the increase is from -100% to 797% with an average increase of 155% at 12-months timescale, whereas at 24-months extreme dry months were increased from -100% to 1112% and an average increase of 218%. The average increase for A2 scenario in the same severity class is 149% (range from -100% to 866%) and 183% (range from -100% to 1036%) at 12- and 24-months timescales respectively.

Table 4.5. Average deficit characteristics of the generated 6-, 12-, 24-months SPEI timeseries for period 2080-2100.

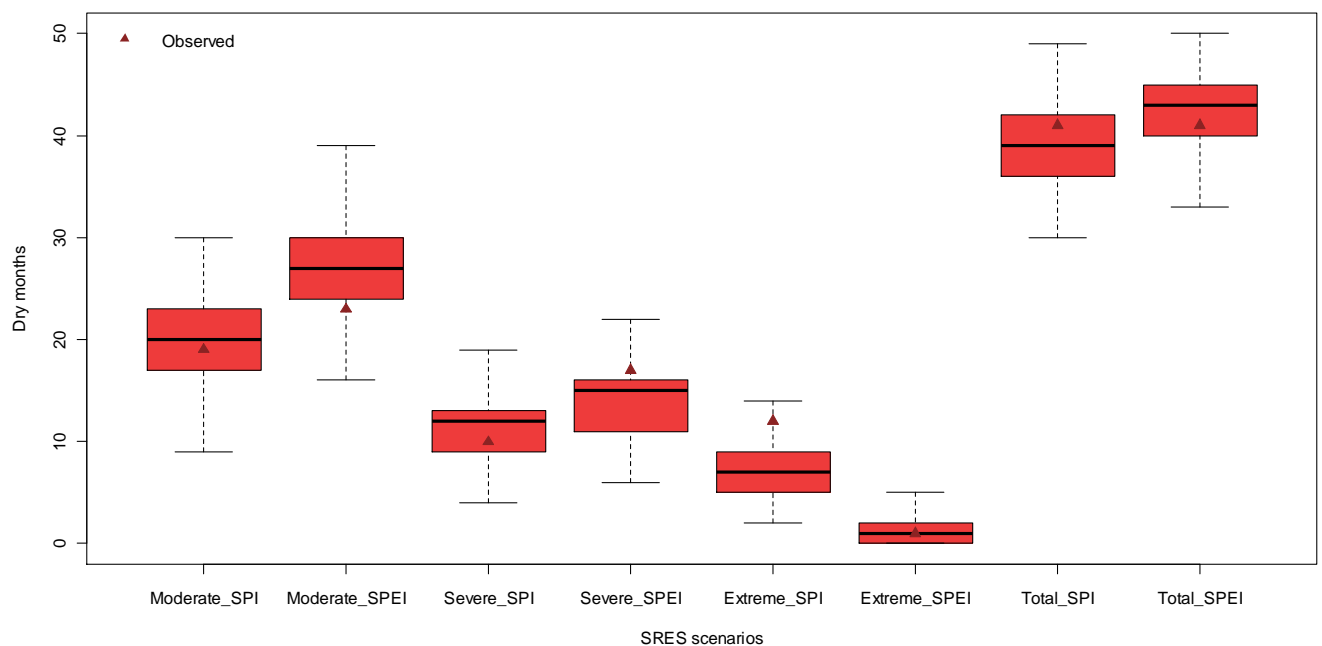|	Timescale 6-months				Timescale 12-months				Timescale 24-months			
	Average	Min	Median	Max	Average	Min	Median	Max	Average	Min	Median	Max
Severity												
Historical	0.42	0.33	0.42	0.55	0.43	0.29	0.43	0.77	0.43	0.24	0.41	0.73
B1	0.45	0.34	0.44	1.13	0.46	0.30	0.45	0.74	0.44	0.20	0.42	0.84
A1B	0.46	0.20	0.46	0.58	0.48	0.30	0.47	0.69	0.49	0.21	0.48	0.82
A2	0.46	0.32	0.46	0.58	0.47	0.30	0.47	0.74	0.47	0.16	0.47	0.89
Maximum cumulative severity												
Historical	4.85	2.72	4.84	8.89	8.86	3.61	8.42	18.31	10.31	3.49	10.56	20.29
B1	5.15	1.13	4.95	10.84	6.69	2.82	6.24	14.36	11.63	1.01	11.42	23.10
A1B	5.66	0.20	5.56	11.66	7.87	2.30	7.16	16.31	14.86	2.17	14.86	27.62
A2	5.73	1.79	5.48	12.30	7.43	3.04	7.04	15.39	13.83	0.72	14.02	26.94
Maximum duration												
Historical	8	5	8	13	14	7	13	35	18	10	18	33
B1	8	1	8	14	10	6	9	26	20	4	21	37
A1B	9	1	8	16	11	6	12	26	23	10	24	62
A2	8	3	8	15	11	5	12	29	22	6	23	62

Table 4.5 shows the results of the threshold level method of the 6-, 12-, 24-months SPEI timeseries for 2080-2100. Overall, for all scenarios the average severity was slightly increased and is rising as the timescales increases. At larger timescales (12- and 24-months) A1B seems more severe than the other two scenarios. For A1B scenario the average increase in severity is 13.38% at 12-months and 30.48% at 24-months timescale. For B1 and A2 scenarios the increase is 5.72% and 9.21% at 12-months and 2.08% and 9.63% at 24-months timescale. Maximum cumulative severity and maximum duration are also increased for the same period. The largest increase was observed at 24-months timescales for the A1B scenario as in the case of average

74

severity and is in the order of 106.07% for maximum cumulative severity and 52% for maximum duration.

4.3.3. Comparison of indices

The SPI and SPEI drought index were estimated for the observed and statistically downscaled time series of the climate data for the Acheloos watershed of period 1980-2000 at multiple timescales. The SPI is based only on the precipitation data, while the SPEI is based on the precipitation and the potential evapotranspiration, which was calculated with the method of Thornthwaite. Figure 4.18 indicate the difference between the total number of dry months (SPI≤-1 and SPEI≤-1) for various severity classes of the SPI and SPEI time series. Based on the observed data, the total number of dry months is equal to 41 for both indices at 6-months timescale. However, the allocation of the dry months in the respective drought classes is quite different. The SPI identifies less moderate and severe drought events than SPEI, but more extreme events. The statistically downscaled time series of the indices have similar patterns with the observed time series at all timescales. SPEI identified more drought events at large timescales but almost no extreme drought events (Fig. 4.18b).

a)

b)
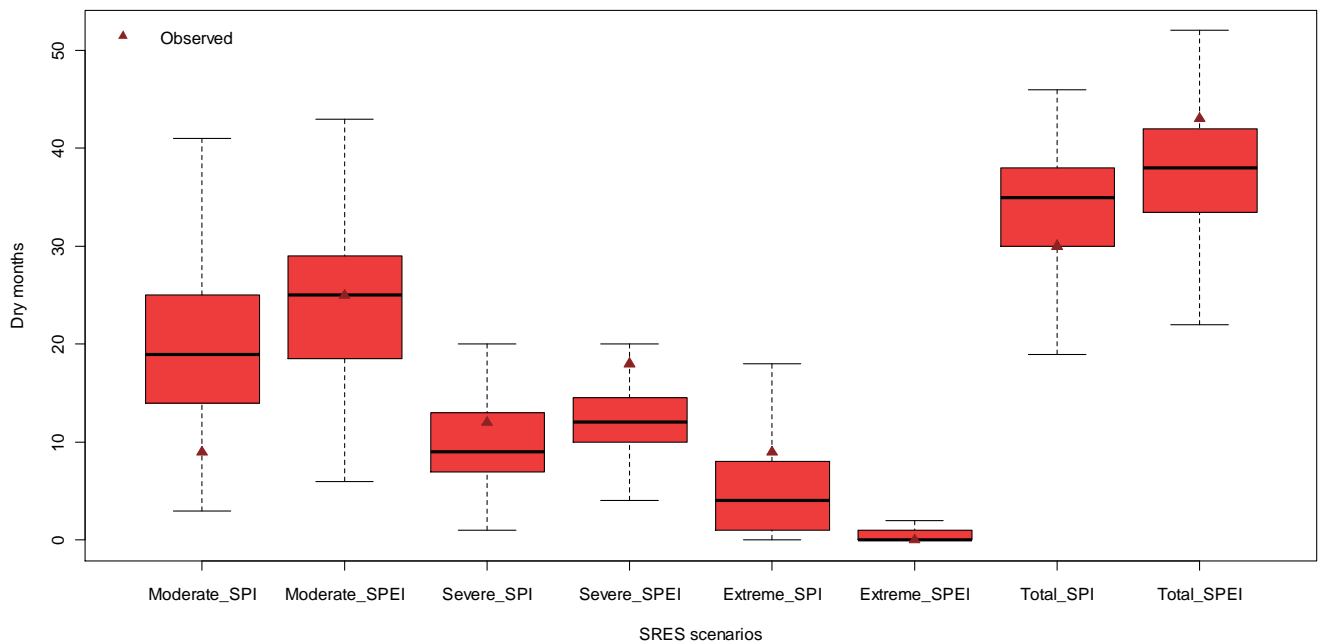
Figure 4.18. Comparison of the historical SPI and SPEI time series for various drought severity classes at 6- and 24-months timescale of period 1980-2000.

SPI and SPEI time series were estimated from the statistically downscaled time series of climate data for two periods (2030-2050 and 2080-2100). The parameters of the distributions assumed to be unchanged in the future. SPI values for the three socio-economic scenarios indicated an increase of the total dry months compared to the historical at multiple timescales. SPEI values have higher increase for the three SRES scenarios compared to the historical and indicated higher number of dry months for all scenarios (fig.4.19). Similar patterns have the SPI and SPEI time series at the other timescales. This is due to the calculation method of the SPEI time series that is based on precipitation and temperature data. For all scenarios an increase in temperature identified from the statistical downscaling method and simultaneous decrease of precipitation for A1B and A2 scenarios. Hence this increase in temperature would have produced a higher water demand by PET.

76

a)
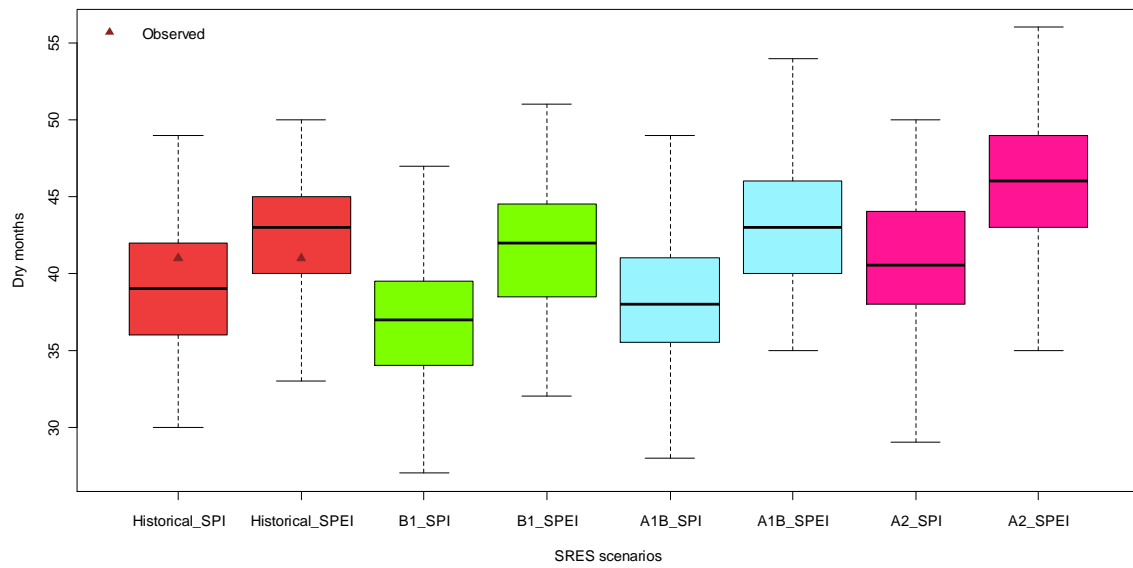
b)
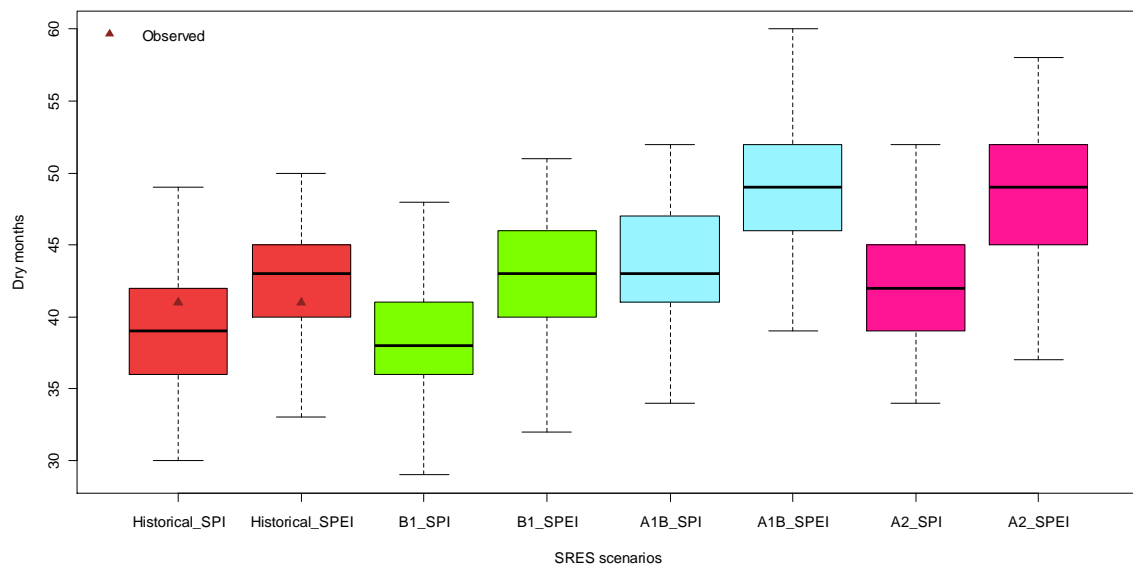
Figure 4.19 Comparison of total dry months for SPI and SPEI time series for the three SRES scenarios at 6-months timescale for a) 2030-2050 and b) 2080-2100.

5. CONCLUSIONS

This study evaluated the impacts of climate change on drought impulses in Acheloos watershed in Western Greece. Climate data of monthly precipitation and temperature from several meteorological stations were available for the basin for the period 1980-2000. The monthly areal precipitation of the watershed was estimated using the modified Thiessen method and the monthly temperature using the temperature gradient method. Moreover, potential evapotranspiration time series were calculated with the Thornthwaite method based on monthly temperature.

The outputs of CGCM3 model have been employed to statistically downscale monthly precipitation and temperature, to account the uncertainty of the downscaling method and to estimate future precipitation and temperature time series for the periods 2030-2050 and 2080-2100. The GCM grid point outputs were downscaled using multiple regression equations between GCM predictor output variables and areal monthly precipitation and temperature.

The mean monthly precipitation and temperature were simulated quite well by the regression model for the historical period 1980-2000 but the variance of the observed precipitation and temperature was not simulated satisfactorily.

The uncertainty of the GCM is included in the stochastic simulation of the residuals of the observed and downscaled time series. Hence, stochastic time series theory was applied to preserve the variance of observed monthly precipitation. A first order autoregressive model (AR(1)) was applied and used to generate annual climate data. Moreover the modified method of fragments applied in order to disaggregate the annual data to monthly climate data. Therefore, 100 synthetic precipitation and temperature time series were produced for historical period. Monthly and annual parameters were estimated for each replicate in order to evaluate the accuracy of the method. The statistical characteristics of the generated time series indicated that the method is able to reproduce the statistical properties of observed monthly precipitation and temperature time series for the period 1980-2000.

Based on the observed and stochastic downscaled time series, two drought indices were estimated at multiple timescales, namely Standardized Precipitation Index (SPI) and Standardized Precipitation Evapotranspiration Index (SPEI).

From the analysis of the SPI and SPEI time series indicated that the statistical downscaling method is capable to simulate drought patterns, since the generated time series produced similar number of total dry months with the observed time series. However, the allocation of the dry months in the respective drought classes was quite different. For the SPI time series moderate and severe droughts at most timescales were simulated satisfactorily by the downscaling method, but smaller number of dry months for extreme drought was produced. For the SPEI index moderate and extreme dry months were simulated well even though the severe drought events were underestimated. However, the observed drought pattern was in the range of the stochastic simulation for both indices.

The threshold level method applied in the observed and synthetic time series of SPI and SPEI for historical period and showed a decrease in the average severity for all the timescales that was applied, except for SPEI time series at 24-months timescale where it was increased. For SPEI an overestimation also exists for the maximum cumulative severity and maximum duration at 24-months timescale, whereas for SPI it is almost similar with the observed value. SPI maximum cumulative severity is underestimated for 6- and 12-months timescale. Finally the observed maximum duration for the 6-month timescale is simulated well, whereas for the other timescales the stochastic method overestimates it. However the observed values are within the inter-quartiles range of the statistical downscaled values.

Monthly and annual time series of precipitation and temperature were also estimated with the statistical downscaled method for two future periods and three socio-economic scenarios, namely SRES B1, SRES A1B and SRES A2, assuming that the residuals remain unchanged in the future. Potential evapotranspiration time series produced for the same periods and scenarios based on the Thorthwaite method. The procedure indicated that the annual temperature was slightly increased for all scenarios and the two future periods. Annual precipitation time series were simulated to decrease for A1B and A2 scenarios, whereas it was increased for the most conservative scenario B1. Similar results were indicated for monthly time series where temperature in almost all months was projected to increase and precipitation was decreased, except for B1 scenario where the precipitation was increased in almost all months. As it was expected the larger change in the average annual

temperature was observed for the long-term period (2080-2100). However, small changes in annual and monthly precipitation and temperature were indicated between the historical and future periods using the outputs of the CGCM3 model.

SPI and SPEI calculation parameters were based according to the present climate and were used to calculate SPI and SPEI time series for the future climate for the three socio-economic scenarios. The accuracy, reliability and uncertainty of the statistical downscaling method for present and future climate conditions was indicated by the results of the study as well as the suitability of the downscaling method for the assessment of climate change on hydrological, agricultural and water resources droughts. The analysis of the SPI and SPEI time series showed an impact of climate change on the severity, the frequency of dry months and the allocation on various severity classes for the three SRES scenarios but the uncertainty is quite large.

For the future period 2030-2050 the total number of dry months (SPI<-1) will be increased only for the A2 SRES scenarios at all time scales. For A1B and B1 scenarios a slight decrease was observed. B1 seems more conservative due to the slight increase of the downscaled annual precipitation and A2 the most severe for this period. According to the analysis of dry months and the categorization in severity classes, the total moderate dry months were estimated to increase for the three scenarios and at all timescales. However, a decrease in severe and extreme dry months was estimated for B1 and A1B scenarios at large timescales while A2 SRES scenarios showed an increase in all drought severity classes.

The total dry months were simulated to increase for all SRES scenarios and at all timescales for period 2080-2100 and as the timescale increases the average number of dry months is rising. Similar with period 2030-2050 an increase in moderate dry months was indicated at all timescales and for all SRES scenarios as well as in extreme dry months at large timescales. For this period A1B seems more severe than the other two scenarios in the estimation of SPI timeseries due to the slight decrease of annual precipitation for this scenario. The threshold level method indicated an increase in the average deficit characteristics of the generated 6-, 12-, 24-months SPI timeseries such as severity, maximum cumulative severity and maximum duration of

80

a drought event. As the timescale increases the difference between the historical and future statistical characteristics is rising.

The analysis of SPEI time series showed similar patterns with the SPI timeseries concerning the total dry months (SPEI≤-1) which will be increased for A2 SRES scenario at all timescales. A2 seems more severe than the others for period 2030-2050 since the downscaled procedure showed a slight decrease in the precipitation pattern for this scenario and an increase in the temperature that probably affected the PET. Extreme dry months were estimated to be increased for all scenarios and at all time scales whereas severe and moderate dry months were decreased for both B1 and A1B scenarios at large timescales.

For period 2080-2100 A1B an increase in total dry months was indicated compared to the historical dry months at all timescales. For all scenarios moderate, severe and extreme dry months at almost all timescales were increased. Similar with SPI timeseries for the same period, A1B is the most severe and B1 the most conservative scenario at all timescales. Furthermore, the threshold level method showed that for all scenarios the average severity, maximum cumulative severity and maximum duration increase as the timescales increases.

Comparing the two indices SPI identifies less moderate and severe drought events than SPEI, but more extreme events. For both indices the statistically downscaled time series have similar patterns with the observed time series at all timescales for the historical period. SPEI identified more drought events at large timescales but almost no extreme drought events for historical period. Under future climate conditions SPEI indicated a larger increase in the frequency of dry months than SPI, due to the dependence of the index on the temperature. The temperature was projected to increase for the three scenarios. Hence, a higher water demand was produced by PET.

The results of this study indicated that even though the changes in precipitation and temperature between historical and future periods using the output of the CGCM3 model were small, future climate change would probably affect drought severity in a region. However, the uncertainty in the future drought episodes should always be accounted for since the range of the drought episodes is quite large especially for

larger timescales. Future drought episodes due to climate change should be handled with caution and always with their respective ranges.

References

Abramopoulos, F., Rosenzweig, C., Choudhury, B., 1988. Improved ground hydrology calculations for global climate models (GCMs). Soil water movement and evapotranspiration. Journal of Climate 1, 921–941.

Abramowitz, M. and I.A. Stegun, 1965: Handbook of Mathematical Functions. Dover Publications, New York.

Allen, R.G., L.S. Pereira, D. Raes, M. Smith, 1998: *Crop evapotranspiration: guidelines for computing crop requeriments*. Irrigation and drainage paper 56. FAO. Roma. Italia.

American Meteorological Society, (AMS), 2004: Statement on meteorological drought, Bull. Am. Meteorol. Soc., 85, pp 771–773.

Bhalme, H. N. and Mooley, D. A., 1980: Large scale droughts/floods and monsoon circulation, Mon. Weath. Rev., 108, pp 1197–1211.

Bordi, I. and Sutera, A.: Fifty years of precipitation: Some spatially remote teleconnections, Water Resour. Manag., 15, 247– 280, 2001.

Bordi, I., Frigio, S., Parenti, P., Speranza, A., and Sutera, A.: The analysis of the Standardized Precipitation Index in the Mediterranean area: regional patterns, Annali di Geofisica, 44, 5–6, 979–993, 2001.

Box, G.E.P., G.M. Jenkins, and G.C. Reinsel, 2008. Time Series Analysis: Forecasting and Control, 4th Edition, John Wiley & Sons.

Brandsma, T. and Buishand, T. A., 1997: Statistical linkage of daily precipitation in Switzerland to atmospheric circulation and temperature, J. Hydrol., 198, pp 98–123.

Burger, G., 1996: Expanded downscaling for generating local weather scenarios, Clim. Res., 7, 111–128.

Cai, W., Cowan, T., 2008. Evidence of impacts from rising temperature on inflows to the Murray–darling basin. Geophysical Research Letters 35, L07701. doi:10.1029/2008GL033390.

Chang, T.J. and Cleopa, X.A., 1991. A proposed method for drought monitoring. Water Resources Bulletin 27, 275–281.

Changnon S, Pielke RP, Changnon D, Sylves RT, Pulwarty R., 2000: Human factors explain the increased losses from weather and climate extremes. Bull Am Meteorol Soc 81: pp 437–442.

Cox, D.R. and lsham, V., 1994. Stochastic models of precipitation. In: Barnett, V. Turkman, K.F. (Eds) Statistics for the Environment 2: Water related issues, Wiley, Chichester, 3-18.

Crane, R.G and Hewitson, B.C. 1998. Doubled CO_2 precipitation changes for the Susquehanna basin: down-scaling from the GENESIS general circulation model. *International Journal of Climatology,* 18, 65-76.

Dibike, B.Y. and Coulibaly, P., 2006: Temporal neural networks for downscaling climate variability and extremes, Journal of Neural Networks, Vol. 19, pp. 135-144.

Dracup, J.A., K. Lee, and E. Paulson, 1980: *On the definition of droughts,* Water Resources Research, Vol 16, Washington D.C. U.S.A, pp 297-302.

Dehn, M. and Buma, J., 1999: Modelling future landslide activity based on general circulation models, Geomorphology, 30, 175–187.

Droogers, P., and R.G. Allen, 2002: Estimating reference evapotranspiration under inaccuratedata conditions. Irrigation and Drainage Systems, 16, 33-45.

Dubrovsky, M., Svoboda, M.D., Trnka, M., Hayes, M.J., Wilhite, D.A., Zalud, Z., Hlavinka, P., 2008: Application of relative drought indices in assessing climate change impacts on drought conditions in Czechia. Theoretical and Applied Climatology 96, 155–171.

Du Pisani, C.G., H.J. Fouché, and J.C. Venter, 1998: Assessing rangeland drought in South Africa. *Agricultural Systems,* **57**, pp 367-380.

Fowler, H. J., Blenkinsop, S., and Tebaldi, C., 2007: Linking climate change modelling to impacts studies: recent advances in downscaling techniques for hydrological modeling, Int. J. Climatol., 27(12), 1547–1578.

Gibbs, W. J. and Maher, J. V., 1967: Rainfall deciles as drought indicators, Australian Bureau of Meteorology Bulletin, No. 48, Commonwealth of Australia, Melbourne, 37.

Giorgi, F., Hewitson, B., Christensen, J., Fu, C., Jones, R., Hulme, M., Mearns, L., Von Storch, H., and Whetton, P., 2001: Regional climate information – evaluation and projections, in: Climate Change 2001: The scientific basis, edited by: Houghton, J. T. et al., Cambridge University Press, 881 pp.

González, J., and J.B. Valdés, 2006: New drought frequency index: Definition and comparative performance analysis, *Water Resources Research,* 42, W11421, doi:10.1029/2005WR004308.

Guttman, N. B., 1998: Comparing the Palmer Drought Index and the Standardized Precipitation Index, J. Am.Water Resour. Assoc., 34, 1, 113–12.

Hayes,M. J., Svoboda, M. D.,Wilhite, D. A., and Vanyarkho, O. V., 1999: Monitoring the 1996 drought using the standardized precipitation index, Bull. Am. Meteorol. Soc., 80, 2, 429–438.

Hayes, M.J. Alvord, C. and Lowrey, J., 2007: Drought indices. *Intermount West Climate Summary*, 3 (6): 2-6.

Heim, R.R., 2000: Drought Indices. A review. In: *Drought: A Global Assessment, Hazards Disaster Series*, Vol.I, Wilhite, D.A. (ed.), Routledge, New York, pp 159-167.

Heim, R.R., 2002: A review of twentieth-century drought indices used in the United States. *Bulletin of the American Meteorological Society,* 83, pp 1149-1165.

Hewitson, B.C. and Crane R.G., 1996: Climate downscaling: techniques and application. Climate Research, 7, pp 85-95.

Hipel, K. and McLeod, A. I., 1994: Time Series Modeling of Water Resources and Environmental Systems, Elsevier, Amsterdam, pp 1013.

Hosking, J.R.M., 1990: L-Moments: Analysis and estimation of distributions using linear combinations of order statistics. *Journal of Royal Statistical Society B,* **52**, 105-124.

Hu, Q. and Willson, G.D., 2000: Effect of temperature anomalies on the Palmer drought severity index in the central United States. International Journal of Climatology. 20, 1899–1911.

Huth, R., 1999: Statistical downscaling in central Europe: Evaluation of methods and potential predictors, Clim. Res., 13, 91–101.

Intergovernmental Panel on Climate Change, (IPCC), 2000: Special Report on Emissions Scenarios, Nebojsa Nakicenovic and Rob Swart (Eds.). Cambridge University Press, UK. pp 570.

Intergovernmental Panel on Climate Change, (IPCC), 2001: Climate Change 2001, The Scientific Basis. Cambridge: Cambridge University Press.

Intergovernmental Panel on Climate Change, (IPCC), 2007: Climate Change 2007: Synthesis Report of the Fourth Assessment Report. IPCC.

IWMI, 2008: *Terms and Definitions of Droughts*. Drought Information Center, International Water Management Institute, Sri Lanka, available at www.iwmi.cgiar.org/drw/info/default.asp?PGID=2.

Jones, P. D. and Hulme, M., 1996: Calculating regional climatic time series for temperature and precipitation: Methods and illustrations, Int. J. Climatol., 16, pp 361–377.

Karl, T. R., Wang, W. C., Schlesinger, M. E., Knight, R. W., and Portman, D., 1990: A method of relating general circulation model simulated climate to observed local climate. Part I: Seasonal statistics, J. Climate, 3, pp 1053–1079.

Keyantash, J. and J. Dracup., 2002: The quantification of drought: an evaluation of drought indices. *Bulletin of the American Meteorological Society*, 83, pp 1167-1180.

Keyantash, J. A., and J.A. Dracup, 2004: An aggregate drought index: Assessing drought severity based on fluctuations in the hydrologic cycle and surface water storage. *Water Resources Research,* 40, W09304, doi:10.1029/2003WR002610.

Kothavala, Z., 1999: The duration and severity of drought over eastern Australia simulated by a coupled ocean-atmosphere GCM with a transient increase in CO2, Envir. Model. Soft., 14, 243–252.

Lana, X., Serra, C., and Burgueno, A.: Patterns of monthly rainfall shortage and excess in terms of the standardized precipitation index for Catalonia (NE Spain), Int. J. Climatol., 21, 13, 1669– 1691, 2001.

Lane, W. L. 1979. Applied stochastic techniques (LAST computer package), user manual. Division of Planning Technical services, Bureau of Reclamation, Denver, Colarado.

Liakouris, D. 1971. Geomorphological and geological research in the area of Acheloos River (upper part), PhD thesis, School of Sciences, University of Athens, Athens.

Lloyd-Hughes, B. and Saunders, M. A.: A drought climatology for Europe, Int. J. Climatol., 22, 1571–1592, 2002.

Loukas, A. and Vasiliades, L., 2004: Probabilistic analysis of drought spatiotemporal characteristics in Thessaly region, Greece, Nat. Hazards Earth Syst. Sci., 4, 719–731.

Loukas, A., and Vasiliades, L., 2005: Identification of the relationship between meteorological and hydrological drought, Geophys. Res. Abstr., 7, 05479.

Loukas, A., Vasiliades, L., and Dalezios, N. R., 2003: Intercomparison of meteorological drought indices for drought assessment and monitoring in Greece". Proceedings of the 8th International Conference on Environmental Science and Technology, 8–10 September 2003, Lemnos, Greece, 484–491.

Loukas, A., Vasiliades, L., and Tzabiras, J., 2007: Evaluation of climate change on drought impulses in Thessaly, Greece, European Water Journal, 17–18(1).

Loukas, A., Vasiliades, L., and Tzabiras, J., 2008: Climate change effects on drought severity, Adv. Geosci., 17, 23–29, http://www.adv-geosci.net/17/23/2008/.

Maheepala, S. and Perera, C. J. C. 1996. Monthly hydrologic data data generation by disaggregation. Journal of Hydrology, 178: 277-291.

Matalas, N. C., 1967. Mathematical assessment of synthetic hydrology. Water Resources Research, 3(4), 937-945.

Mavromatis, T., 2007: Drought index evaluation for assessing future wheat production in Greece, Int. J. Climatol., 27(7), 911–924.

McCabe, G. J. andWolock, D. M., 1999: General-Circulation-Model simulations of future snowpack in the western United States, J. Am. Water Resour. Assoc., 35(6), 1473–1484.

McKee, T. B., Doesken, N. J., and Kleist, J., 1993: The relationship of drought frequency and duration to time scales, Preprints, 8th Conference on Applied Climatology, Anaheim, CA, Amer. Meteor. Soc., 179–184.

McKee, T. B., Doesken, N. J., and Kleist, J., 1995: Drought monitoring with multiple time scales, Preprints, 9th Conference on Applied Climatology, Dallas, TX, Amer. Meteor. Soc., 233–236.

Mearns, L. O., Giorgi, F., Whetton, P., Pabon, D., Hulme, M., and Lal, M., 2004: Guidelines for use of climate scenarios developed from regional climate model experiments, Tech. Rep., Data Distribution Centre of the IPCC.

Mejia, J. M. and Rouselle, J. 1976. Disaggregation models in hydrology revisited. Water Resources Research, Vol. 12(2): 185-186.

Murphy, J.M., 1999: An evaluation of statistical and dynamical techniques for downscaling local climate. *Journal of Climate,* 12, pp 2256-228.

National Observatory of Athens, 2001: Climate Changes in Mediterranean. Scientific Report, National Observatory of Athens, Athens.

Nicholls, N., 2004. The changing nature of Australian droughts. Climatic Change 63, 323–326.

Niemeyer S., 2008: New drought indices. Options Méditerranéennes. Série A : Séminaires Méditerranéens 80 : pp 267-274.

Obasi GOP, 1994: WMO's role in the international decade for natural disaster reduction. Bull Am Meteorol Soc 75: 1655–166.

Palmer, W. C., 1965: Meteorological drought. Research Paper No. 45, U.S. Weather Bureau, Washington, D.C., pp 58.

Piechota, T. C. and Dracup, J. A., 1996: Drought and regional hydrologic variation in the US: associations with the El Ni˜no-Southern Oscillation, Water Resour. Res., 32, 5, 1359–1373.

Porter, J. W. and Pink, B. J. 1991. A Method of synthetic fragments for disaggregation in stochastic data generation. Hydrology and Water Resources Symposium, Institution of Engineers, Australia: 187-191.

Potop V., 2011: Evolution of drought severity and its impact of corn in the Republic of Moldova. Theor Appl Climatol. DOI:10.1007/s00704-011-0403-2.

Potop V. and Možný M. (2011): The application a new drought index – Standardized precipitation evapotranspiration index in the Czech Republic. In: "Mikroklima a mezoklima krajinných structur a antropogenních prostředí".2- 4February, Brno.

Salas, J. D., 1993: Analysis and Modeling of Hydrologic Time Series, in Handbook of Hydrology, edited by Maidment, D. R., McGraw- Hill, Inc., New York, Chap. 19, 19.1–19.72.

Sandford, S., 1978: *Towards a definition of Drought* Botswana Drought Symposium, del 5 al 8 de Junio de 1978, Gaborone Botswana, pp 305.

Singh, V.P. and F.X.Y. Guo, 1993: Parameter estimation for 3 parameter log-logistic distribution (LLD3) by Pome. Stochastic Hydrology and Hydraulics, 7, 163-177.

Srikanthan, R. and McMahon, T.A., 1985. Stochastic generation of rainfall and evaporation data. AWRC Technical Paper No. 84, 301pp.

Srikanthan, R. and McMahon, T.A., 2001. Stochastic generation of annual, monthly and daily climate data: A review. Hydrology & Earth SystemSciences, 5(4), pp. 653-670.

Subrahmanyam, V. P., 1967: *Incidence and Spread of Continental Drought,* WMO Report No 2, Geneva Switzerland, pp 53.

Syed, T.H., Famiglietti, J.S., Rodell, M., Chen, J., Wilson, C.R., 2008. Analysis of terrestrial water storage changes from GRACE and GLDAS. Water Resources Research 44, W02433. doi:10.1029/2006WR005779.

Tallaksen, L.M. (2000) Streamflow drought frequency analysis, In*: Drought and Drought Mitigation in Europe* (ed. by J.V.Vogt and F.Somma), Kluwer Academic Publishers, the Netherlands, 103-117.

Tate, E.L. and Gustard, A., 2000: Drought definition: a hydrological perspective, In*: Drought and Drought Mitigation in Europe* (ed. by J.V.Vogt and F.Somma), Kluwer Academic Publishers, the Netherlands, 23-48.

Thyer, M. A. and Kuczera, G. A., 2000. Modelling long-term persistence in hydro-climatic time series using a hidden state Markov model. Water Resources Research, 36(11): 3301-3310.

Thornthwaite, C.W., 1948: An approach toward a rational classification of climate. Geographical Review, 38, 55-94.

Tsakiris, G. and Vangelis, H.: Towards a drought watch system based on spatial SPI, Water Resour. Manag., 18, 1–12, 2004.

van Rooy, M. P., 1965: A rainfall anomaly index independent of time and space, Notos, 14, pp 43–48.

Varis, O., Kajander, T., and Lemmela, R., 2004: Climate and water: From climate models to water resources management and vice versa, Clim. Change, 66, pp 321–344.

Vasiliades, L., 2010: Drought spatiotemporal analysis, modelling and forecasting in Pinios river basin of Thessaly, PhD Thesis, Department of Civil Engineer, University of Thessaly, pp 391 (in Greek with English abstract).

Vasiliades, L. and A. Loukas, 2006. "Hydrological Drought Evaluation with the Use of Meteorological Drought Indices" *EGU General Assembly*, 2-7 April 2006, Vienna, Austria (Geophysical Research Abstracts, Vol. 8).

Vasiliades, L. and A. Loukas (2009). "Hydrological Response Evaluation to Meteorological Drought Using the Palmer Drought Indices in Thessaly, Greece" Desalination, 237 (1-3), 3-21. B. 37.

Vasiliades, L., Loukas, A. and Liberis, G., 2011: "A Water Balance Derived Drought Index for Pinios River Basin, Greece." *Water Resources Management,* 25, 1087-1101.

Vasiliades, L., Loukas, A. and Patsonas, G., 2009. Evaluation of a statistical downscaling procedure for the estimation of climate change impacts on droughts. Natural Hazards and Earth Systems Sciences, 9, 879-894.

Vicente-Serrano S. M., Beguería S., López-Moreno J.I., 2010: A Multi-scalar drought index sensitive to global warming: The Standardized Precipitation Evapotranspiration Index – SPEI. Journal of Climate 23(7):1696- 1718, DOI: 10.1175/2009JCLI2909.1.

Vicente-Serrano, S. M. and López-Moreno, J. I., 2005: Hydrological response to different time scales of climatological drought: an evaluation of the Standardized Precipitation Index in a mountainous Mediterranean basin, Hydrol. Earth Syst. Sci., 9, 523–533, http://www.hydrol-earth-syst-sci.net/9/523/2005/.

Vongt, J.V. and Somma, F. (eds), 2000: *Drought and Drought Mitigation in Europe. Advances in Natural and Technological Hazards Research*, 14, Kluwer Academic Publishers, Dordrecht.

von Storch, H., 1995: Inconsistencies at the interface of climate impacts studies and global climate research, Meteorol. Zeitschrift 4, pp 72-80.

von Storch, H., 1999: On the use of "inflation" in statistical downscaling. Journal of Climate, 12, pp 3505-3506.

Von Storch, H., Zorita E. and Cubasch, U. 1993. Downscaling of global climate change estimates to regional scales: An application to Iberian rainfall in wintertime. *Journal of Climate,* 6, 1161-1171.

Wells, N., S. Goddard, and M.J. Hayes, 2004: A self-calibrating Palmer Drought Severity Index. *Journal of Climate,* 17, pp 2335-2351.

Wilby, R. L. and Wigley, T. M. L., 1997: Downscaling General Circulation Model output: a review of methods and limitations, Prog. Phys. Geogr., 21, 530–548.

Wilby, R.L., Conway, D. and Jones, P.D., 2002: Prospects for downscaling seasonal precipitation variability using conditioned weather generator parameters, Hydrological Processes, Vol. 16, pp 1215-1234.

Wilby, R. L., Charles, S. P., Zorita, E., Timbal, B., Whetton, P., and Mearns, L. O., 2004: Guidelines for use of climate scenarios developed from statistical downscaling methods, Tech. Rep., Data Distribution Centre of the IPCC.

Wilhite,D.A., 2000: Drought as a natural hazard: Concepts and definition. In: *Drought: A Global Assessment,* Vol. 1, Wilhite, D.A. (ed.). Routledge, New York, pp. 1-18.

Wilhite, D.A. and Buchanan, M., 2005: Drought as hazard: Understanding the natural and social context. In *Drought and Water Crisis: Science, Technology, and Management Issues,* Wilhite, D.A. (ed.). CRC Press (Taylor and Francis), New York, pp 3-29.

Wilhite, D. A. and Glantz, M. H., 1985: Understanding the drought phenomenon: The role of definitions, Water Inter., 10, 2, pp 111–120.

Wilks, D.S. and Wilby, R.L., 1999: The weather generation game: A review of stochastic weather models. *Progress in Physical Geography,* 23, pp 329-357.

Wilson, E. B. and M.M. Hilferty, 1931. Distribution of Chi-square. Proceedings National Academy of Science, 17, 684-688.

World Meteorological Organization, 1975: *Drought and agriculture WMO Technical Note Number 138,* Report of CAg Working Group on the Assessment of Drought, Geneva Switzerland, pp 53*.*

Xu, C. Y., 1999: From GCMs to river flow: A review of downscaling techniques and hydrologic modeling approaches, Prog. Phys. Geogr., 23, 229–249.

Xu, C. Y., Widen, E., and Halldin, S., 2005: Modelling hydrological consequences of climate change – progress and challenges, Adv. Atmos. Sci., 22(6), 789–797.